

https://dspace.org/

Synthesis gas conversion into dimethyl ether and light hydrocarbons via methanol over a hybrid gold-based catalyst

Kalala, Mbuyi Gabriel

2012-07-19
http://hdl.handle.net/10539/11694

Downloaded from a DSpace repository. https://dspace.org/

SYNTHESIS GAS CONVERSION INTO DIMETHYL ETHER AND LIGHT HYDROCARBONS VIA METHANOL OVER A HYBRID GOLD-BASED CATALYST

Mbuyi Gabriel Kalala

A dissertation submitted to the Faculty of Engineering and the Built Environment, University of the Witwatersrand, Johannesburg, in fulfilment of the requirements for the degree of Master of Science in Engineering.

Johannesburg, 2012

DECLARATION

I declare that this dissertation is my own, unaided work. It is being submitted for the Degree of Master of Science in Engineering in the University of Witwatersrand, Johannesburg. It has not been submitted before for any degree or examination in any other University.

(Signature of candidate)

---------- day of----------2012

ABSTRACT

Dimethyl ether (DME) has attracted an increasing amount of attention in recent years because its properties are similar to those of transportation fuels and it can be used as a substitute for diesel. The two-step process required to produce DME is a proven technology that has already been commercialised. However its capital and operating costs remain high because two different reactors are required for methanol synthesis and methanol dehydration, and a number of recycles are needed to improve the overall CO conversion in the methanol synthesis step.

A number of researchers have proposed a new process design named synthesis gas-to-DME (STD) process to overcome the limitations of the current technology for producing DME. This innovation uses one reactor for both methanol and DME synthesis, and a hybrid catalyst that leads to higher conversions of synthesis gas to DME. Both of these features reduce the capital and operating costs of the process.

In this dissertation we record the results of thermodynamic research into the STD process, which confirm that it offers more advantages than the two-step process. The system remains pressure-sensitive, as the methanol synthesis is the most active component of the process. The experimental results also matched the trends of thermodynamic predictions of selectivities.

For the experimental work we used a gold-based catalyst to convert synthesis gas to DME and by-products (light hydrocarbons C_1 to C_5). The results showed that DME selectivity is high at a low temperature (340^{o}–380^{o}C), but that under these conditions the catalyst exhibited a low level of activity. An increase in temperature increased the production of hydrocarbons but imposed kinetic limits on the conversion of MeOH to DME. Deactivation of the catalyst occurred at 460^{o}C because of carbon deposits on its surface.

To

My parents, brothers and sisters

ACKNOWLEDGEMENTS

I owe thanks to many people, whose assistance was indispensable to the completion of this project.

Firstly, I express my sincere gratitude to my supervisors, Professors Diane Hildebrandt, Mike S. Scurrell and David Glasser, for their guidance and advice throughout the course of this research project.

I would like to thank Mr. Basil Chassoulas for his technical assistance in the laboratory.

Also I must express my gratitude to my colleagues in the Centre of Materials and Process Synthesis (COMPS) and the Catalysis, Organo-Metallic and Materials (CATOMMAT) group for creating a supportive and friendly working environment.

I am indebted to the National Research Foundation (NRF), the Centre of Materials and Process Synthesis (COMPS) and the University of the Witwatersrand, Johannesburg for financial support.

Most importantly, I would like to thank my family: my parents, brothers and sisters for their support, encouragement and love throughout my life.

Lastly, I offer my regards and blessings to all of those who supported me in many different ways during the period I spent working on this project.

CONTENTS

DECLARATION ..... **ii**

ABSTRACT ..... **iii**

DEDICATION ..... **iv**

ACKNOWLEDGEMENTS ..... **v**

CONTENTS ..... **vi**

LIST OF FIGURES ..... **ix**

LIST OF TABLES ..... **xi**

LIST OF SYMBOLS ..... **xiii**

LIST OF ACRONYMS ..... **xv**

CHAPTER 1 INTRODUCTION **1**

CHAPTER 2 LITERATURE REVIEW **3**

2.1 Introduction 3

2.2. Supported catalysts 4

2.2.1 Methods of catalyst preparation 5

2.2.2 Preparation of highly-dispersed gold catalysts 8

2.2.3 Factors that affect gold catalysis 9

2.3 MeOH synthesis 10

2.4 Water-gas shift reaction 15

2.5 Dimethyl ether synthesis 16

2.5.1 Catalysts for DME synthesis 19

2.5.2 DME formation mechanism 21

2.5.3 Raw materials used for DME synthesis 22

2.5.4 Synthesis gas-to-DME (STD) process reactors 24

2.5.5 DME process technologies 25

2.5.6 Catalyst deactivation 28

2.6 Summary of the literature review 29
2.7 Objectives of the research 30
CHAPTER 3 EXPERIMENTAL 31
3.1 Introduction 31
3.2 Catalyst preparation 32
3.3 Characterization methods 33
3.3.1 Catalyst composition by atomic emission spectroscopy 33
3.3.2 Size determination by transmission electron microscopy 34
3.3.3 Surface area and pore size determination by the Brunauer-Emmett-Teller method 35
3.4 The rig and reactor 37
3.5 Analytical method 40
3.6 Data generation and processing 43
3.7 Calculation of outlet gas compositions, conversion, reaction rates and selectivity 45
CHAPTER 4 RESULTS AND DISCUSSION 47
4.1 Introduction 48
4.2. Process analysis 48
4.2.1 Mass balances 49
4.2.2 Equilibrium equations 50
4.2.3 Case 1. The MeOH synthesis reaction is the only reaction that occurs 53
4.2.4 Case 2. Both the MeOH and DME synthesis reactions occur in the reactor 55
4.2.5 Case 3. The MeOH, DME and WGS reactions all occur simultaneously in the reactor 58
4.2.6 Case 4. MeOH–WGS system 61
4.2.7 Case 5. The MeOH, DME, WGS and CH_4 reactions all occur simultaneously in the reactor 62
4.3 Conversion of synthesis gas into DME using a gold based-catalyst 64
4.3.1 Catalyst characterization 65

4.3.2 Effect of temperature on product selectivity and CO conversion over Au/ZnO/γ-Al_2O_3 66

4.3.3 Effect of pressure on product selectivity and CO conversion over Au/ZnO/γ-Al_2O_3 70

4.3.4 Effect of space velocity on product selectivity and CO conversion Au/ZnO/γ-Al_2O_3 72

4.3.5 Catalyst stability 74

4.3.6 Effect of the temperature on the equilibrium constant 75

4.4 Conclusion 81

CHAPTER 5 GENERAL CONCLUSIONS 84

REFERENCES 85

LIST OF FIGURES

CHAPTER 2

Figure 2.1 MeOH synthesis process flow diagram 15
Figure 2.2 The chemical structure of DME with hydrogen atoms in white, carbon atoms in black, and oxygen atoms in red..... 16
Figure 2.3 Schematic diagram of the DME two-step process..... 27
Figure 2.4 Schematic diagram of the one-step DME synthesis process 27
Figure 2.5 Illustration of the integrated DME synthesis process 28

CHAPTER 3

Figure 3.1 Schematic diagram showing the preparation of Au/ZnO/γ- Al_2O_3 bifunctional catalyst 32
Figure 3.2 Linear plot of the Brunauer-Emmett-Teller equation..... 36
Figure 3.3 Schematic diagram of the rig..... 38
Figure 3.4 Simplified scheme of the reactor 39
Figure 3.5 Six-way sampling valve..... 40
Figure 3.6 FID chromatograms of calibration gas 42
Figure 3.7 TCD chromatogram of calibration gas 43

CHAPTER 4

Figure 4.1 Simplified DME process 49
Figure 4.2 Effect of temperature on the CO equilibrium conversion at different pressures when the MeOH synthesis reaction (Equation 4.1) is the only reaction occurring in the reactor. The feed to the reactor is CO:H_2 = 1:2 54
Figure 4.3 (A) Equilibrium conversion of CO as a function of temperature in the combined DME–MeOH system at a range of pressures, and (B) comparison of the equilibrium CO conversion for the MeOH and MeOH–DME systems at a pressure of 40 bar 57

Figure 4.4 (A) Equilibrium MeOH selectivity as a function of temperature at different pressures, and (B) DME selectivity as a function of temperature at different pressures in the MOH–DME system 57
Figure 4.5 (A) Effect of temperature on equilibrium conversion of CO in the combined MeOH–DME–WGS system at different pressures, and (B) Comparison of the equilibrium conversion of CO as a function of temperature for the three cases (MeOH synthesis, combined MeOH–DME synthesis and combined MeOH–DME–WGS system) at 40bar 58
Figure 4.6 (A) Effect of temperature on MeOH selectivity, and (B) DME selectivity at different pressures in the combined MeOH–DME–WGS system 60
Figure 4.7 (A) Effect of temperature on H_2O selectivity, and (B) CO_2 selectivity at different pressures in the combined MeOH–DME–WGS system.....60
Figure 4.8 Effect of temperature and pressure on CO_2:H_2 ratio for the MeOH–DME–WGS system 61
Figure 4.9 (A) CO conversion as function of temperature in the MeOH–WGS system, and (B) Comparison of the MeOH, MeOH–DME, MeOH–DME–WGS and MeOH–WGS systems at 50bar.....62
Figure 4.10 Effect of temperature on the CO equilibrium conversion at different pressures when the MeOH synthesis reactions (4.1), DME synthesis (4.2), WGS reaction (4.3) and CH_4 synthesis (4.4) are simultaneously occurring in the reactor.....63
Figure 4.11(A) Effect of temperature on CO_2 selectivity, and (B) H_2O selectivity at different pressures in the combined MeOH–DME–WGS–CH_4 system.....63
Figure 4.11C Effect of temperature on CH_4 selectivity at different pressures in the combined MeOH–DME–WGS–CH4 system.....63
Figure 4.12 TEM results for the gold-based catalyst.....66
Figure 4.13 Selectivity of products as a function of temperature at a SV of 0.75 $dm^3.h^{-1}.g^{-1}$, and pressures of 20 bar (A) and 35 bar (B).....66
Figure 4.13C Selectivity of products as a function of temperature at a SV of 0.75 $dm^3.h^{-1}.g^{-1}$, and pressure of 50 bar.....66
Figure 4.14 CO conversion as a function of temperature at a SV of 0.75 $dm^3.h^{-1}.g^{-1}$, and pressures of 20, 35 and 50 bar 69
Figure 4.15 Selectivity of products as a function of pressure at a SV of 0.75 $dm^3.h^{-1}.g^{-1}$, and temperatures of 380^oC (A) and 420^oC (B).....70
Figure 4.15C Selectivity of products as a function of pressure at a SV of 0.75 $dm^3.h^{-1}.g^{-1}$, and temperature of 460^oC 70

Figure 4.16 Selectivity of products as a function of SV at a constant pressure of 50 bar and temperatures of 380^{o}C (A) and 420^{o}C (B) 72
Figure 4.17 Selectivity of products as a function of SV at a constant pressure of 50 bar and temperature of 460^{o}C 73
Figure 4.18 CO conversion as a function of SV at temperatures of 340, 380, 420 and 460^{o}C 73
Figure 4.19 CO conversion as a function of time on stream at 340 (A), 380 (B), 420 (C) and 460^{o}C (D) respectively 74
Figure 4.20 Theoretical Ln (Kp) function of temperature for the reactions 4.1 for MeOH; 4.2 for WGS; 4.3 for DME; and 4.4 for CH_4 formation 76
Figure 4.21 Calculated Ln (Kp) and experimental Ln (Kp) as a function of temperature at 35 bar and 0.75 $dm^3.h^{-1}.g^{-1}$, of the WGS reaction (A), DME formation (B), CH_4 formation (C) and MeOH synthesis (D) 77
Figure 4.22 Calculated Ln (Kp) and experimental Ln (Kp) as a function of temperature at 50 bar and 0.75 $dm^3h^{-1}g^{-1}$ for WGS reaction (A), DME formation (B), CH_4 formation (C), and MeOH synthesis (D) 78
Figure 4.23 Experimental DME selectivity (A) and theoretical DME selectivity (B) for the DME–MeOH–WGS system at different temperatures and pressures 79
Figure 4.24 Experimental MeOH selectivity (A) and theoretical MeOH selectivity (B) for the DME–MeOH–WGS system at different temperatures and pressures 80

LIST OF TABLES

CHAPTER 2

Table 2.1 Commercial MeOH synthesis catalysts [14] 14
Table 2.2 Properties of DME and MeOH [15] 18
Table 2.3 Properties of DME compared with those of diesel fuel, propane and butane [15, 20, 21] 19
Table 2.4 Conversions for MeOH, DME, and co-production MeOH-DME at 250°C and 52 bar [46, 74] 26

CHAPTER 3

Table 3.1 GC operating conditions (parameter and setting) 42
Table 3.2 Relative response factors for hydrocarbon products[4] 44

CHAPTER 4

Table 4.1 BET results 65

LIST OF SYMBOLS

Symbol	Designation	Units
A_j	Integrated area of the GC peak for component *j*	–
C_j	Concentration (molar percentage) of component *j*	–
Fj	Molar flowrate of component *j*	$mol.h^{-1}$
$G_{f,j,T}$	Gibbs free energy of formation of species *j* at *T*	$kJ.mol^{-1}$
$G_{rx,k,T}$	Gibbs free energy of reaction for reaction *k* at *T*	$kJ.mol^{-1}$
Ha	Heat of adsorption	$kJ.mol^{-1}$
Hc	Heat of condensation	$kJ.mol^{-1}$
$K_{p,k,T}$	Reaction equilibrium constant for reaction *k* at *T*	–
n	Carbon number	–
N	Total number of mole flowing out of the reactor	mol
N_j	Number of mole of component *j* in the product stream	mol
N_j^o	Number of mole of component *j* in the feed stream	mol
P	Pressure	bar
p_j	Partial pressure of component *j*	bar
p_o	Saturation pressure	bar
R	Molar gas constant	$J.mol^{-1}.K^{-1}$
T	Temperature	^oC or K
$RF_{j,k}$	Relative response factor of the component *j*	–
r_j	Rate of formation of product *j*	$mol.h^{-1}.g^{-1}$
y_j	Mole fraction of component *j*	–
γ_{jk}	Stoichiometric coefficient of component *j* in reaction *k*	–

ξ_k	Extent of reaction k	–
S_j	Percentage selectivity of component j in the product	–
V	volume	dm^3
X_{CO}	Percentage conversion of CO	–

LIST OF ACRONYMS

ATR	Autothermal reforming
BET	Brunnauer, Emmett and Teller
CTL	Coal-to-liquid
DME	Dimethyl ether
FID	Flame ionisation detector
FTIR	Fourier Transform Infrared spectroscopy
GC	Gas chromatograph
GTL	Gas-to-liquid
HRTEM	High-resolution transmission electron microscopy
ICP-AES	Inductively coupled plasma atomic emission spectroscopy
LPG	Low pressure gas
MeOH	Methanol
POX	Partial oxidation
ppb	Part per billion
SEM	Scanning emission microscopy
SMR	Steam methane reforming

STD	Synthesis gas-to-DME
SV	Space velocity
TCD	Thermal conductivity detector
TGA	Thermo-gravimetric Analysis
WGS	Water-gas shift
XPS	X-ray Photoelectron Spectroscopy
XRD	X-ray diffraction
XTL	(Synthesis gas , Coal, biomass) to liquid fuel

CHAPTER 1

INTRODUCTION

Energy consumption has increased dramatically in recent years all over the world, especially in developing countries such as China and South Africa. A great deal of research is being conducted to meet the rising demand for energy by developing new and more sustainable technologies that use available raw materials like coal, natural gas or biomass instead of petroleum. Synthesis gas produced from these potential energy sources can be converted into useful hydrocarbons and oxygenates with high calorific energy content. Well-known examples of technologies that convert synthesis gas to liquid fuel are the Fisher-Tropsch and methanol synthesis processes. These produce fuel containing fewer pollutants than that obtained from the traditional methods using petroleum. This is an advantage, because the 'cleaner' the fuel is, the less damage it can do to the environment.

A number of catalysts have proved effective in the conversion of synthesis gas to liquid fuel. Cobalt- and iron-based catalysts are extensively used in the Fisher-Tropsch process, while copper-based catalysts are used for methanol synthesis. The latter is an important intermediate step in the manufacture of petrochemical and chemical products.

The research described in this dissertation focuses on the synthesis of dimethyl ether (DME) and light hydrocarbons from synthesis gas using gold-based catalysts. The paragraphs below set out the content of the chapters that follow.

Chapter 2 contains a review of the historical background of the production of DME in terms of the literature published on the subject. It introduces some important concepts concerning catalysis by gold, specifies the preparation methods required for gold

catalysts, and identifies the factors that affect catalysis by gold. Methanol synthesis, which is an essential first step in the DME synthesis process, is explained in greater detail. This chapter also introduces relevant aspects of DME such as its properties, synthesis, catalysts and process. Thereafter we resume the literature review. The final section sets out the objectives of this study.

Chapter 3 introduces the experimental component of the investigation. We describe the material and methods used, and outline how the catalyst samples were prepared and analysed. We explain the experimental protocol and the data generation and processing procedures.

Chapter 4 deals with the findings on thermodynamic calculations concerning the DME synthesis process. We investigate different scenarios for the reactions of methanol synthesis, dimethyl ether formation, water gas shift reaction and methane synthesis in order to determine which design for a DME synthesis process is most effective, and to predict the optimal operating conditions in the reactor. It also comprises our report on the experimental investigation into synthesis gas conversion to DME using gold-based catalysts. We discuss the effect of pressure, temperature and space velocity on the synthesis gas conversion, the selectivities and the catalyst deactivation.

Chapter 5 concludes the dissertation by summarising the findings of this research project.

CHAPTER 2

LITERATURE REVIEW

2.1 Introduction

Almost 90% of industrial chemical processes are based on catalysis[1, 2], which initiates or alters the rate of a chemical reaction. The estimated value of catalyst-based processes used in commercially manufactured products across the world is $900 billion a year.[2] The most commonly-used catalysts, which are applied in such divergent fields as manufacturing, pharmaceutical and environmental conservation processes, are heterogeneous. The growing need for catalysts that are more active and environmentally friendly is particularly acute in the area of energy generation and transformation, and has prompted a great deal of research into the subject. Of the many materials available for use as catalysts, gold has recently attracted attention because of its interesting catalytic properties when it is reduced to nano size.

In this chapter we review some of the concepts governing supported catalysts, with a particular emphasis on supported gold catalysts. We also explain some of the basic requirements of MeOH synthesis, such as mechanism of MeOH formation, the preparation of MeOH catalysts and the process itself, to provide a context for DME synthesis. This is followed by an extended section on DME that ranges from its important properties as an alternative fuel to the technology/chemistry of its production. We also give an overview of the raw materials and catalysts for DME to show the multiple sources that can be used for its manufacture.

2.2. Supported catalysts

When a metal that is catalytically active is dispersed on a porous material, it forms a catalyst that is said to be supported because the material on which the metal is deposited plays a secondary role.[3] The most common catalyst supports used in industry are aluminosilicates, aluminium oxides, ceramics, silica gel, MgO, TiO_2, ZrO_2, activated carbon and zeolites.[3]

It is essential to support a catalyst in order to reduce the cost of the regeneration process and that of the active metal, which is usually expensive. Another reason for using a support is that it improves the physicochemical properties of the catalyst (activity and selectivity) and its mechanical strength.

A good support stabilizes the active metal, and is able to increase the specific surface area (its most important role). It also assists the formation, fixation and dispersion of the active metal. In many cases catalytic activity rises with an increase in the catalyst surface area, although often the opposite occurs for selectivity. For hydrogenation and reactions involving the activation of hydrogen, such as hydrodesulphurization and hydrodenitrogenation, it is good practice to use supports with a high surface area. On the other hand, selective oxidations (such as olefin epoxidation) require lower surface areas to prevent undesirable reactions. [5]

It is very important to choose a support suitable for the specific metal used, because the rate of reaction depends on the type of support. Another consideration to be borne in mind is that the support material chosen must maintain its stability under the operating conditions in the reactor (like temperature, pressure and flow of fluid). If the catalyst is used in a liquid phase, the support must be inert in the solvent. The support loading and

the support size are also determined by the requirements of the process. Pellet supports are indicated in gas and liquid continuous processes, but powders are often used in batch liquid phase systems.

The support can also play a significant role in delaying catalyst deactivation by sintering because of its interactions with the active metal. These include electronic effects, the formation of new phases at the boundary surface, van der Waals forces and the formation of reduced support species on the metal surface. [2, 5]

The supported catalysts most frequently used in industry are small metal particles bonded on a support with a large surface area between 10–1000 m^2 per gram of catalyst, which allows the catalytic reaction to occur at the surface of the metal particles. The particle size of the metal can be expressed by the diameter of the metal particles, the area of the metal surface and the dispersion, which is defined as the fraction of all metal atoms present at the surface. A catalyst consists of porous material that contains micro pores (with a diameter of 1 nm or less) or macro pores (with a diameter of 100 nm or more) of undefined shape. Macro pores are formed as cracks between crystallites, while micro pores are formed by the roughness of the surface.[4] Porous materials with pores in the 1-100 range are called mesocatalysts.

2.2.1 Methods of catalyst preparation

The properties of heterogeneous catalysts depend on the method employed in preparing the support and subsequent treatments, such as heat and catalyst activation. The preparation of supported metal and oxide catalysts follows the sequence: precipitation or co-precipitation or impregnation; drying; calcination; and activation. [3]

a) Precipitation and co-precipitation

The precipitation method consists of mixing one solution containing the active metal with another solution, or a suspension containing the metal support. The solid obtained is washed and filtered (or filtered and washed) several times before being dried, calcined and crushed (if necessary to a fine powder). The catalyst can be designed so as to take on its definitive form before or after calcination. When the solid is being filtered for industrial purposes, the designer has to take precautions to prevent blockages, because a blocked filter will slow down the manufacturing process. The precipitation process is influenced by the rate of mixing solutions, the pH and the maturation of precipitate.[5]

i) Mechanism of precipitation

Nucleation and growth are taking place during precipitation. Nucleation occurs at high super-saturation that is when the solubility product of ions in solution is very high compared with the initial solubility constant of the solids in solution. Growth of the precipitate occurs as it approaches equilibrium conditions.

ii) Effect of common ions on precipitation

The composition of the precipitate is influenced by the nature of the ions contained in the solution. In a system containing the same anions or cations, the solids obtained do not have the same composition because of changes in the properties of solution over time resulting from the different dispersion of the precipitate. [2-5]

iii) Precipitation procedure

A prepared solution containing an active metal is added drop-wise to the precipitating solution, or vice versa. Fine precipitates are formed because the low solubility constant leads to high super-saturation. Ideally, the solution should be kept homogeneous to allow the metal and the support to precipitate simultaneously. However, it is difficult to control the precipitation process because of variations in pH and diffusion problems that occur during precipitation.

b) Deposition-precipitation

Deposition-precipitation consists of deposing an active metal (for instance Ni) onto a support (like SiO_2) in suspension in the precipitating solution (such as Ni $(NO_3)_2$). The progressive addition of a precipitating agent such as urea raises the pH of the solution, which becomes supersaturated. This makes it possible for the nucleation process to occur at the interface between the liquid and the support. Constant stirring is recommended in order to ensure that the pH remains uniform throughout the solution, and that the homogeneity of the composition and the texture of the precipitate are maintained. The deposition-precipitation technique applicable to gold requires the ageing of an aqueous solution of $HAuCl_4$ (pH 6-10) in the presence of a metal oxide support. [2-4]

c) Impregnation

In the impregnation technique, the pores of the support are filled with an active metal when a solution of a metal salt is sprayed onto it. The phenomenon called incipient wetness can be observed when the pores are filled by the solution, after which the

outside becomes wet. Interactions between the support and the metal can lead to an excellent catalytic dispersion of the metal over the support. [3]

The metal salt can be deposited homogeneously throughout the porous support, or concentrated near the outside. The distribution of the metal is controlled by either the pH or the addition of chelating agents to the impregnation liquid.

2.2.2 Preparation of highly-dispersed gold catalysts

Conventional Au catalysts are prepared by the impregnation method. This consists of immersing a metal oxide support in a solution of $HAuCl_4$, and then removing the water by drying to disperse $HAuCl_4$ crystallites on the support. The precursor is then calcined in air at a temperature above 200^{o}C, and activated by reduction in flowing hydrogen. This technique leads to Au particle sizes larger than 30 nm that are not well dispersed on the surface support.[6] This can be contrasted with the calcination and reduction of platinum group metals, which results in a high dispersion on the support. The reason for the difference is that the dispersion of gold nanoparticles on the support demands strong interaction between the gold and the support. Good dispersion is obtained when the precursor is prepared by co-precipitation of the gold hydroxide and the metal support. Calcination in air between 573-673K of the mixed precursor produces gold particles that bind on the metal oxide.[6]

The catalytic properties of gold vary with the catalyst preparation method used,[7] which dictate the size and structure of the gold deposited on the support. Au/Fe, Au/Al_2O_3, Au/ZnO, and Au/TiO_2 are examples of effective gold-based catalysts prepared by co-precipitation and deposition-precipitation methods. During the preparation procedure, gold tetrachloride anion is transformed into a gold hydroxide precursor before being

mixed with the hydroxide of a metal (co-precipitation) or deposited on a metal oxide support (deposition-precipitation).[8] For example, gold supported on ZnO is prepared by co-precipitation from a solution consisting of a mixture of $HAuCl_4$ and Zn $(NO_3)_2$, following the procedure of deposition-precipitation.[7] Precipitated wet metal hydroxides M.OH are obtained by hydrolysis of the corresponding nitrates (M = Fe, Mn, Ni, Co, Ce, Zn, Mg, Cu, La and so on) or alkoxides (M = Ti) with an aqueous solution of H_2O, NH_4OH or Na_2CO_3.

Another method of preparing very active gold catalysts is to use phosphine complexes. This method shows the effect that the nature of the support has on the activity of the catalyst. When phosphine complexes, such as $AuPPh_3NO_3$ or $[Au_9(PPh_3)_8](NO_3)_3$, are added to a metal hydroxide, the gold catalyst shows a higher activity for CO oxidation than when it is prepared using metal oxide as a support. The morphology and the specific surface area also play a significant role in catalysis. Their effect can be predicted by characterization studies of the support using scanning emission microscopy (SEM), thermo-gravimetric analysis (TGA), x-ray diffraction (XRD), x-ray photoelectron spectroscopy (XPS) and fourier transform infrared spectroscopy (FTIR). The results obtained from catalysts using commercial supports provide evidence that the CO oxidation activity increases with a suitable type of catalyst and a larger surface area. [9-10]

2.2.3 Factors that affect gold catalysis

The catalytic properties of gold depend on the contact structure, support selection, and particle size,[6, 7] whereas the activity of gold-supported catalysts are influenced by the dispersion of the metal and the interaction between metal and support.[9, 10] It is difficult

to disperse gold on the support during the preparation process owing to the risk of agglomeration inherent in the low melting-point of this metal.[9] Agglomeration of the gold can lead to the deactivation of the catalyst. Another factor to be borne in mind is that the preparation method used can lead to a specific range of sizes in the gold catalyst particles.

Dispersed Au particles on oxide surfaces are obtained by:

1. choosing a suitable support leading to a specific morphology and range of sizes (such as Au complexes as precursors);[11]

2. using precipitated wet metal hydroxides as precursors for oxide supports, which have many surface OH groups reactive to the Au complexes; and

3. transforming both precursors to gold particles and oxides simultaneously under their chemical interactions by temperature-programmed calcinations.[9, 12]

Many authors have reported that gold-supported catalysts are widely used for CO oxidation, ethyne hydrochlorination,[10] selective oxidation of alcohol,[7] water-gas shift and hydrogenation processes.[1, 13]

2.3 MeOH synthesis

Originally, MeOH was produced by burning wood and condensing the resultant vapour. In ancient Egypt its properties were used to embalm the dead. In 1660, Robert Boyle isolated MeOH, and in 1860 a French scientist named Eugène Marcelin Berthelot synthesised MeOH. It was only in around 1923 that synthesis of MeOH from synthesis gas (CO and H_2) began to be practised on large scale in Germany by BASF.[3] This was a high-pressure (250–350 bar) synthesis process using a ZnO/Cr_2O_3 catalyst and

operating at 350–400°C. Much later (in 1966) ICI and Lurgi developed a more active $CuO/ZnO/Al_2O_3$ catalyst that was effective at 220–300°C and 50–100 bar (a low-pressure process). Currently the low-pressure synthesis process operates at maximum efficiency at 80–100 bar using low-temperature copper-based catalysts.[14, 15]

Many sources have reported that MeOH synthesis occurs via the combined reactions described below in Equations 2.1 and 2.2. However, some scientists noted the effect of CO_2 on the MeOH synthesis process because of the excess H_2 consumption that took place during the process of converting synthesis gas to MeOH when CO_2 was present in the feed. This led to the postulation that there may be another, third, reaction, as shown in Equation 2.3, which takes place in the MeOH synthesis process.

MeOH formation

$$CO + 2H_2 \leftrightarrow CH_3OH \quad \Delta H_{298K} = -92\ kJ.mol^{-1} \tag{2.1}$$

Reverse water-gas shift

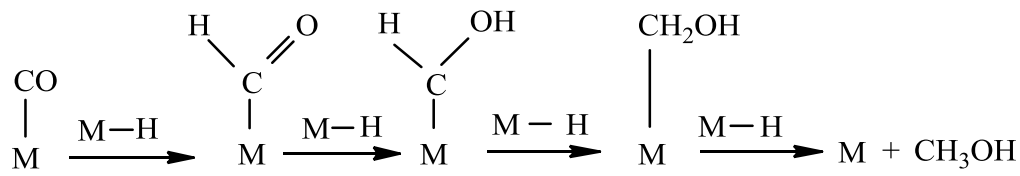
$$CO_2 + H_2 \leftrightarrow CO + H_2O \quad \Delta H_{298K} = +41.3\ kJ.mol^{-1} \tag{2.2}$$

Carbon dioxide hydrogenation

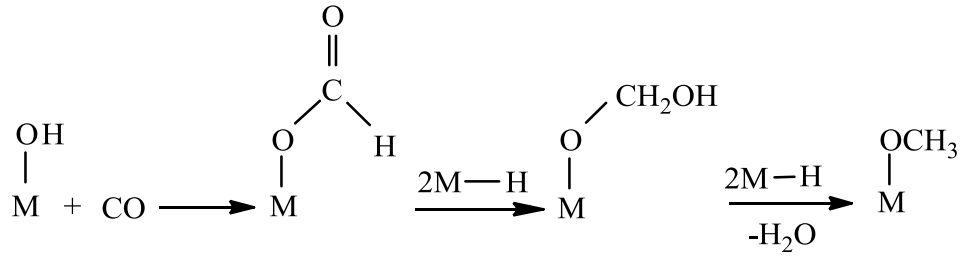
$$CO_2 + 3H_2 \leftrightarrow CH_3OH + H_2O \quad \Delta H_{298K} = -50\ kJ.mol^{-1} \tag{2.3}$$

The mechanism of MeOH synthesis is still not very well understood. There are two controversial theories that attempt to explain the origin of the carbon contained in the MeOH structure (CH_3OH), and to determine whether carbon comes from CO or CO_2 hydrogenation.[16]

First it was assumed that CO is adsorbed on the surface of the catalyst and then reacts with dissociated hydrogen on copper active sites in successive hydrogenation steps until MeOH is formed (Equation 2.4). The second approach (represented in Equation 2.5) posits that CO reacts with OH to give formate, after which hydrogenation and dehydration in succession lead to a surface methoxyl group and then to MeOH formation. This theory is supported by the fact that formate ions are created when CO reacts with a strong basic component (such as ZnO) contained in the MeOH catalyst, after which the copper in the active site allows the hydrogenation of formate to MeOH. [3]



(2.4)

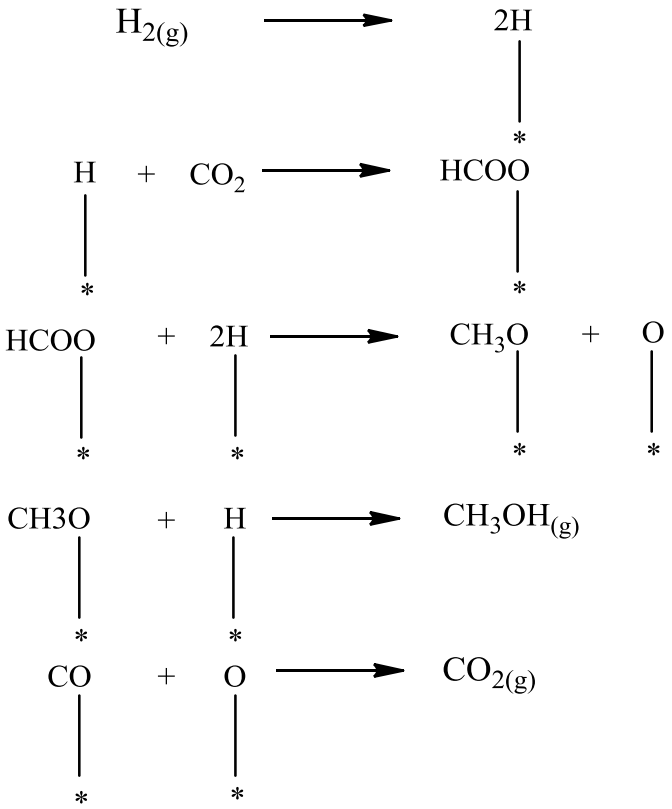




(2.5)

However, studies on the origin of C in MeOH that apply isotopic labelling methods provide strong evidence that C is the result of CO_2 (Equation 2.6). CO is combined with the oxygen present on the catalyst surface to give CO_2. Also, scientists have observed that when MeOH is produced from H_2 and CO, the reaction rate is around 100 times slower than when CO_2 is co-fed. Further CO_2 and H_2 are produced from CO via the reverse water-gas shift (WGS) reaction. Spectroscopic investigations of elementary

steps of MeOH show that the most abundant species present on the Cu surface are formate, methoxide, formyl, and carbonates. ZnO does not play a specific role in the catalyst. Nevertheless, supports and promoters play a significant role because they control the rate of reaction of CO and CO_2.[3, 13-14] For example, when a Cu/Zr catalyst is used, the rate of reaction of CO is half the rate of CO_2, while on a Cu/ZnO catalyst the rate of CO is only slightly slower than that of CO_2.



(2.6)

Most of the MeOH catalysts used in industry are copper-based, among them Cu/Zn/Al, Cu/Zn/Cr and Cu/Zn/Zr.[17] Table 2.1 shows some of the formulations of commercial MeOH synthesis catalysts that have been published.

Table 2.1 Commercial MeOH synthesis catalysts [14]

Manufacturer	Cu at %	Zn at %	Al at %	Other	Patent date
IFP	45–70	15–35	4–20	Zn-2-18	1987
ICI	20–35	15–50	4–20	Mg	1965
BASF	38.5	48.8	12.9	–	1978
Shell	71	24	–	Rare Earth oxide-5	1973
Sud Chemie	65	22	12	–	1987
Dupont	50	19	31	–	–
United Catalyst	62	21	17	–	–
Haldor Topsoe MK-121	>55	21–25	8–10	–	–

MeOH is currently produced from synthesis gas over a copper-based catalyst using the low-process technology (220–300^{o}C and 50–100 bar). [13-14] Natural gas is converted into synthesis gas during the reforming step, which involves either steam methane reforming (SMR) or autothermal reforming (ATR), after which the resultant gas is fed into the MeOH reactor. A distillation and cooling system separates the MeOH produced from the unreacted synthesis gas, by-products and water. The MeOH is removed, and the synthesis gas is sent back to the feed of the reactor via a recycle loop. The overall CO conversion can reach 99%. The operating temperature is maintained at under 300^{o}C, as already indicated, to reduce the risk of catalyst sintering.

A typical MeOH synthesis flow diagram is illustrated in Figure 2.1.

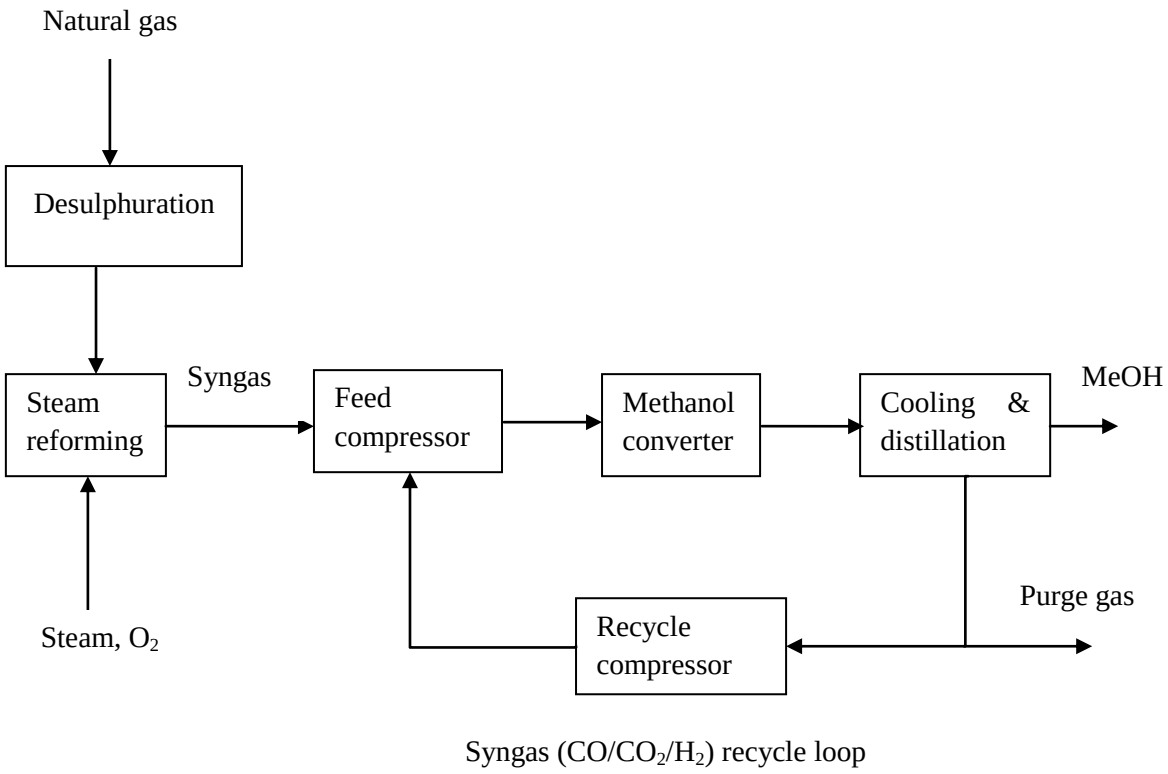


Figure 2.1 MeOH synthesis process flow diagram

2.4 Water-gas shift reaction

The reverse water-gas shift reaction (RWGS) (Equation 2.2) plays an important role in MeOH and DME synthesis. Researchers have observed that the rate of MeOH synthesis is much higher when MeOH is produced from a mixture of $CO/CO_2/H_2$ than when the feed contains CO and H_2 only. The WGS reaction leads to the production of CO_2 and H_2 in the methanol synthesis, while it contributes to the synergy effect when DME is produced directly from synthesis gas. In the MeOH and DME processes a low-temperature copper-based catalyst is used to catalyze both the MeOH synthesis and the WGS reactions. The low-temperature process overcomes the equilibrium limitations of

the WGS reaction and MeOH synthesis. However, under these conditions the catalyst is more sensitive to poisoning by sulphur and other impurities that may be present in the feed stream.

2.5 Dimethyl ether synthesis

DME synthesis is a combination of the MeOH synthesis reactions (Equations 2.1 and 2.3), the WGS reaction (reverse of Equation 2.2) and the MeOH dehydration reaction (Equation 2.7).

$$2CH_3OH \leftrightarrow CH_3OCH_3 + H_2O \qquad \Delta H_{298K} = -23.0\ kJ.mol^{-1} \tag{2.7}$$

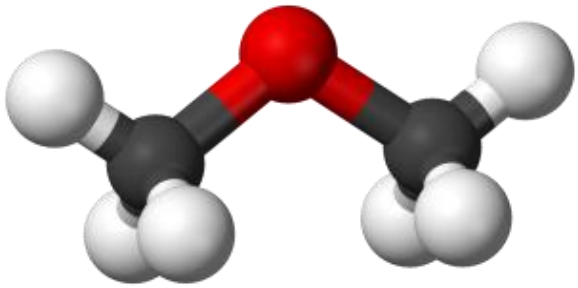


Figure 2.2 The chemical structure of DME with hydrogen atoms in white, carbon atoms in black, and oxygen atoms in red

Figure 2.2 shows the structure of DME. Its physical properties are summarized in Tables 2.2 and 2.3. The latter Table shows that DME possesses physical properties similar to those of some transportation gases such as propane and butane, which are easily liquefied.[15, 18, 19] The DME cetane number is high: greater than that of methane, propane and MeOH, but similar to that of diesel.[20, 21] Furthermore, because the DME autoignition temperature is low (350^{o}C), DME is suitable for use in a diesel engine, and is recommended for cold-starting engines.[22] Its high flammability limit (3.4–17%) also

ensures that DME is safe to use. Its oxygen content is low (35 %) compared with that of MeOH (50%) (as shown in Table 1.2), and it contains no sulphur; and emits less smoke and NO_x on combustion, and fewer hydrocarbons than LPG and conventional diesel fuel.[23, 24]. The energy content of DME is higher than that of MeOH, and the former can be handled and stored using the same technology as is applicable to low-pressure gas (LPG).[20, 25, 26] There is one difference in that more attention has to be paid to avoiding leakage of DME, as its density is lower than that of diesel, falling between that of propane and butane. It is non-toxic (for example when used as a propellant in an aerosol);[27, 28] DME can also be used in fuel cells and gas turbines, and to generate power in combined cycle plants. Further, it is an intermediate in the production of dimethyl sulphate, methyl acetate, light olefins and high-value oxygenated compounds.[29]

Depending on the operating conditions and the catalysts, the formation of hydrocarbons (paraffins and olefins) can occur as follows:

$$CO + 3H_2 \leftrightarrow CH_4 + H_2O \quad (2.8)$$

$$CH_3OCH_3 \rightarrow Hydrocarbons + H_2O \quad (2.9)$$

$$n\,CO + 2n\,H_2 \leftrightarrow C_nH_{2n} + n\,H_2O \quad (2.10)$$

$$n\,CO + (2n+1)H_2 \leftrightarrow C_nH_{2n+2} + n\,H_2O, (n = 1, 2\ldots) \quad (2.11).$$

Table 2.2 Properties of DME and MeOH [15]

Properties	**MeOH**	**DME**
Chemical formula	CH_3OH	CH_3OCH_3
Molecular weight	32.04	46.07
Carbon content (%)	37.5	52
Hydrogen content (%)	12.5	13
Oxygen content (%)	50	35
Melting point (^oC)	-97.6	-138.5
Boiling point (^oC)	64.6	-25
Density at 20^oC (Kg m^{-3})	971	668
Energy content (kcal kg^{-1})	5420	6880
Energy content (kcal mol^{-1})	173.6	317
Energy of vaporization (kcal mol^{-1})	9.2	55-60
Flash point (^oC)	11	-41
Auto ignition temperature (^oC)	455	350
Explosive limit in air (%)	7-36	3.4-17

Table 2.3 Properties of DME compared with those of diesel fuel, propane and butane [15, 20, 21]

Properties	**DME**	**Diesel**	**Propane**	**Butane**
Boiling point (^{o}C)	-25	180–360	-42.1	-0.5
Vapour pressure at 20^{o}C(bar)	5.1	–	8.4	2.1
Liquid density at 20^{o}C (kg m^{-3})	668	840–890	501	610
Heating value (kcal kg^{-1})	6 880	10 150	11 090	10 920
Cetane number	55–60	40–55	5	–
Autoignition temperature (^{o}C)	350	200–300	470	–
Flammability limits in air (vol. %)	3.4–17	0.6–6.5	2.1–9.4	1.9–8.4

2.5.1 Catalysts for DME synthesis

A survey of MeOH dehydration catalysts reveals that the original method of producing DME was to heat MeOH with a strong acid such as H_2SO_4. This process was found to have many disadvantages. It was toxic, and therefore represented an environmental hazard; it made catalyst recovery difficult; and it was expensive. The use of strong acid was abandoned in favour of solid acid catalysts. Dehydration catalysts such as γ-Al_2O_3, zeolites, Amberlyst 35, heteropolyacids and mesoporous aluminosilicate have been

tested and proved to be effective.[20] The varieties of γ-Al_2O_3 and H-ZSM are the most commonly used in academic and industrial contexts at present.

The conventional production route for DME is via dehydration of MeOH over an acidic catalyst, such H-ZSM-5 and γ-Al_2O_3.[30] As previously noted, the process occurs in two stages, using different reactors and catalysts. Copper-based catalysts are used in the first reactor for MeOH synthesis, and H-ZSM-5 and γ-Al_2O_3 commonly provide the catalysts for MeOH dehydration in the second reactor.[31, 32]

The bifunctional catalyst used in the direct process, synthesis gas-to-DME (STD), is made by a physical mixture of CuO/ZnO/Al_2O_3 (MeOH synthesis catalyst) and H-ZSM-5 (MeOH dehydration catalyst), which combine high activity in the metallic function and a suitable level of acidity for the acidic sites.[33] H-ZSM-5 reduces the side reactions attendant on the transformation of MeOH and DME into hydrocarbons. The latter which eventually deposit on the catalyst as coke, and deactivate it.[29, 34, 35]

While H-ZSM-5 possesses Bronsted acidity and is not sensitive to water, γ-Al_2O_3 has Lewis acidity. The lower deactivation of H-ZSM-5 in the presence of water may indicate the different roles of Bronsted and Lewis acid sites in the reaction.[36]

Studies of the zeolites NaZSM and H-ZSM-5 revealed that when the ratio Si/Al decreases, the acid strength of ZSM-5 increases, leading to a change in rate of MeOH dehydration. Furthermore, the results elicited from a comparative study on other dehydration catalysts, such as γ-alumina, H-ZSM-5, tungsten-zirconia and sulphated-zirconia, confirmed that the rate of DME formation in direct synthesis is a function of the acid strength and the number of acid sites of the dehydration catalyst.[37] A less acidic zeolite results in a lower activity of MeOH dehydration, whereas a more acidic

one leads to an interaction between the MeOH catalyst ($CuO/ZnO/Al_2O_3$) and the zeolite, and partial conversion of the DME to hydrocarbons.[37, 38] Therefore weak and medium acidic sites favour the dehydration of MeOH to DME, while strong acidic sites allow the formation of by-products.[39, 40]

Recently Liu *et al*. (2010) prepared and tested a new type of catalyst adapted to application in a slurry reactor. The slurry catalyst, which contained a crystal phase AlO(OH) that was used for dehydration of MeOH to DME, exhibited good stability and performed better than the traditional commercial catalyst γ-Al_2O_3.[39]

Research on the co-production of MeOH/DME revealed that the use of gold, supported by ZnO, as a MeOH synthesis catalyst combined with γ-Al_2O_3 for dehydration of MeOH, led to the production of hydrocarbons. Gold-based catalysts also showed low selectivity for hydrocarbons and greater stability at high temperatures than the commercial hybrid copper-based catalyst used to convert synthesis gas into hydrocarbons. The selectivity of DME was much higher when γ-Al_2O_3/Au/ZnO was used rather than zeolite-Y/Au/ZnO.[41, 42]

2.5.2 DME formation mechanism

The proposed DME synthesis mechanism is: [30, 32]

- MeOH synthesis:

  $CO + s1 \rightarrow COs1$

  $H_2 + s2 \rightarrow 2Hs2$

  $COs1 + Hs2 \rightarrow HCOs1 + s2$

  $HCOs1 + Hs2 \rightarrow H_2COs1$

$$H_2COs1 + Hs2 \rightarrow H_3COs1$$

$$H_3COs1 + Hs2 \rightarrow CH_3OH + s1 + s2,$$

where s1 and s2 are two different active sites.

- MeOH dehydration:

$$CH_3OH\ (g) \rightarrow CH_3OH\ (a)$$

$$O + CH_3OH\ (a) \rightarrow CH_3O\ (a) + OH$$

$$CH_3OH\ (a) + CH_3O\ (a) \rightarrow CH_3OH\ (g) + OH$$

$$CH_3O\ (a) + CH_3O\ (a) \rightarrow CH_3OCH_3\ (g) + O$$

$$2OH \rightarrow H_2O\ (g) + O,$$

where O is a surface oxide which is assumed to cover the surface, and 'a' may be either acidic or basic sites.

The mechanisms of MeOH formation and dehydration make it possible to deduce that H_3COs1 and CH_3OH (a) or CH_3O can react and increase the rate of DME production. Because the dispersion of oxides in the hybrid catalyst improves the activity of the catalyst by bringing the oxides of the catalyst closer to each other, a better dispersion is obtained by using the co-precipitation method for catalyst preparation. [22-23]

2.5.3 Raw materials used for DME synthesis

In the early stages of its development, DME was a by-product of MeOH synthesis. Currently DME is produced by the dehydration of MeOH from synthesis gas, which can be made from a multiplicity of raw materials, such as natural gas, coal, oil residue, petroleum coke, biomass and wastes.[21, 43]

The technologies that have been developed for the production of synthesis gas from methane are the steam reforming of methane; the partial oxidation of methane; autothermal reforming; a combination of steam reforming with partial oxidation (two-step reforming); and CO_2 reforming of methane.[44]

In steam methane reforming (SMR), methane and steam are converted to hydrogen and carbon monoxide over a catalyst, for instance, Ni at 800^{o}C (Equation 2.8). The SMR process is endothermic, while partial oxidation (POX) is an exothermic and non-catalysed process in which methane reacts with oxygen to produce synthesis gas (Equation 2.9). The compositions of synthesis gas mixtures resulting from SMR and POX differ: steam reforming leads to a much higher H_2 : CO ratio than is found in synthesis gas produced through partial oxidation. Despite their dissimilarity, both technologies are suitable for gas-to-liquid applications. Autothermal reforming (ATR) combines steam methane reforming and partial oxidation in one reactor, while endothermic reforming reactions are assisted by the combustion of a portion of the feed hydrocarbons.[45, 46]

Equations 2.12 to 2.15 describe the major reactions involved in each process, but the actual reactions are more complex than those shown below.

Steam reforming

$$CH_4 + H_2O \leftrightarrow CO + 3H_2 \qquad \Delta H_{298K} = +206\ kJ.mol^{-1} \tag{2.12}$$

Partial oxidation

$$CH_4 + \tfrac{1}{2}O \rightarrow CO + 2H_2 \qquad \Delta H_{298K} = -36\ kJ.mol^{-1} \tag{2.13}$$

CO_2 reforming

$$CH_4 + CO_2 \leftrightarrow CO + 2H_2 \qquad \Delta H_{298K} = +247\ kJ.mol^{-1} \tag{2.14}$$

Reforming (Equations 2.12 and 2.14) and partial oxidation (Equation 2.13) are used to produce synthesis gas from biomass and methane. Gasification (Equation 2.15) is used to produce synthesis gas from coal, petroleum coke and oil residue.

Coal gasification

$$C + H_2O \leftrightarrow CO + H_2 \qquad \Delta H_{298K} = +131.3\ kJ.mol^{-1} \tag{2.15}$$

The production of DME from coal at a mine site offers certain advantages. These include the possibility of using low-quality coal or lignite coal; a reduction in the cost of transportation and the cleaning step, as coal can be used directly at the source; and a lower environmental impact because no ash disposal treatment and desulphurisation are required. DME also provides a highly-efficient means of producing electricity.[21]

2.5.4 Synthesis gas-to-DME (STD) process reactors

Because DME synthesis involves reactions that are exothermic, it is essential to control the operating temperature in the reactor so as to achieve higher conversion and avoid damaging the catalyst.[47]

Most of the reactors commonly used for DME synthesis are of the fixed-bed type. This is a simple reactor design which offers the dual advantages of requiring lower loading of the bifunctional catalyst, and achieving higher conversion, which in turn reduces the need for recycling. The greatest disadvantage in the operation of a fixed-bed reactor is the difficulty of controlling the temperature to prevent hot spots.[36]

The proposed slurry phase reactor offers a greater control of the temperature. The heat generated by the reactions is absorbed by the solvent, which has a high heat capacity.[48] Moreover, there is no temperature gradient within the reactor and diffusion limitations are reduced.[49] This type of reactor affords lower catalyst loading than the fixed-bed reactor, and provides good mixing and excellent heat removal.[23] On the other hand, the slurry reactor has a complex design and is difficult to operate because of the three phases in the system (catalyst, solvent and gas). Also, the catalyst is vulnerable to attrition, which reduces its mechanical strength and active life.

The slurry consists of the suspension in a solvent of fine catalyst particles that possess different active sites for MeOH synthesis and dehydration, and water-shift reaction. The shape and the strength of the catalyst are not limited by the same restrictions as in the fixed-bed reactor.[19, 21]

The fluidized bed reactor can operate within a large range of temperatures, and can overcome diffusion limitation problems,[50, 51] so it is regarded as an ideal reactor for DME synthesis. Recently Vakilia *et al.* investigated the direct production of DME from synthesis gas in a heat-exchanger reactor, in which endothermic and exothermic reactions are combined. One side of the reactor produces heat by the dehydrogenation of cyclohexane to benzene, after which the synthesis of DME proceeds on the other side.[52] These researchers found that the conversion was much higher than that achieved in a fixed-bed reactor. .

2.5.5 DME process technologies

As described earlier, the conversion of synthesis gas to DME can be done in two steps (the indirect process) or in one step (the direct process). The indirect process involves

the production of DME using two separate reactors for MeOH synthesis and for the dehydration step. Synthesis gas is first converted into MeOH over a MeOH catalyst, and then MeOH is converted into DME over an acidic catalyst in a second reactor. This process is associated with a relatively low conversion because of the equilibrium limitations of MeOH. This in turn increases the cost of the equipment required for the overall process.[53, 54]

In the single-step process a hybrid catalyst can be used. There is a synergy between reactions 2.1, 2.2 and 2.7 which allows a higher MeOH conversion to be achieved in the direct process than in the indirect version described above.[36, 55] MeOH from reaction 1 is converted into DME and water, after which the water reacts with CO in reaction 2.2 and shifts reaction 2.7 to the right. Hydrogen produced in the WGS reverse reaction 2.2 favours reaction 2.1 (shifts to the right), leading to further MeOH formation.[56-58]

Table 2.4 allows a comparison of published experimental results to be made of the per-pass and total CO conversion in the synthesis of MeOH, DME and MeOH-DME co-production over a catalyst containing CuO-ZnO-Al2O3 and γ-alumina-supported copper. [46, 74] It shows that the CO conversion is increasing in this order MeOH synthesis < MeOH –DME synthesis < DME synthesis.

Table 2. 4 Conversions for MeOH, DME, and co-production MeOH-DME at 250^{o}C and 52 bar [46, 74]

Conversion	**MeOH**	**DME**	**MeOH-DME**
Per-pass (%)	14	50	18
Total (%)	77	95	85

Lurgi, MGC, Udhe and Toyo Engineering have developed the two-step processes for DME synthesis (Figure 2.3). One-step technologies, which are illustrated schematically in Figure 2.4, have been licensed by JFE Holdings, Korea Gas Corporation, and Haldor Topsoe, and a liquid phase technology for direct synthesis of DME from synthesis gas has been designed by Air Products.[59, 60]

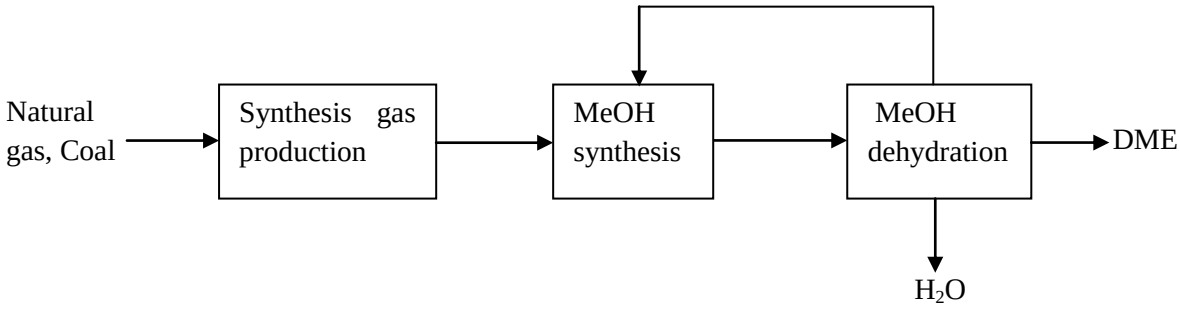


Figure 2.3 Schematic diagram of the DME two-step process

In the direct process the cost of MeOH separation and transportation are eliminated, since the synthesis of DME occurs in one reactor without removing MeOH to dehydrate it. Moreover, in this process the thermodynamic limitation of conversion in MeOH synthesis is overcome, as the MeOH produced is directly converted into DME.[53]

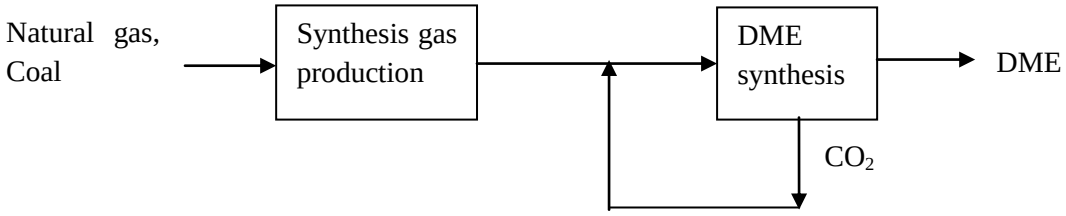


Figure 2.4 Schematic diagram of the one-step DME synthesis process

The integrated approach (Figure 2.5) is a combined system in which synthesis gas and DME production units are interrelated in a loop. CO_2 from DME synthesis is sent back to the synthesis gas generation unit. This new design makes better heat management

possible, and reduces both CO_2 emission and the costs involved in capturing and storing CO_2 by reusing it for CO_2 reforming.[49]

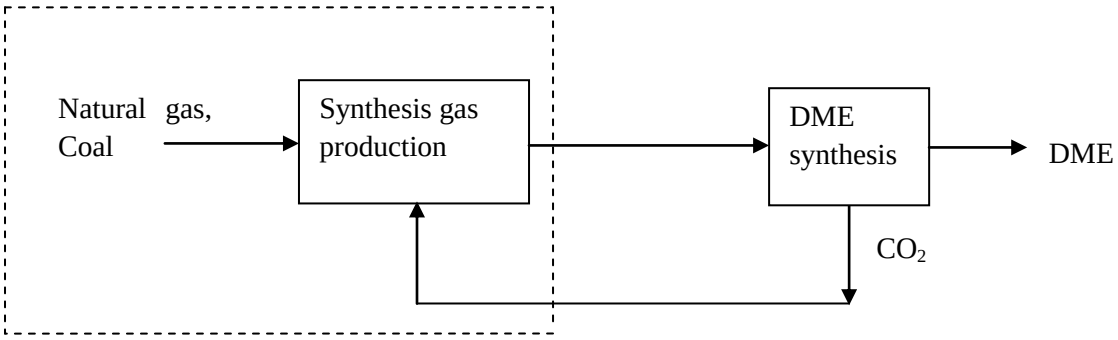


Figure 2.5 Illustration of the integrated DME synthesis process

2.5.6 Catalyst deactivation

As the main reactions involved in converting synthesis gas to DME are exothermic, it is desirable to operate the reactor at low temperatures to avoid the deactivation of the catalyst by sintering and carbon deposition. [15] Catalyst deactivation is a serious problem in the dehydration process for MeOH conversion, and is most commonly the result of carbon deposition, which can be significantly reduced by adding ZnO to the catalyst CuO/HZSM-5. [29]

According to Seo *et al.*, the kinetics of the commercial hybrid catalyst $CuO/ZnO/Al_2O_3$ indicated that catalyst deactivation was observed during DME synthesis at high space velocities and a high ratio of dehydration catalyst. [23] Moradi *et al*. reported that CuO-based catalysts can be deactivated at high temperatures by the presence of water or by carbon deposition, and that a catalyst involving the use of a platinum group metal had proved more stable. [61]

The deactivation of the DME bifunctional catalyst is attributable to coke deposits derived from the degradation of the lower hydrocarbons (C_{1-4} paraffins) produced as by-products. Deactivation has the greatest effect on the acidic function (dehydration component) of the catalyst, which is the main contributor to the conversion of MeOH into DME. The optimal activity and selectivity of DME decrease more when the feed composition contains only CO and H_2 than when CO_2 is also included in the feed .[29] The deactivation of the DME catalyst can also occur when it is exposed to high temperatures (300–350^{o}C), which lead to agglomeration of copper [27] and a reduction in the surface of the catalyst. An environment containing sulphur can lead to catalyst deactivation by poisoning.

2.6 Summary of the literature review

Throughout the literature review we have shown that many techniques are used to prepare supported catalysts. Most of the DME catalysts currently in use are copper-based catalysts, but in this research we have investigated the use of gold as the active metal instead of copper, because it has higher activity and resistance to water-induced sintering than copper-based catalysts.

The co-precipitation preparation method for gold is one of the most extensively-used techniques to disperse active gold nano particles on a support, as it results in highly active gold-based catalysts. However, gold sintering, which reduces the activity of the catalyst occurs at high temperatures, so work should be carried out at carefully controlled temperature to avoid it.

2.7 Objectives of the research

A previously-published article on the co-production of DME and MeOH by Mpela *et al.*[46] suggested that gold might be used as the catalyst for co-production. This provided the context for the extensive study of the production of DME on which this dissertation is based.

We carried out a wide range of experiments with gold catalysts, using different operating conditions (pressure, temperature and space velocity) to seek answers to the following questions:

- Can gold-based catalysts sustain activity at high temperatures?
- How do the operating conditions affect the CO conversion and selectivities of the products?
- Is the process kinetically or thermodynamically limited?
- Is a gold-based catalyst suitable for DME synthesis?
- What are the practical limits of the temperatures used for DME synthesis with a gold-based catalyst?
- What is the best way to relate the thermodynamic predictions to the experimental results?

However, the larger aim of the research was to answer two further questions: What is the best process design for DME production? And why is the production of DME in one step believed to be a better option than the two-step process? Addressing these involves not only a close scrutiny of the production process itself but also the technical and economic considerations that govern it.

CHAPTER 3

EXPERIMENTAL

3.1 Introduction

The experiments we designed to elicit insight into the synthesis of oxygenates and hydrocarbons from synthesis gas required meticulous attention to detail at every stage, from the preparation of the catalyst to the testing and data processing that followed. In this chapter we start by providing technical information on the procedure used to ready the bi-functional catalyst Au/ZnO/γ-Al_2O_3 (a mixture of the Au/ZnO MeOH prepared catalyst and the commercial γ-Al_2O_3 catalyst for MeOH dehydration) by the co-precipitation method. The section that follows describes the three different methods that were used to determine the composition, surface area and particle size in samples of the catalyst: inductively coupled plasma atomic emission spectroscopy(ICP-AES), the Brunauer-Emmett-Teller (BET) method and transmission electron microscopy(TEM).

We then present a schematic diagram of the experimental set-up to accompany a description of the equipment used, which includes gas lines, the reactor and major apparatus. Gas chromatography was applied to quantify the amounts of inlet and outlet gas in the system. The results, which were shown on a computer screen (PC), were then processed so that the researcher could evaluate the performance of the catalyst in terms of activity and selectivity, using the systematic approach of mass balance. To minimize errors, the values obtained were the average of recurring data at steady state. These were validated for carbon, hydrogen and oxygen balance in the range of 93–97%.

3.2 Catalyst preparation

The samples of the Au/ZnO/γ-Al_2O_3 catalyst were prepared by co-precipitation of chloroauric acid ($HAuCl_4 \cdot 3H_2O$) and zinc nitrate (Zn $(NO_3)_2 \cdot 6H_2O$), followed by calcination and then the physical mixing of the resultant Au/ZnO powder with gamma alumina (γ-Al_2O_3, 300-500μm) in the ratio 1:1.Figure 3.1 is a schematic diagram of the various chemicals and the sequence of procedures involved in preparation by co-precipitation.

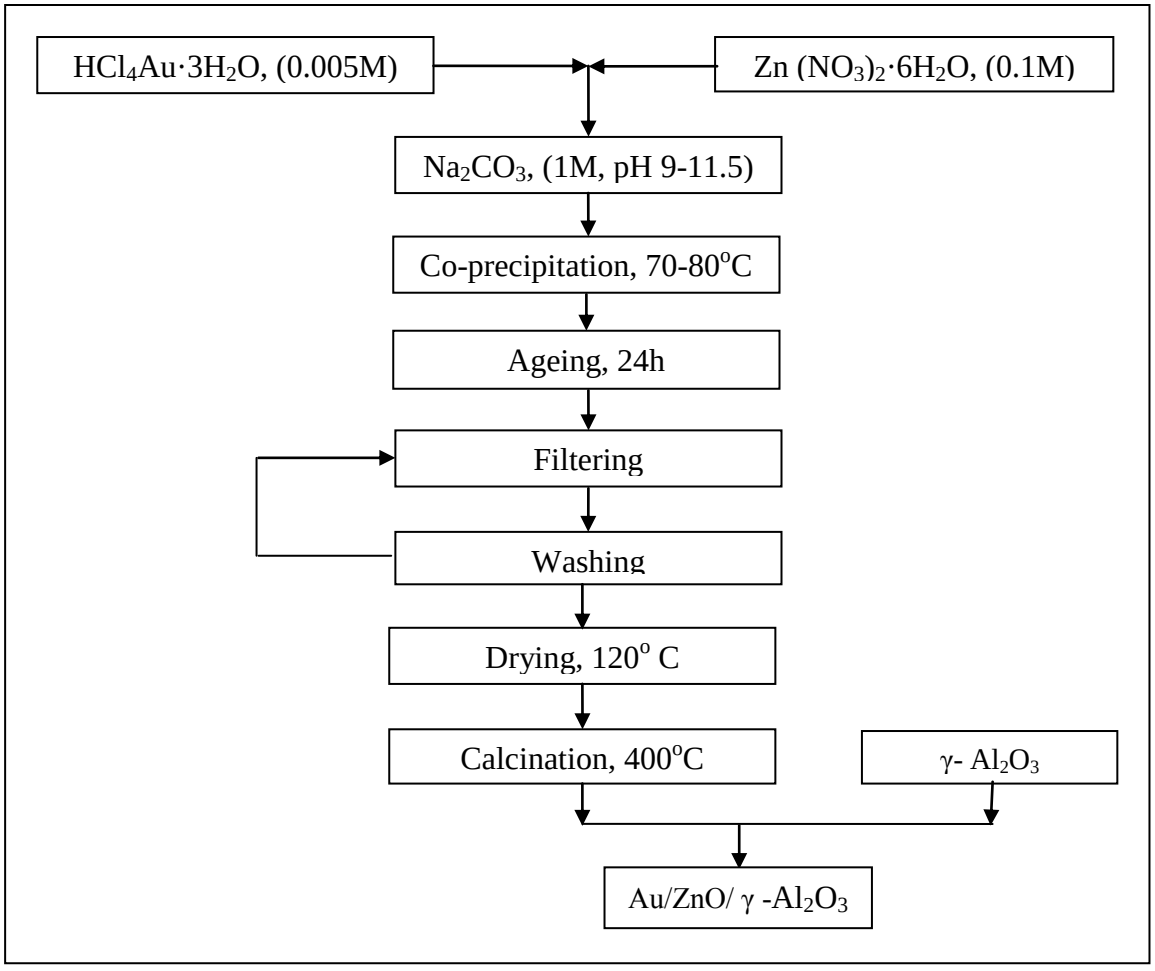


Figure 3.1 Schematic diagram showing the preparation of Au/ZnO/γ- Al_2O_3 bifunctional catalyst

A solution of $HAuCl_4 \cdot 3H_2O$ (0.005M) was mixed with a solution of pure crystals of $Zn(NO_3)_2 \cdot 6H_2O$ (0.1M). The pH of precipitation was kept within the range of 9–11.5 by adding a solution of Na_2CO_3 (1M), at a constant rate of 7.5 ml/min, to the mixed solution under vigorous stirring (600 rpm). The temperature was fixed between 70–80^oC for the 90–120 minutes duration of precipitation. After being aged overnight, the precipitate was filtered and washed with warm distilled water to remove residual sodium ions. The solid product obtained was then dried at 120^oC and subsequently calcined at 400^oC for 6 hours. Thereafter the Au/ZnO powder was physically mixed with γ-Al_2O_3 to obtain the Au/ZnO/ γ-Al_2O_3 hybrid catalyst.[41, 42]

3.3 Characterization methods

3.3.1 Catalyst composition by atomic emission spectroscopy

The Au loading composition was determined using the ICP-AES method, which is a technique for identifying and quantifying elements on the basis of the emission of energy by excited electrons at a given wavelength when they return to ground state. Each element emits energy at specific wavelengths that are characteristic of its chemical character.[62] The intensity of the energy emitted by the atoms and ions is proportional to their concentration in the analyzed sample. The wavelengths and their intensities make it possible to determine the elemental composition of the analyzed sample relative to a reference standard. The ICP can be used for chemical analysis of sample traces lower than ppb. [2]

The Inductively coupled plasma atomic absorption spectroscopy GENESIS ICP-AES SPECRO, Analytical Instruments model was used in our analysis. As required by the ICP-AES technique, we dissolved the catalyst sample by means of a combined acid

attack, employing HF, HNO_3, and HCl acids and a $LiBO_2$ flux-fusion technique. This was followed by successive dilutions of the solution obtained, which were then analyzed. [7]

3.3.2 Size determination by transmission electron microscopy

Transmission electron microscopy (TEM)analyses were performed for determining the particle size distribution of the catalyst using FEI Tecnai G2 Spirit electron microscope at 120 kV.TEM is a characterization technique that provides information on the size, shape, lattice structure and chemical composition of individual particles in the catalyst sample. The interaction of the metal particles with the support reveals their shape. This method also enables the researcher to observe the migration of portions of the support to the surface of the metal particles.[63]Furthermore, TEM can provide a real space image of the atom distribution in a nanocrystal and on its surface. The typical operating resolution of a TEM instrument is 0.5 nm, although the high-resolution transmission electron microscope HRTEM can provide chemical information on nanophase material at a spatial resolution of 0.2 nm or even better.[14, 64]

The determination of particle (crystallite) size and distribution for supported metals is based on the principle of transmission of a focused parallel electron beam to a fluorescent screen and on these assumptions: the size of the imaged particle is proportional to the size of the actual particle, and the detection probability is the same for all particles, independent of their dimensions. [8]

3.3.3 Surface area and pore size determination by the Brunauer-Emmett-Teller method

We evaluated the specific surface area of the catalyst using the BET method by means of a Quantachrome Autosorb (Tristar 3000 V6.05), which is based on the multilayer adsorption of gas (N_2) on a surface. The amount of gas adsorbed at a given pressure enables the researcher to determine the surface area by measuring nitrogen adsorption-desorption isotherms. Three assumptions are made: that the surface of the sample is homogeneous, and that there are no lateral interactions occurring between the molecules and the topmost layer is in equilibrium with the vapour phase.[65]

The plot of a BET equation [66] (see Figure 3.2 below) can be used to determine the total surface area, *A*, of the catalyst sample; the total volume, *V*, of the gas adsorbed at partial pressure, *p*, of N_2; and V_m, the volume of gas adsorbed on the monolayer when the entire surface of one monolayer is covered. This can be expressed as follows:

$$A = \sum_{i=0}^{\infty} S_i \qquad V = V_0 \sum_{i=0}^{\infty} i S_i \qquad V_m = V_0 A \tag{3.1},$$

where V_0 is the volume of gas adsorbed on $1cm^2$ when it is covered by a complete unimolecular layer; and S_i is the surface area covered by *i* layers. At saturation pressure p_o, the number of layers becomes infinite.

The BET isotherm is:

$$\frac{p}{V\,(p_o - p)} = \frac{1}{V_m C} + \frac{C-1}{V_m C} \times \frac{p}{p_o} \tag{3.2}$$

$$C = e^{\frac{H_a - H_c}{RT}} \tag{3.3},$$

where C is a constant related exponentially to the heat of adsorption, H_a, on the first layer and to the heat of condensation of the gas, H_c, on all the other layers. p_o is the saturation pressure of adsorbed gas at the experimental temperature.

The graph $p/V\ (p_o - p)$ versus p/p_o in Figure 3.2 gives a straight line, the slope and intercept of which are used for the evaluation of V_m and C.

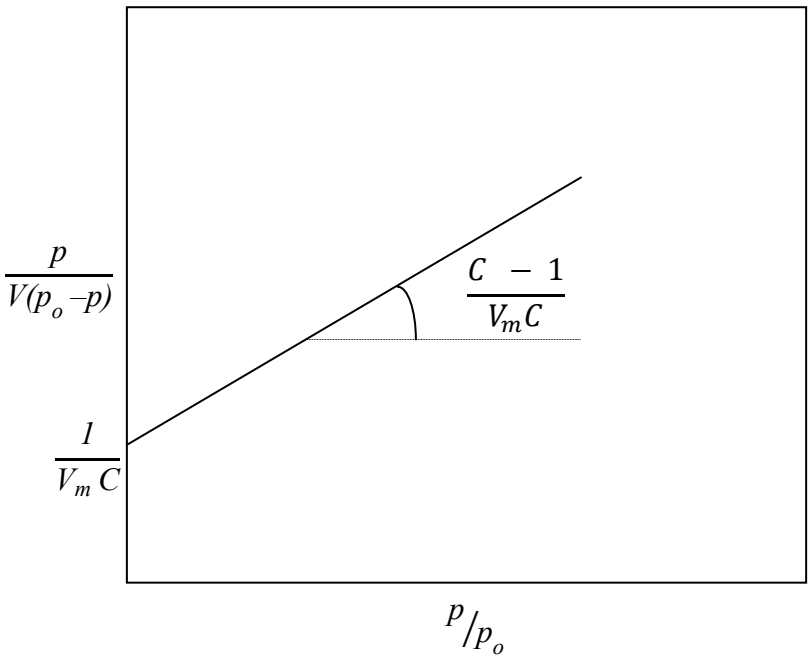


Figure 3.2 Linear plot of the Brunauer-Emmett-Teller equation

The sample was degassed at 150^{o}C for 4 hours under vacuum. It was then cooled to liquid-nitrogen temperature, after which a known quantity of nitrogen gas was admitted and allowed to equilibrate. The amount of nitrogen adsorbed was calculated at equilibrium pressure by using the equation of state pV = NRT. The procedure was repeated to yield a series of values of volume adsorbed that corresponded with a set of increasing values for the equilibrium pressure.[6]

3.4 The rig and reactor

A schematic diagram of the rig used in the experiments is shown in Figure 3.3. The major pieces of equipment it contains are the reactor, gas cylinders, piping and gas chromatographs (GCs).

During the experiments, the feed gas (synthesis gas) flowing from the cylinder ($CO+H_2$) was sent to the reactor (RX) via a mass flow controller (MFC Brooks Model 5850), which maintained a constant flow rate at the specified operating conditions. The temperature of the reactor was monitored by thermocouples (TCs) connected to a control box. The cold trap under the reactor separated the liquid from the gaseous products.

Two online GCs, a flame ionization detector (FID) and a thermal conductivity detector (TCD) were used to create chromatograms that could be read on a computer (PC). These made it possible to analyze the products of the reactor. A continuous supply of hydrogen and air flowed from cylinders or gas lines to the FID to keep the GC flame alight, while argon was used as a carrier gas for both the FID and TCD. Valves V_1 to V_8, each with a pressure indicator (PI), were manually operated to control the flow, and the back pressure regulator (BPR) kept the pressure in the reactor at the set operating pressure. It also released atmospheric pressure for GC analysis.

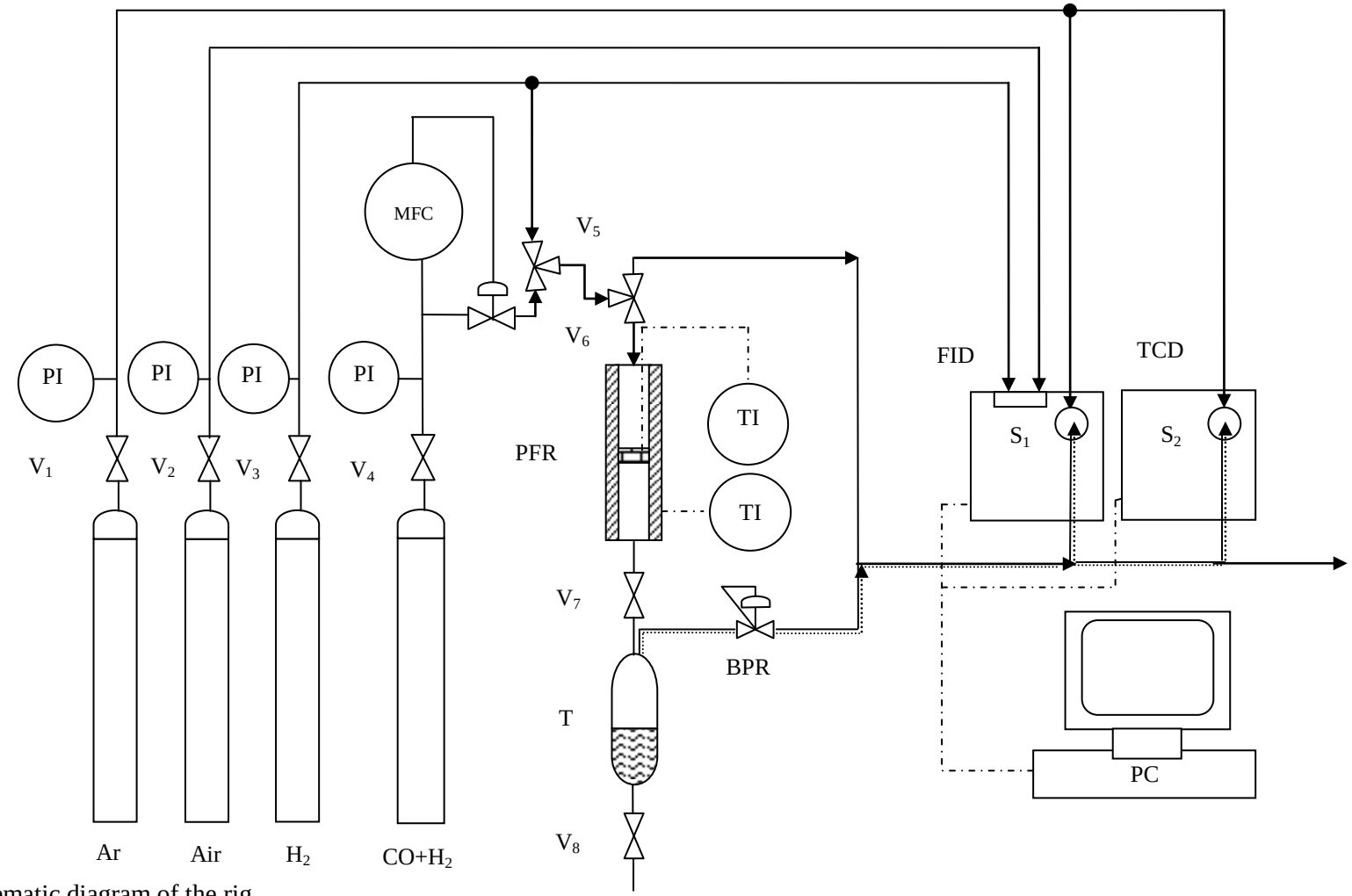


Figure 3.3 Schematic diagram of the rig

PFR: plug flow reactor; BPR: back pressure regulator; TI: temperature indicator; PI: pressure indicator; $V_{1\text{-}8}$: shut off valves; FID: flame ionized detector; TCD: thermal conductivity detector; MFC: mass flow controller; T: trap, Ar, Air; H2, CO+H2: cylinders; S_1 and S_2: six ways sampling valves

The fixed bed reactor used in this study was made of stainless steel tubing (35 cm in length and with a 5 mm ID), as shown in Figure 3.4. A thermocouple inserted in the centre of the reactor controlled the inside temperature, while another, placed outside the reactor, allowed the reading of the temperature of the heating jacket. The reactor was loaded with 0.6 g of catalyst packed between two layers of quartz wool.

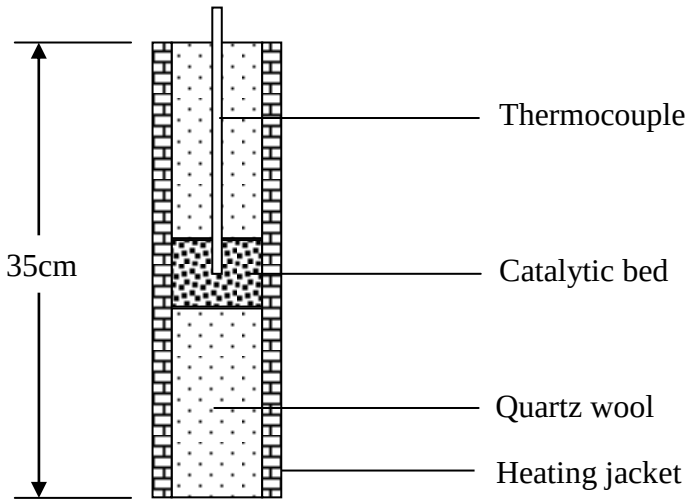


Figure 3.4 Simplified scheme of the reactor

The synthesis gas flowed through the catalytic bed from the top to the bottom of the reactor. The downstream 3.2 mm stainless steel tubing line below the reactor exit was wrapped with electrical heating tape, under which a thermocouple connected to an Omega digital readout had been inserted. The tubing was kept at 150°C in order to avoid any condensation of the product to be analyzed by the GC.

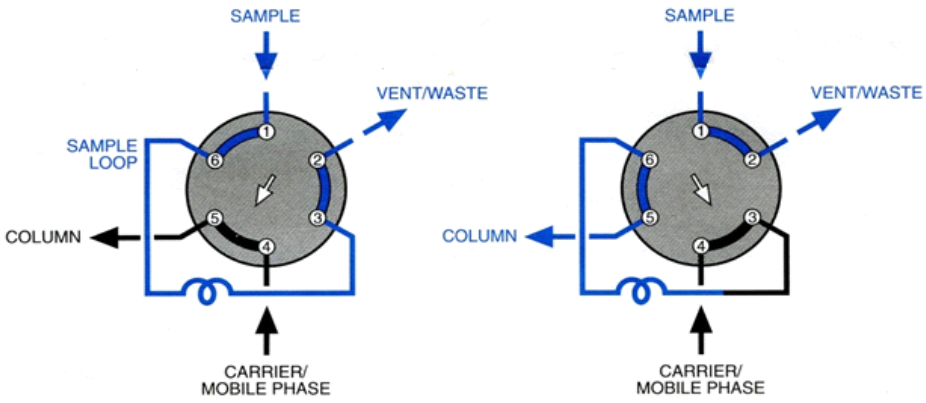
Based on previous research on CO hydrogenation and co-production of DME/MeOH over gold-based catalysts [41, 42], the experiments were carried out between 340–460^{o}C at different pressures ranging from 20–50 bar and different space velocities. For each experimental run, 0.6 g of catalyst (physical mixture of 0.3 g Au/ZnO and 0.3 g γ-Al_2O_3) was loaded into the reactor between plugs of quartz wool. Catalyst activation was performed at 300^{o}C for six

hours using pure hydrogen. Before any run the reactor system was first pressure- tested with inert gas (nitrogen or argon) under the planned operating conditions to check for any possible leak of gas along the reactor and piping. The feed composition was a mixture of 10 vol. % N_2, 30 vol. % CO and 60 vol. % H_2.

3.5 Analytical method

The GC technique was used to determine the composition of products from the reactor. It is a method of analyzing complex compound mixtures that uses the physical properties (volatility and thermal stability) of sample components to identify and quantify them.[2]

The gas product coming from the reactor flows through the GC column via an automatic six-way sampling valve, which allows the gas to pass through the injector, which vaporizes the sample, after which the carrier gas conveys it to the column for separation into its components identifiable by the detector.



(a) **(b)**

Figure 3.5 Six-way sampling valve

The sampling valve operates as shown in Figure 3.5. In position (a), the sample enters the sampling loop and is then vented (sequence 1-6-3-2), while the carrier gas flows through to

the column (sequence 4-5). Position (b) shows that a portion of the sample is retained in the sample loop and transported by the carrier gas into the column for analysis (sequence 4-3-6-5), whereas the fresh sample is vented (sequence 1-2). The valve was programmed to extract a sample every 2 hours. The analysis of the sample lasted for 40 minutes. Thereafter the column was maintained at 220^{o}C for 1 hour in position (a) to clean the column.

The gaseous products are identified while they pass through the detector at a specific rate. The gas that moves most rapidly is the first to be detected, while the others are identified in a sequence dictated by the amount of time that elapses between injection and their becoming detectable (retention time). The detector is connected to a digital read-out that transforms the signal generated by the contact gas detector into a chromatogram that is shown on the computer screen. The area of the peaks on the chromatogram indicates the amount of the gas that is being analyzed.

The retention time of the products depends on the type of column used for the analysis and the operating conditions of the GC. A Porapak column (80–100 mesh, 3 m x 1/8" x 2.2 mm, SS) was used on the FID for the detection of oxygenate and hydrocarbon compounds, while a Carboxen column (80–100 mesh, 2 m x 1/8" x 2.0 mm, SS) on the TCD enabled the researcher to identify the components of the synthesis gas, CO, CO_2, H_2, and N_2. The carrier gas used was Argon. Table 3.1 below sets out the operating conditions for the GCs.

Table 3.1 GC operating conditions (parameter and setting)

Parameter	Setting
Injector temperature (^{o}C)	150
Detector temperature (^{o}C)	220
Sampling valve temperature (^{o}C)	220
Initial temperature (column) (^{o}C)	20
Final temperature (column) (^{o}C)	220
Initial time (min)	0
Ramp rate (^{o}C.min^{-1})	5
Final time (min)	20

Figures 3.6 and 3.7 below give examples of chromatograms of calibration gas from a FID and TCD. The retention times show the identifying peaks as 1-4-7 for CH_4, 2-5-8 for C_2H_4 and 3-6-9 for C_2H_6 on the FID. Those on the TCD are 1-4-7 for H_2, 2-5-8 for N_2 and 3-6-9 for CO.

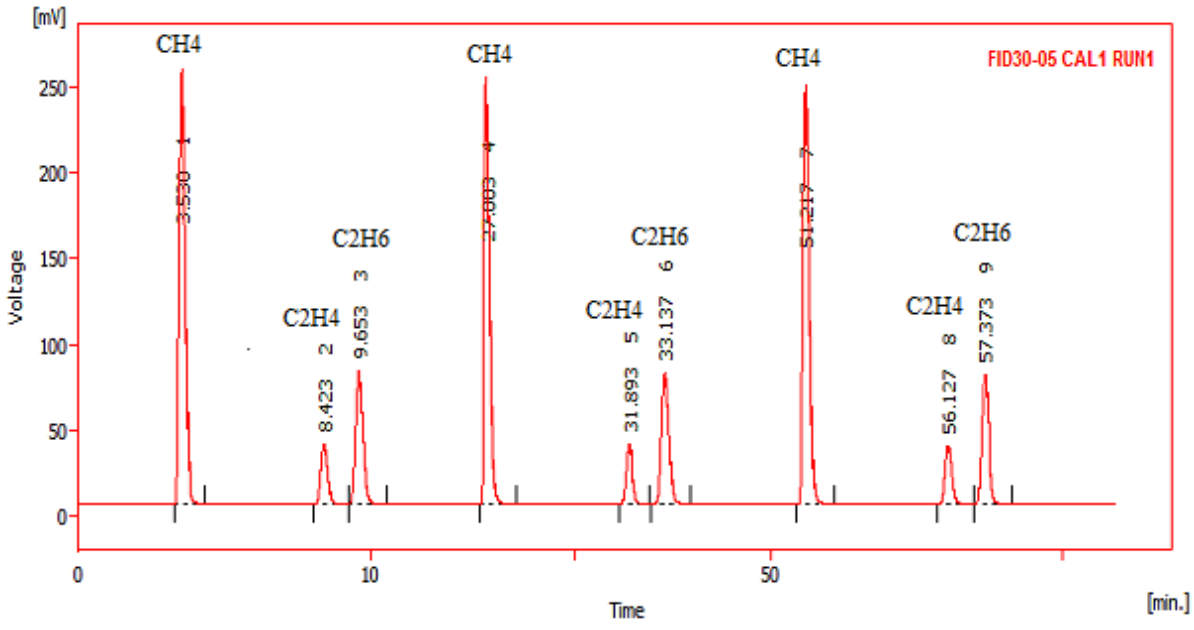


Figure 3.6 FID chromatograms of calibration gas

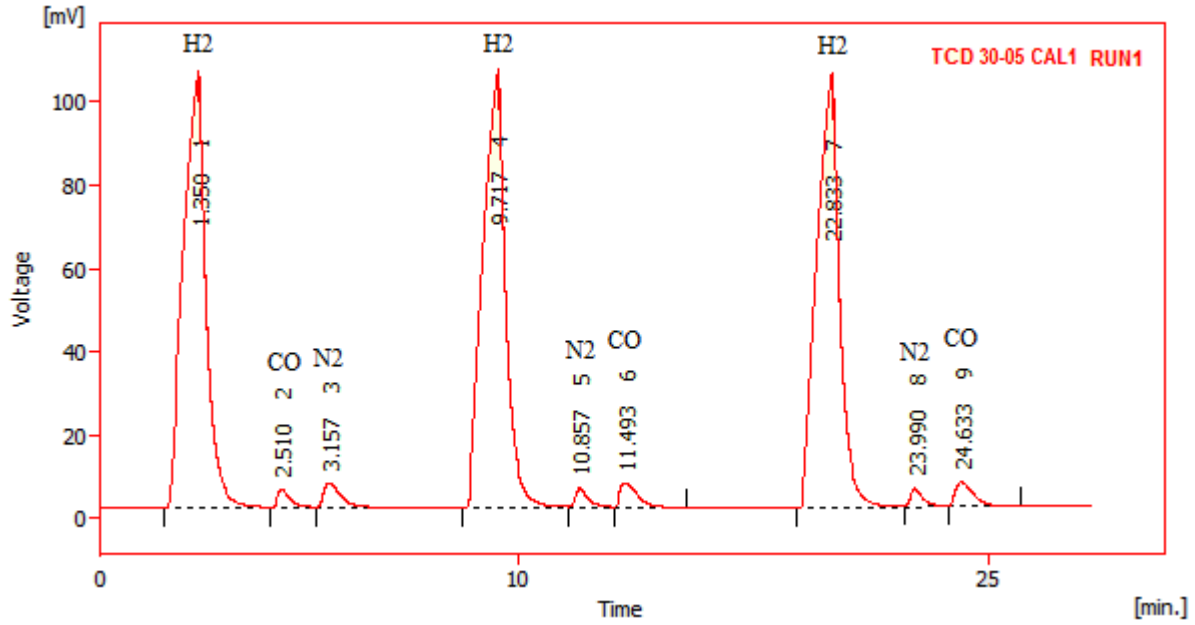


Figure 3.7 TCD chromatogram of calibration gas

3.6 Data generation and processing

Data were collected from the GC traces (chromatograms) and processed on Excel worksheets to determine the CO conversion, rates of consumption of reactants and product formation, space velocity and selectivity of products.[61]

A mixture of selected gases with a known volumetric composition was used as the standard for calibration. It consisted of 2.5% CH_4, 0.2% C_2H_4, 0.5% C_2H_6, 10.0% CO, 5.0% CO_2 and $N_2$to make up the balance. The calibration gas mixture was sent to the GCs to determine the areas $A_{j,cal}$ of the integrated peaks on the chromatograms (provided by the readout from Clarity software) that corresponded with the percentages $(\%)_{j,cal}$ of calibration gas.

The molar percentage of a compound *j* in the gas was calculated as follows:

$$(\%)_j = \frac{A_j}{A_{j,cal}} \times (\%)_{j,cal} \qquad (3.4),$$

where $(\%)_j$ is the molar percentage of compound *j* in the analyzed gas; A_j is the integrated

area of the GC peak corresponding to compound *j* in the analyzed gas; $A_{j,cal}$ is the integrated area of the GC peak corresponding to compound *j* in the calibration mixture; and $(\%)_{j,cal}$ is the molar percentage of compound *j* in the calibration mixture.

The following expression was used to evaluate the molar percentage of compounds in cases where the calibration data could not be obtained directly from the calibration mixture:

$$(\%)_j = \frac{A_j}{A_{l,cal}} \times (\%)_{k,cal} \times RF_{j,l} \qquad (3.5),$$

where $(\%)_j$ *is* the molar percentage of compound *j* in the analyzed gas; A_l,*cal* is the integrated area of the GC peak corresponding with compound *l* in the analysed gas; $(\%)_{l,cal}$ is the molar percentage of the reference compound *l* in the calibration mixture; and $RF_{j,l}$ is the relative response factor of the compound *j* with respect to the reference compound *l*.

C_2H_4 was used as the reference for olefins while C_2H_6 was used as the reference for paraffins. Relative response factors (RFs) for hydrocarbon products are presented in the Table below.

Table 3.2 Relative response factors for hydrocarbon products [4]

Carbon Number	Olefin	Paraffin
2	1.00	1.00
3	0.70	0.74
4	0.78	0.55
5	0.47	0.47

The RFs and concentration of MeOH and dimethyl ether were determined using the single point external standard method. This involves first analyzing a sample with a known

concentration (C_1) on the GC, and recording the peak area (A_1). Then a sample of the same product (MeOH or DME), but with an unknown concentration (C_2), is sent to the GC and the peak area (A_2) recorded. The RF and C_2 are calculated as follows:

$$RF_{MeOH} = \frac{A_1}{C_1} \tag{3.6}$$

$$C_2 = \frac{A_2}{RF_{MeOH}} \tag{3.7}$$

The RF was obtained by averaging at least three measurements, which had been repeated to ensure accuracy.

3.7 Calculation of outlet gas compositions, conversion, reaction rates and selectivity

The mass flow controller placed in the inlet stream before it reached the reactor measured the inlet volumetric flow rate and from this the molar flow rate F_{in}, was determine and the bubble meter placed in the outlet stream after it left the reactor calibrated the flow meter.[61] The outlet molar flow rate was established by applying the following equation:

$$F_{in} \times (\%)_{N_2,in} = F_{out} \times (\%)_{N_2,out} \tag{3.8},$$

where F_{in} is the total molar flow rate (moles/min) of the inlet stream of the reactor; F_{out} is the total molar flow rate (moles/min) of the reactor outlet gas stream; $(\%)_{N_{2,in}}$ is the mole fraction of nitrogen in the inlet stream of the reactor; and $(\%)_{N_{2,out}}$ is the mole fraction of nitrogen in the outlet gas stream of the reactor.

The molar flow rate of CO in the feed stream $F_{\text{CO,in}}$ and molar flow rate of CO in the product stream $F_{CO,out}$ were defined respectively as:

$$F_{CO,in} = F_{in} \times (\%)_{CO,in} \tag{3.9},$$

$$F_{CO,out} = F_{out} \times (\%)_{CO,in} \quad (3.10).$$

The conversion of CO, X_{CO} was evaluated using the following equation:

$$X_{CO} = \left\{1 - \left(\frac{(\%)_{CO,out}}{(\%)_{CO,in}}\right) \times \left(\frac{(\%)_{N_2,in}}{(\%)_{N_2,out}}\right)\right\} \times 100 \quad (3.11).$$

The rate of consumption of CO, r_{CO} (mol.min^{-1}.g^{-1}) was defined as:

$$r_{CO} = \frac{F_{CO,in} - F_{CO,out}}{g_{cat}} \quad (3.12)$$

where g_{cat} is the mass of catalyst in grammes.

The rate of formation of product j, r_j was defined as:

$$r_j = \frac{F_{out} \times (\%)_{j,out}}{g_{cat}} \quad (3.13).$$

The selectivity of product j, S_j was defined as:

$$S_j(\%) = \frac{n \times F_{j,out}}{r_{CO}} \times 100 \quad (3.14),$$

where n is the carbon number in the analyzed compound j.

The selectivity of oxygenates (S_O) in the product and the selectivity of DME in the oxygenates ($S_{DME\ in\ O}$) were evaluated as follows:

$$S_O(\%) = \frac{2 \times F_{DME,out} + F_{MeOH,out}}{F_{CO,in} - F_{CO,out}} \times 100 \quad (3.15)$$

$$S_{DME\ in\ O}(\%) = \frac{2 \times F_{DME,out}}{2 \times F_{DME,out} + F_{MeOH,out}} \times 100 \quad (3.16),$$

The space velocity SV ($dm^3.g^{-1}.h^{-1}$), was defined as:

$$SV = \frac{V_{out}}{g_{cat}} \qquad (3.17),$$

where V_{out} is the outlet volume flow rate ($dm^3.h^{-1}$) under standard conditions of pressure and temperature.

This chapter was intended to provide a background for understanding the material and methods used in subsequent chapter.

CHAPTER 4

RESULTS AND DISCUSSION

4.1 Introduction

In this chapter, we apply thermodynamic reaction equilibrium theory to analyze the DME process. We show how parameters such as temperature, pressure and the catalyst affect the conversion and selectivity of the process in terms of the different reactions that occur on the catalyst. Further results and discussion report on the experimental work done, in laboratory, on the synthesis of DME using a gold based-catalyst.

4.2. Process analysis

In designing this series of experiments, we used synthesis gas (CO and H_2) as a feed to a Gibbs reactor, which is a type of reactor in which the reactions reach chemical equilibrium. The products of the reactor could include MeOH, DME, CO_2 and H_2O, as well as unreacted CO and H_2. The reactions we were analyzing form MeOH, DME, CH_4 and/or H_2O.

Figure 4.1 shows a simplified scheme of the DME process. There are seven species of interest: H_2, CO, CO_2, H_2O, CH_3OH, CH_3OCH_3 and CH_4. There are four independent mass balances or reactions that can be used to relate the feed to the potential products. We will consider these independent reactions to be MeOH synthesis (as described in Equation 4.1), DME formation (as in equation 4.2), water-gas shift (WGS) reaction (Equation 4.3) and the CH_4 synthesis (Equation 4.4).

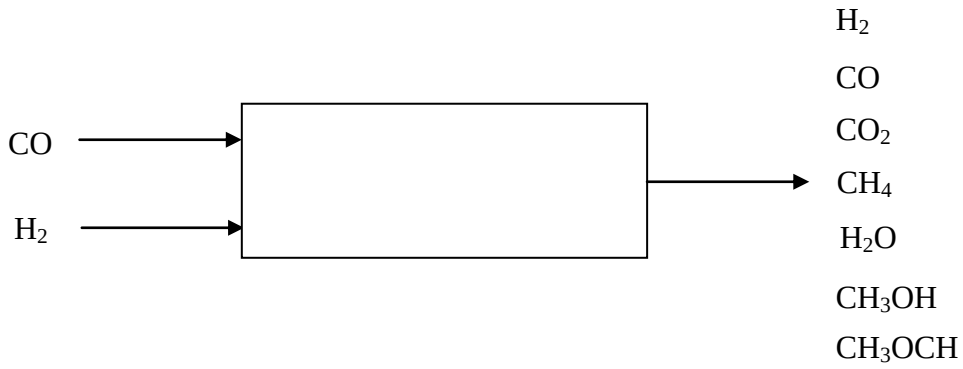


Figure 4.1 Simplified DME process

$$CO + 2H_2 \leftrightarrow CH_3OH \qquad \Delta H_{298K} = -90.70\ kJ.mol^{-1} \qquad (4.1)$$

$$2CH_3OH \leftrightarrow CH_3OCH_3 + H_2O \qquad \Delta H_{298K} = -23.00\ kJ.mol^{-1} \qquad (4.2)$$

$$CO + H_2O \leftrightarrow CO_2 + H_2 \qquad \Delta H_{298K} = -41.19\ kJ.mol^{-1} \qquad (4.3)$$

$$CO + 3H_2 \leftrightarrow CH_4 + H_2O \qquad \Delta H_{298K} = -205.9\ kJ.mol^{-1} \qquad (4.4)$$

Overall net reaction

$$3CO + 4H_2 + CH_3OH \rightarrow CH_3OCH_3 + H_2O + CH_4 + CO_2 \qquad \Delta H_{298K} = -360.79\ kJ.mol^{-1} \qquad (4.5)$$

4.2.1 Mass balances

Assuming that the system is allowed to reach equilibrium, the number of moles N_j of component *j* in the product stream can be obtained using the relationship between the number of mole N_j^o of component *j* in the feed stream and the extent of reaction *k*, $\xi_{k,}$, as follows:

$$N_j = N_j^o - \sum_k \gamma_{jk} \xi_k \qquad (4.6),$$

where γ_{jk} is the stoichiometric coefficient of component *j* in reaction *k*.

It follows that if all three reactions occur, the number of moles of species in the outlet of the process are related as follows:

$$N_{CO} = N^o_{CO} - \xi_1 - \xi_3 - \xi_4 \qquad \geq 0 \tag{4.7}$$

$$N_{CO_2} = N^o_{CO_2} + \xi_3 \qquad \geq 0 \tag{4.8}$$

$$N_{H_2} = N^o_{H_2} - 2\xi_1 + \xi_3 - 3\xi_4 \qquad \geq 0 \tag{4.9}$$

$$N_{H_2O} = N^o_{H_2O} + \xi_2 - \xi_3 + \xi_4 \qquad \geq 0 \tag{4.10}$$

$$N_{DME} = N^o_{DME} + \xi_2 \qquad \geq 0 \tag{4.11}$$

$$N_{MeOH} = N^o_{MeOH} + \xi_1 - 2\xi_2 \qquad \geq 0 \tag{4.12}.$$

$$N_{MeOH} = N^o_{CH_4} + \xi_4 \qquad \geq 0 \tag{4.13}$$

N, the total number of moles flowing out of the reactor, is given by:

$$N = \sum_p N_j = N^o_{CO} + N^o_{CO_2} + N^o_{H_2} + N^o_{H_2O} + N^o_{DME} + N^o_{MeOH} + N^o_{CH_4} - 2\xi_1 - 2\xi_4 \qquad \geq 0 \tag{4.14}.$$

4.2.2 Equilibrium equations

The Gibbs free energy of formation of species *j* at temperature *T*, $G_{f,j,T}$, and the Gibbs free energy of reaction for reaction *k* at temperature *T*, $G_{rx,k,T}$, were determined using the following equations :

$$G_{f,j,T} = a_j + b_j T + c_j T^2 \tag{4.15}$$

$$\Delta G_{rx,k,T} = \sum_k \gamma_{j,k} (G_{f,j,T})_{products} - \sum_k \gamma_{j,k} (G_{f,j,T})_{reactants} \quad (4.16),$$

where a_j, b_j and c_j are constant coefficients relative to a given component j, and T is the temperature in K. The units of Gibbs free energy are kJ.mole^{-1}. The reaction equilibrium constant for reaction k at temperature T, $K_{P_{k,T}}$, is given by:

$$K_{P_{k,T}} = exp\left(\frac{-\Delta G_{rx,k,T}}{RT} \right) \quad (4.17),$$

where R is the molar gas constant (8.314 J.mole^{-1}.K^{-1}).

The equilibrium constants $K_{P_k T}$ are function of temperature and allow to determine the extents ξ_k of the reactions at equilibrium. In order to calculate the equilibrium constant, we assumed that all components involved in the process were ideal gases. The mole fraction of component j, y_j, and the partial pressure of component j, p_j, are expressed as:

$$y_j = \frac{N_j}{N} \quad (4.18)$$

$$p_j = y_j \times P \quad (4.19),$$

where P is the total pressure in bar. The equilibrium constant can thus be written in terms of partial pressures as:

$$K_{P_{k,T}} = \frac{\left(\prod_k p_j^{\gamma_{j,k}} \right)_{products}}{\left(\prod_k p_j^{\gamma_{j,k}} \right)_{reactants}} \quad (4.20).$$

Combining Equation 4.17 with Equation 4.20, we calculate the equilibrium constant as follows:

For the MeOH synthesis reaction

$$K_{P_1,T} = \frac{P_{MeOH}}{(P_{CO})(P_{H_2})^2} = \frac{\left(N^o_{MeOH} + \xi_1 - 2\xi_2\right)(N)^2}{(N^o_{CO} - \xi_1 - \xi_3 - \xi_4)(N^o_{H_2} - 2\xi_1 + \xi_3 - 3\xi_4)^2} \times \frac{1}{P^2} \tag{4.21}$$

For DME formation

$$K_{P_2,T} = \frac{(P_{DME})(P_{H_2O})}{(P_{MeOH})^2} = \frac{\left(N^o_{DME} + \xi_2\right)(N^o_{H_2O} + \xi_2 - \xi_3 + \xi_4)}{(N^o_{MeOH} + \xi_1 - 2\xi_2)^2} \tag{4.22}$$

For the WGS reaction

$$K_{P_3,T} = \frac{\left(P_{CO_2}\right)\left(P_{H_2}\right)}{(P_{CO})(P_{H_2O})} = \frac{\left(N^o_{CO_2} + \xi_3\right)\left(N^o_{H_2} - 2\xi_1 + \xi_3 - 3\xi_4\right)}{(N^o_{CO} - \xi_1 - \xi_3 - \xi_4)(N^o_{H_2O} + \xi_2 - \xi_3 + \xi_4)} \tag{4.23}$$

For CH_4 synthesis

$$K_{P_4,T} = \frac{\left(P_{CH_4}\right)\left(P_{H_2O}\right)}{(P_{CO})(P_{H_2})^3} = \frac{\left(N^o_{CH_4} + \xi_4\right)\left(N^o_{H_2O} + \xi_2 - \xi_3 + \xi_4\right)}{(N^o_{CO} - \xi_1 - \xi_3 - \xi_4)(N^o_{H_2} - 2\xi_1 + \xi_3 - 3\xi_4)^3} \times \frac{N^2}{P^2} \tag{4.24}.$$

Notice that only the MeOH reaction and CH_4 synthesis depend on pressure.

If we consider that the feed is synthesis gas and the ratio of CO: H_2 in the feed of the reactor is 1:2, the equilibrium constant equations (Equations 4.21–4.24) become:

$$K_{P_1,T} = \frac{\left(\xi_1 - 2\xi_2\right)(3 - 2\xi_1 - 2\xi_4)^2}{(1 - \xi_1 - \xi_3 - \xi_4)(2 - 2\xi_1 + \xi_3 - 3\xi_4)^2} \times \frac{1}{P^2} \tag{4.25}$$

$$K_{P_2,T} = \frac{\left(\xi_2\right)(\xi_2 - \xi_3 + \xi_4)}{(\xi_1 - 2\xi_2)^2} \tag{4.26}$$

$$K_{P_3,T} = \frac{\left(\xi_3\right)\left(2 - 2\xi_1 + \xi_3 - 3\xi_4\right)}{(1 - \xi_1 - \xi_3 - \xi_4)(\xi_2 - \xi_3 + \xi_4)} \tag{4.27}$$

$$K_{P_1,T} = \frac{\xi_4\left(\xi_2 - \xi_3 + \xi_4\right)(3 - 2\xi_1 - 2\xi_4)^2}{(1 - \xi_1 - \xi_3 - \xi_4)(2 - 2\xi_1 + \xi_3 - 3\xi_4)^3} \times \frac{1}{P^2} \quad (4.28)$$

We can now examine various cases in order to understand the impact on the product distribution and conversion at equilibrium of the temperature, the pressure, and the reactions that occur in the reactor.

4.2.3 Case 1. The MeOH synthesis reaction is the only reaction that occurs

If we assume that the only reaction that occurs in the reactor is the MeOH synthesis reaction (Equation 4.1), we can also assume that the reaction equilibrium is described by Equation 4.25, and that in this case, ξ_2, ξ_3 and ξ_4 are 0.

By solving the reaction equilibrium (Equation 4.25) we can find the equilibrium CO conversion as a function of temperature at different pressures for MeOH synthesis (Equation 4.1), as shown in Figure 4.2. The graphs in this study were generated in Excel, and the non-linear equations were solved using MathCAD 14. The thermodynamic data used were taken from the book of *The Properties of Gases and Liquids*. [67]

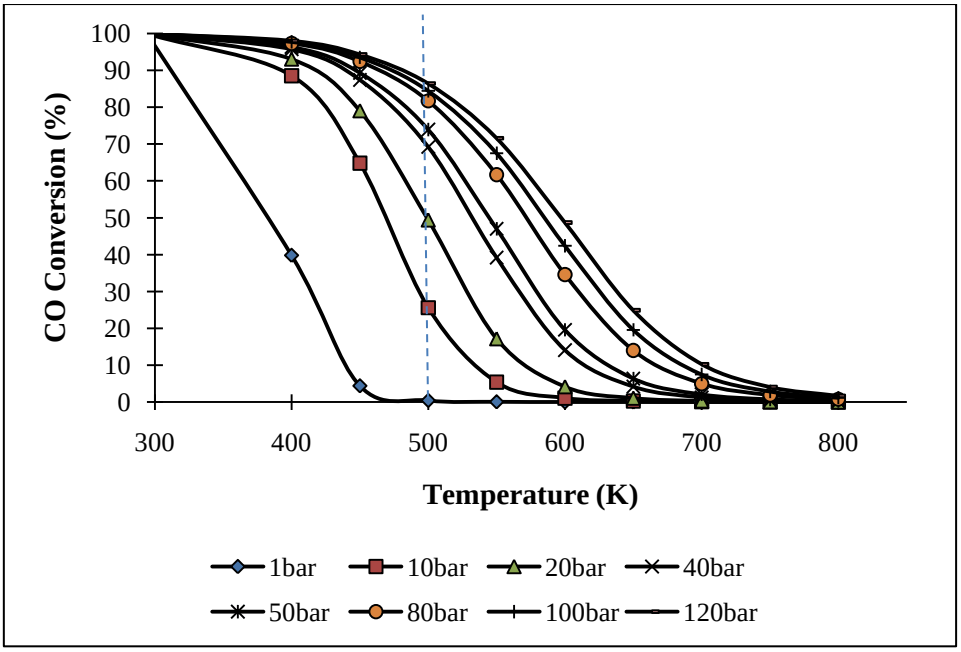


Figure 4.2 Effect of temperature on the CO equilibrium conversion at different pressures when the MeOH synthesis reaction (Equation 4.1) is the only reaction occurring in the reactor. The feed to the reactor is $CO:H_2 = 1:2$

The MeOH synthesis reaction is exothermic, which causes the CO conversion to reduce with an increase in temperature. For practical reasons, such as catalyst activity, the MeOH synthesis is carried out around 220–275^{o}C and at high pressure (50–100 bar), and typically achieves a CO conversion above 50%. The ideal situation would be to work at a relatively low temperature to keep the CO conversion as high as possible (which would avoid the need to recycle large amounts of unreacted CO and H_2, and incur the costs of separation and recycle compression). The higher the pressure of the process (reactor), the higher the equilibrium conversion and the smaller the size of the equipment required for separation and recycling. As a result, the power requirements of the recycle compressor will decrease, while those of the feed compressor will rise. It is clear that a trade-off must be found between the technical aspects of the process (that is, the operating conditions) and the costs (relative to equipment and energy use). The choice a process is motivated by considerations like amount of DME and Methanol to be produced (or selectivity) and CO conversions, bearing in mind

the economic aspect of the process. For a feed where the percentage in inert gas is low the recycle process is preferred to the cascade (duplication of series of reactors) for improving CO conversion for the overall process. Using a cascade system will increase capital cost (reactors, catalysts...) For a feed containing higher percentage of inert the cascade process is indicated because recycling lead to higher energy consumption (big compressors) and operating cost.

4.2.4 Case 2. Both the MeOH and DME synthesis reactions occur in the reactor

As part of the project to arrive at a better understanding of the process of DME synthesis equilibrium, we assumed in this case that both the MeOH synthesis reaction (Equation 4.1) and the DME synthesis reaction (Equation 4.2) occurred simultaneously and reached reaction equilibrium, but that the WGS reaction and CH_4 synthesis reaction did not take place because the nature of the catalyst set kinetic limits on the reactions. This limitation would apply even if the WGS reaction was thermodynamically feasible. Jia *et al*. cited a similar scenario in relation to their work on Fischer-Tropsch synthesis in which the use of a cobalt catalyst for CO hydrogenation did not lead to the conversion of water to hydrogen. Conversely, iron-based catalysts produce CO_2 as the main by-product via the WGS reaction.[68]

We addressed Equations 4.25 and 4.26 simultaneously with the extents of the WGS reaction, ξ_3, and CH_4 formation, ξ_4 set to 0. Figure 4.3A shows the effect of temperature on the equilibrium conversion of CO for the combined reactions of MeOH and DME synthesis under different reactor pressures. We can see that the overall equilibrium conversion of CO drops as the temperature rises, which is not surprising, as both reactions are exothermic. Furthermore, increasing the pressure at fixed operating temperature improves the equilibrium conversion. Thus the pressure dependence of the MeOH synthesis reaction continues to

dominate the pressure sensitivity of the combined reaction system, even though the DME synthesis reaction is not dependant on pressure.

In Figure 4.3B we compare the equilibrium CO conversion of the MeOH-synthesis-only reaction (Case 1) with the simultaneous MeOH and DME synthesis reactions. For Case 2 we adopted a fixed pressure of 40 bar, but varied the temperature. The CO conversion of the combined reaction system is higher than that of the MeOH-only synthesis. For example, at 40 bar and 500 K, the CO conversion for the reaction involving MeOH alone was 69.2%, as against 86.6% for the combined MeOH–DME process. Thus the DME synthesis reaction raises the achievable level for the equilibrium conversion of CO higher than the MeOH-only reaction can. The implications for DME synthesis are that we could achieve higher conversions and thus lower recycle flow rates if we ran the reactor at the same temperature and pressure as in the MeOH-only process; or that we could obtain the same conversion as in a MeOH synthesis process if the catalyst was operated at lower temperatures and pressures.

The selectivities of MeOH and DME in the case of the MeOH–DME system are not particularly pressure-sensitive as can be observed in Figures 4.4 A and B. Furthermore, the MeOH selectivity improves, and conversely the DME selectivity decreases, in response to a rise in temperature. At 300 K we would, at equilibrium, produce mainly DME, while at 750 K, the selectivity of DME would drop to 70%.

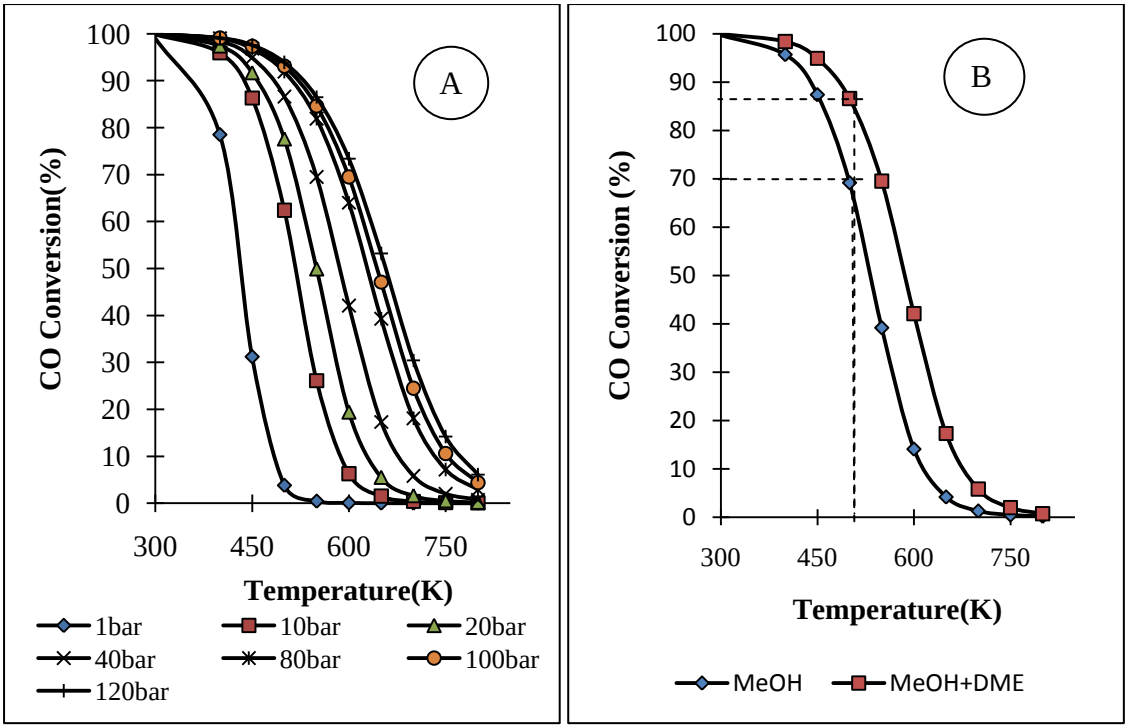


Figure 4.3 (A) Equilibrium conversion of CO as a function of temperature in the combined DME–MeOH system at a range of pressures, and (B) comparison of the equilibrium CO conversion for the MeOH and MeOH–DME systems at a pressure of 40 bar

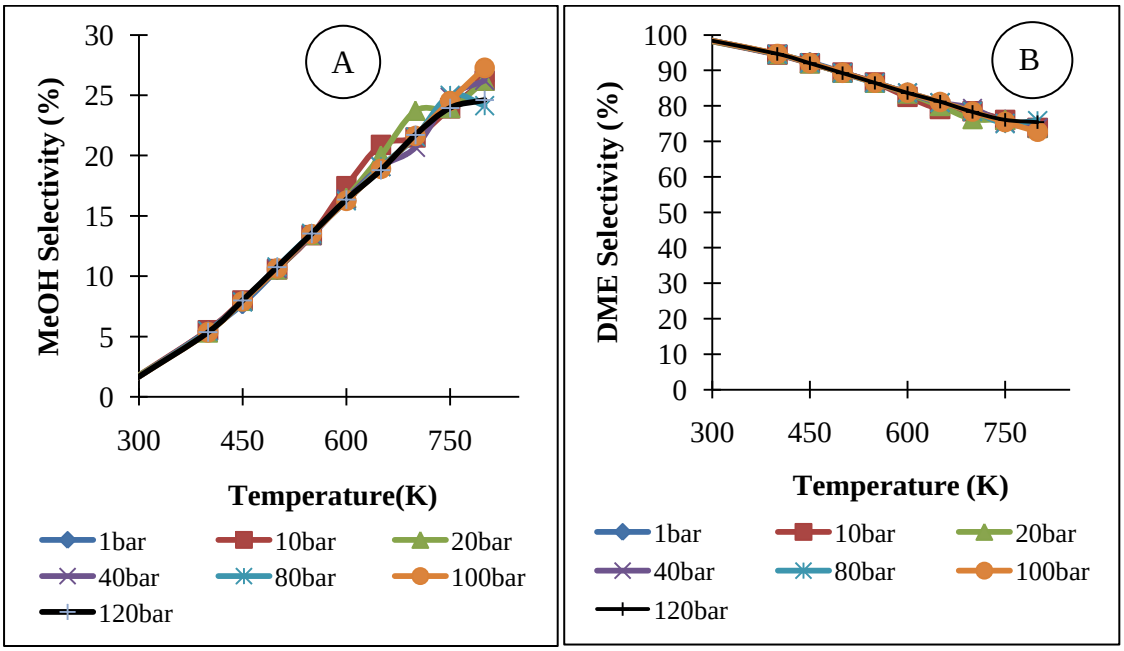


Figure 4.4 (A) Equilibrium MeOH selectivity as a function of temperature at different pressures, and (B) DME selectivity as a function of temperature at different pressures in the MOH–DME system

4.2.5 <u>Case 3</u>. The MeOH, DME and WGS reactions all occur simultaneously in the reactor

Typically, the WGS reaction occurs on MeOH synthesis catalysts. We now examine the impact of the WGS (Equation 4.3) on the reactor conversion and selectivity at equilibrium when both the MeOH synthesis reaction (Equation 4.1) and the DME synthesis reaction (Equation 4.2) are also occurring at the same time. The equilibrium CO conversion as a function of temperature at different pressures is shown in Figure 4.5A.

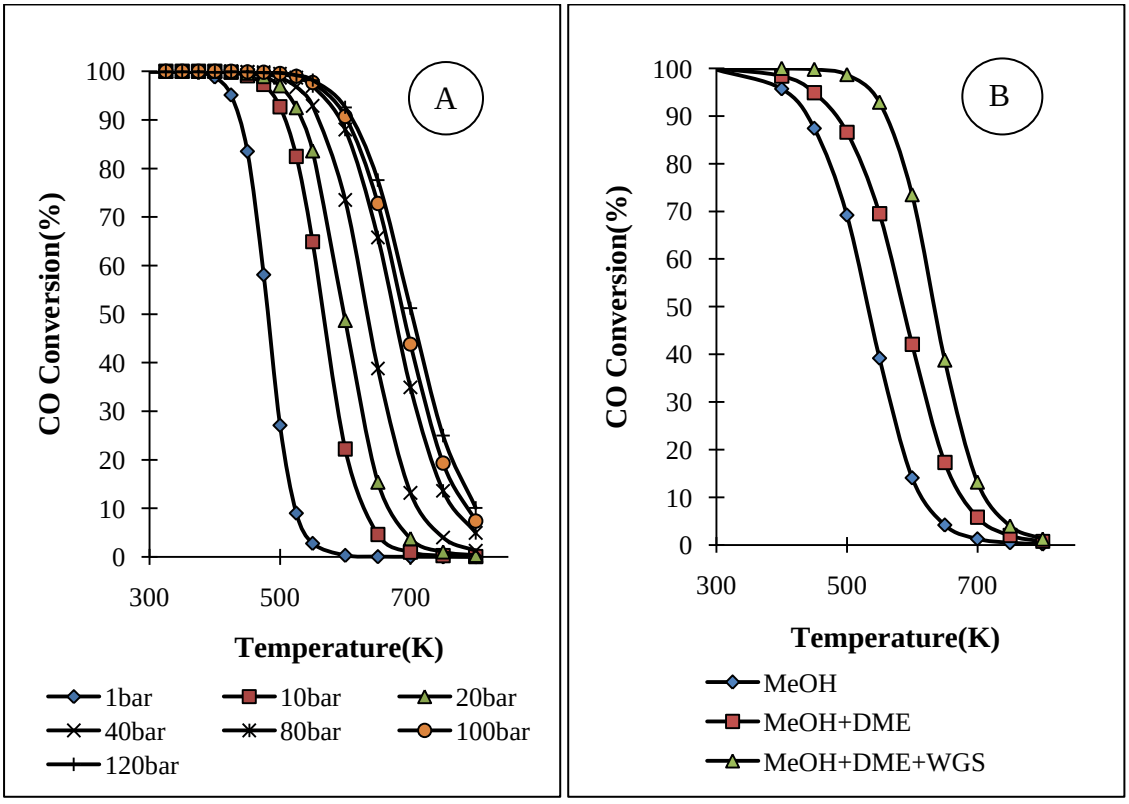


Figure 4.5 (A) Effect of temperature on equilibrium conversion of CO in the combined MeOH–DME–WGS system at different pressures, and (B) Comparison of the equilibrium conversion of CO as a function of temperature for the three cases (MeOH synthesis, combined MeOH–DME synthesis and combined MeOH–DME–WGS system) at 40bar

We again observe that the CO conversion decreases with increasing temperature, as occurs in an exothermic reaction. Furthermore the equilibrium conversion of CO improves as the pressure is raised at a fixed temperature. Again, the same would occur if the number of

moles decreases with the reaction. The MeOH reaction must drive this effect, as neither the DME nor the WGS reactions bring about a mole change.

In Figure 4.5B we compare the equilibrium CO conversion at a fixed pressure for the three different Cases (MeOH synthesis, combined MeOH–DME syntheses and the combined MeOH–DME–WGS system). This Figure shows that we achieve an even higher CO conversion when the three reactions occur simultaneously than in Cases 1 and 2. We attributed this phenomenon to the reaction of the water formed in the DME system with CO in the WGS reaction, resulting in a raised overall CO conversion.

On the other hand, the water created in this way causes the MeOH selectivity in the MeOH–DME–WGS system (Figure 4.6A) to fall below that of the MeOH–DME system (Figure 4.4A).[3] To compensate for this, and in accordance with le Chatelier's principle, reaction 4.2 must proceed in the direction of dehydration of more MeOH and thereby produce more water. As consequence of the decrease in MeOH selectivity the DME selectivity (Figure 4.6B) sinks to a level lower than that in Case 2 (Figure 4.4B).

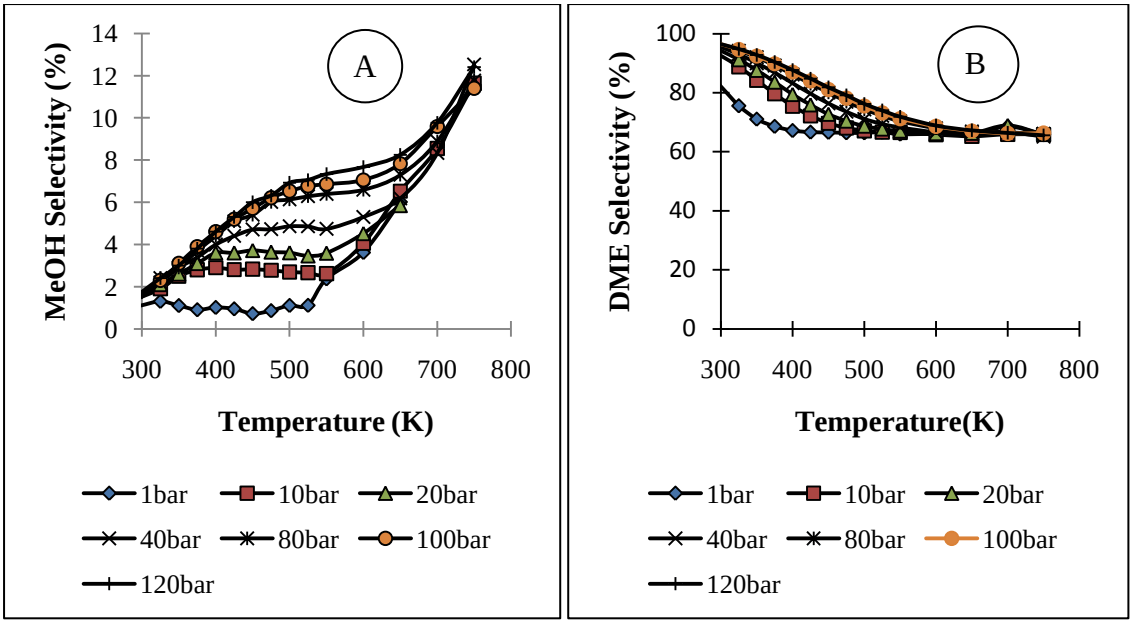


Figure 4.6 (A) Effect of temperature on MeOH selectivity, and (B) DME selectivity at different pressures in the combined MeOH–DME–WGS system

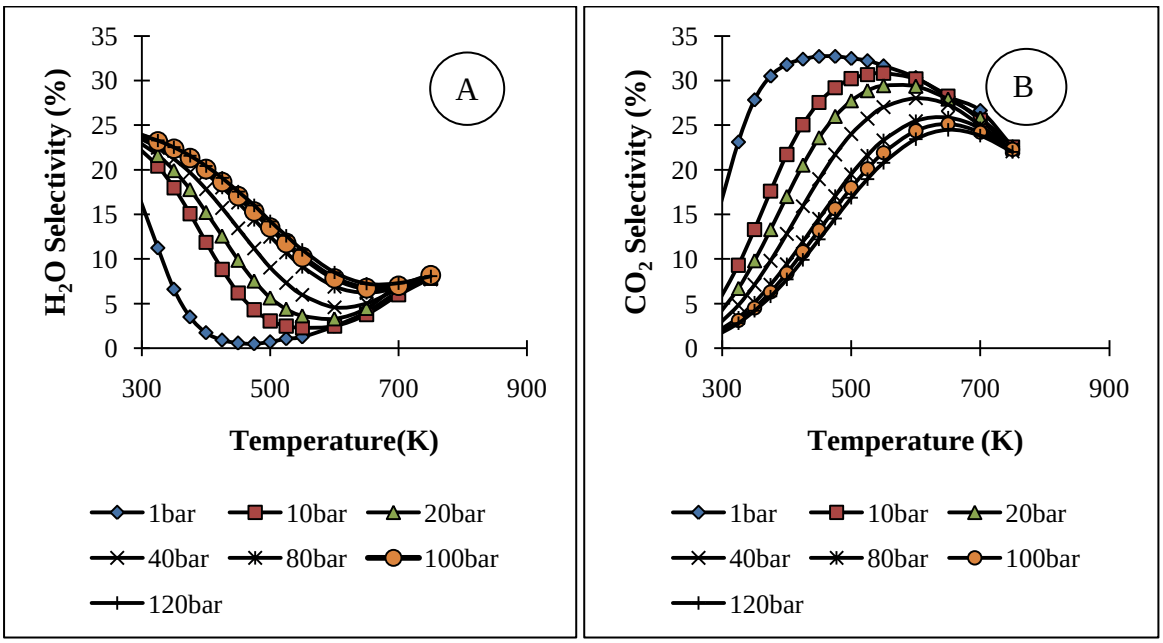


Figure 4.7 (A) Effect of temperature on H_2O selectivity, and (B) CO_2 selectivity at different pressures in the combined MeOH–DME–WGS system

The H_2O selectivity initially falls with the increase of temperature. The trend then reverses, and the selectivity rises slightly as temperature climbs further (Figure 4.7A). The temperature

at which the minimum selectivity occurs becomes higher as the pressure increases. Figure 4.7B shows that CO_2 selectivity is reduced as the pressure is raised, and reaches a maximum when the temperature is varied at constant pressure. The temperature at which this maximum occurs rises with increasing pressure. The CO_2:H_2O ratio as a function of temperature and pressure (Figure 4.8) reveals that the ratio is very pressure-sensitive at low pressures (around 1 bar), and becomes relatively insensitive at higher pressures. Furthermore, at low temperatures and raised pressures the CO_2:H2O ratio is close to zero, which indicates that the WGS reaction is not occuring to any appreciable extent.

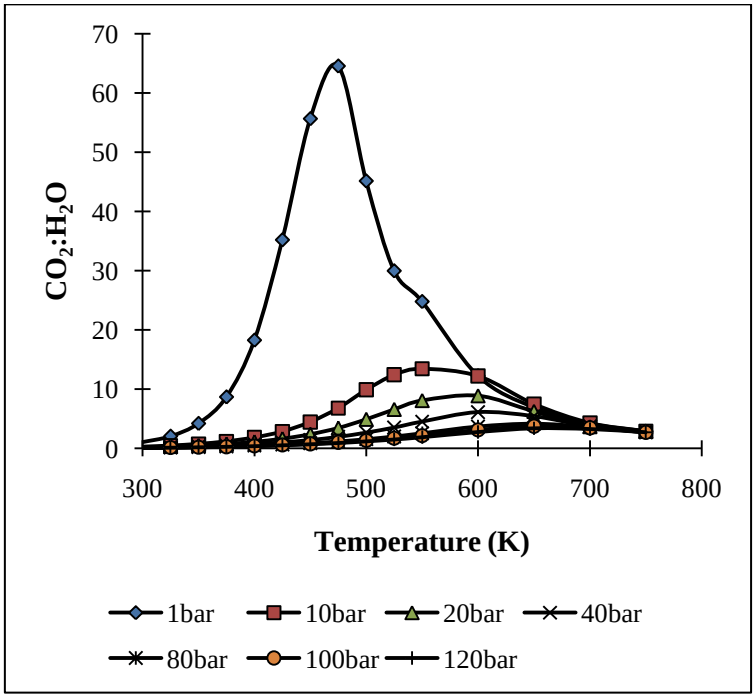


Figure 4.8 Effect of temperature and pressure on CO_2:H_2 ratio for the MeOH–DME–WGS system

4.2.6 Case 4. MeOH–WGS system

Figure 4.9A shows that pressure has little influence on the MeOH–WGS system, but brings about higher CO conversions that reduce with an increase of temperature. The trend of the

curves in this Figure looks different from those that illustrate the situation in previous Cases 1–3 (MeOH, MeOH–DME, MeOH–DME–WGS systems). The comparison of the four different systems in Figure 4.9B shows that the reactions of DME formation and WGS, when combined with the MeOH synthesis reaction, improve the CO conversion and allow high conversions to be achieved at reduced pressure.

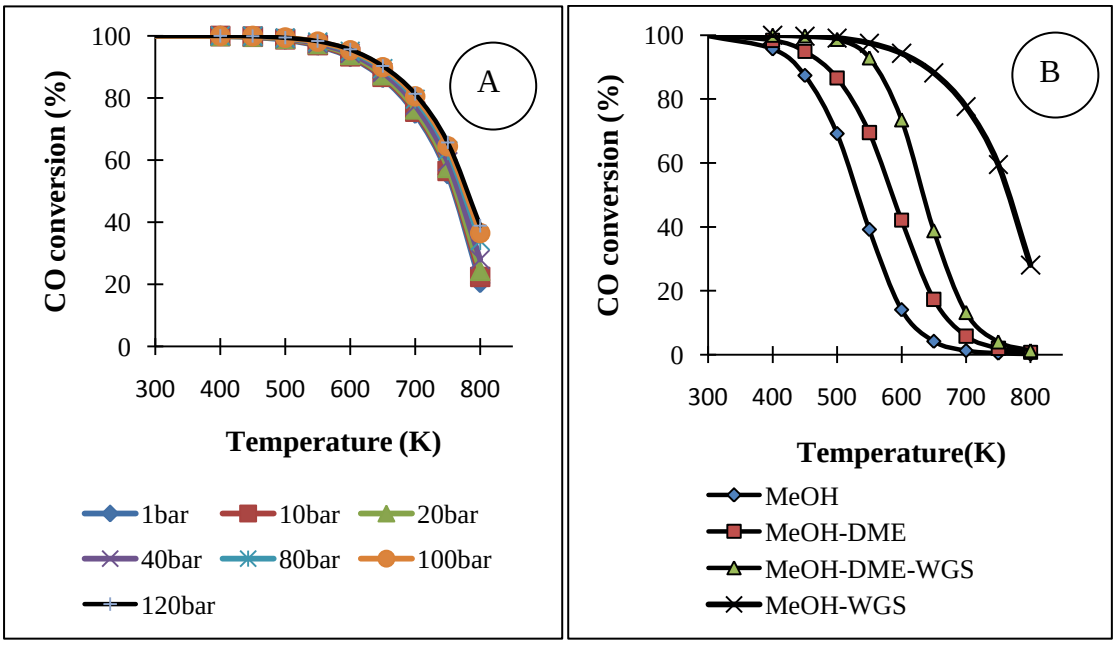


Figure 4.9 (A) CO conversion as function of temperature in the MeOH–WGS system, and (B) Comparison of the MeOH, MeOH–DME, MeOH–DME–WGS and MeOH–WGS systems at 50bar

4.2.7 <u>Case 5</u>. The MeOH, DME, WGS and CH_4 reactions all occur simultaneously in the reactor

Figures 4.10 and 4.11 report the result of the effect of the methane reaction equilibrium on DME and methanol production from synthesis gas. We have assumed that reactions 4.1-4 are occurring simultaneously in the same reactor and allowed to reach equilibrium. Figure 4.10 shows that the CO conversion is complete in the range of temperature 300-750K chosen for this conducted study and does not depend on the change in pressure even that reactions 4.1 and 4.4 are favoured by an increase in pressure. The synergetic effect between the four reactions involved in the system plays a significant role: product of reaction from one is

consumed by another in a cyclic way which allows the synthesis gas to be more consumed leading to the attainment of higher CO conversion.

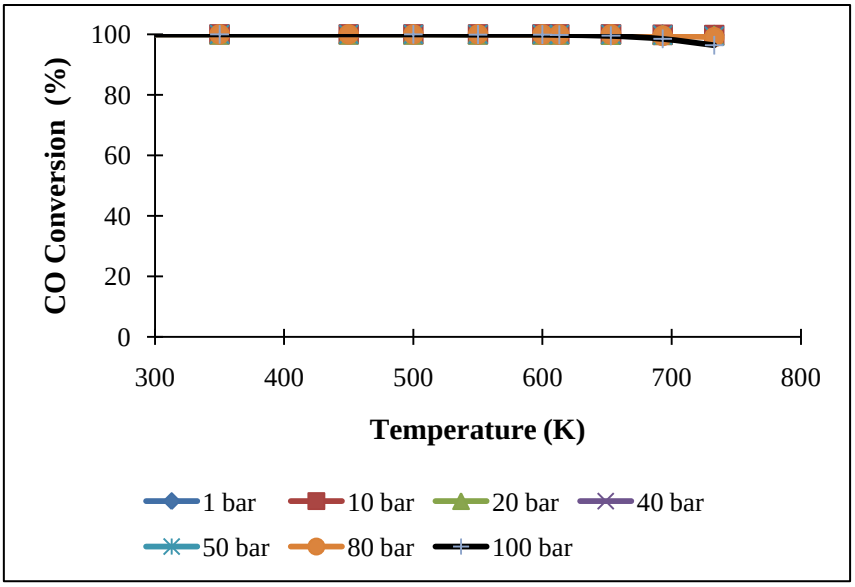


Figure 4.10 Effect of temperature on the CO equilibrium conversion at different pressures when the MeOH synthesis reactions (4.1), DME synthesis (4.2), WGS reaction (4.3) and CH_4 synthesis (4.4) are simultaneously occurring in the reactor.

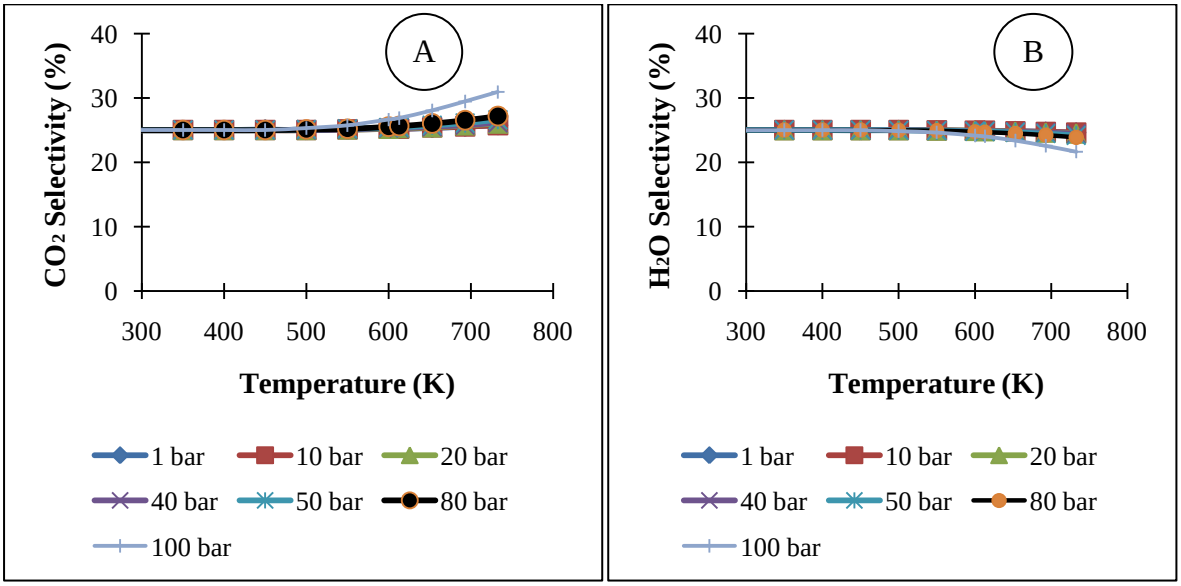


Figure 4.11(A) Effect of temperature on CO_2 selectivity, and (B) H_2O selectivity at different pressures in the combined MeOH–DME–WGS–CH_4 system

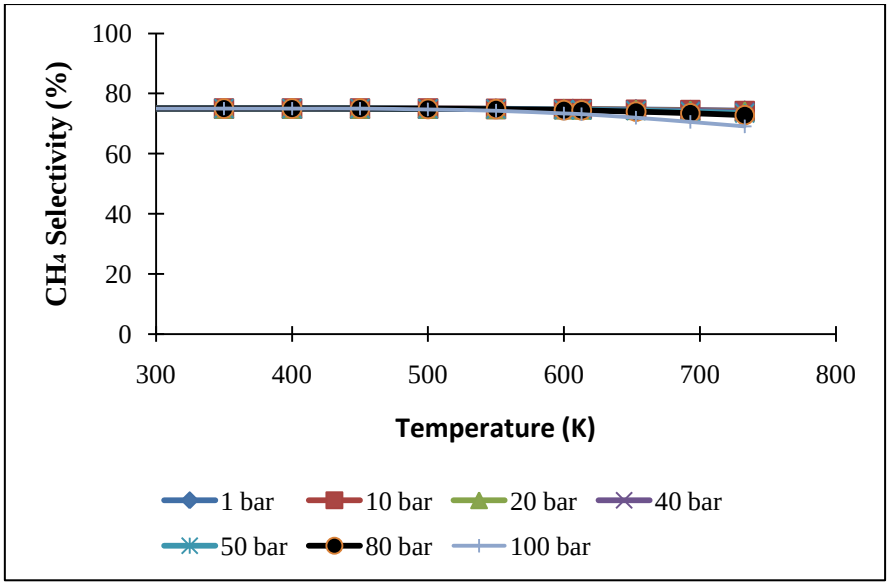


Figure 4.11C Effect of temperature on CH_4 selectivity at different pressures in the combined MeOH–DME–WGS–CH_4 system

The analysis of the product distribution reveals that CH_4, CO_2 and H_2O are the only compounds present in the reactor at equilibrium, there is no DME as we could predict from the net reaction (Equation 4.5). Methane and H_2O selectivities are quite constant with the rise in temperature but decrease slightly at high temperatures and pressures while the CO_2 selectivity increases with a rise in temperature and pressure. This situation can be observed if the catalyst used is highly active and possesses high selectivity to methane.

The methane synthesis reaction (Equation 4.4) is the one which is driving the all process as its equilibrium constant is far higher than the equilibrium constant of the three other reactions (Equations 4.1-3) taking place in the system.

4.3 Conversion of synthesis gas into DME using a gold based-catalyst

In this part of the research, undertaken for the study described in this dissertation, we explored the use of a gold-based catalyst to gain new insights into its catalytic behaviour and

the effects of process variables on the process of the conversion of synthesis gas to dimethyl ether. As described in Chapter 3, we tested a gold-based catalyst to determine its stability and the effect of the operating conditions (pressure, temperature, and space velocity) on CO conversion and selectivity to DME and by-products.

4.3.1 Catalyst characterization

The results of the BET analysis are displayed in Table 4.1. The Au/ZnO prepared for MeOH synthesis showed a very low specific surface area, which was improved by the addition of γ-Al_2O_3 for MeOH dehydration.

Table 4.1 BET results

Catalyst	**Surface area** ($m^2.g^{-1}$)	**Pore volume** ($cm^3.g^{-1}$)	**Pore size** (nm)
γ-Al_2O_3	208	0.36	6.93
Au/ZnO	4.72	0.024	20.4
Au/ZnO+ γ-Al_2O_3	107	0.19	7.13

The ICP (ES) analysis confirmed the 5% gold loading in the catalyst, and showed that the catalyst was pure at 99.99%. The iron concentration was very low, and the catalyst displayed some Fischer-Tropsch synthesis activity toward CH_4, and C_2-C_5.

The TEM images in Figure 4.12 showed that the gold particle size in the prepared catalysts was below 10μm and the particles were thoroughly dispersed on the ZnO support. The spherical shape of the gold was also noted. The smaller size of gold in the range below 10μm is thought by Kozlov *et al*. to have a positive effect on the activity of the catalyst.[69]

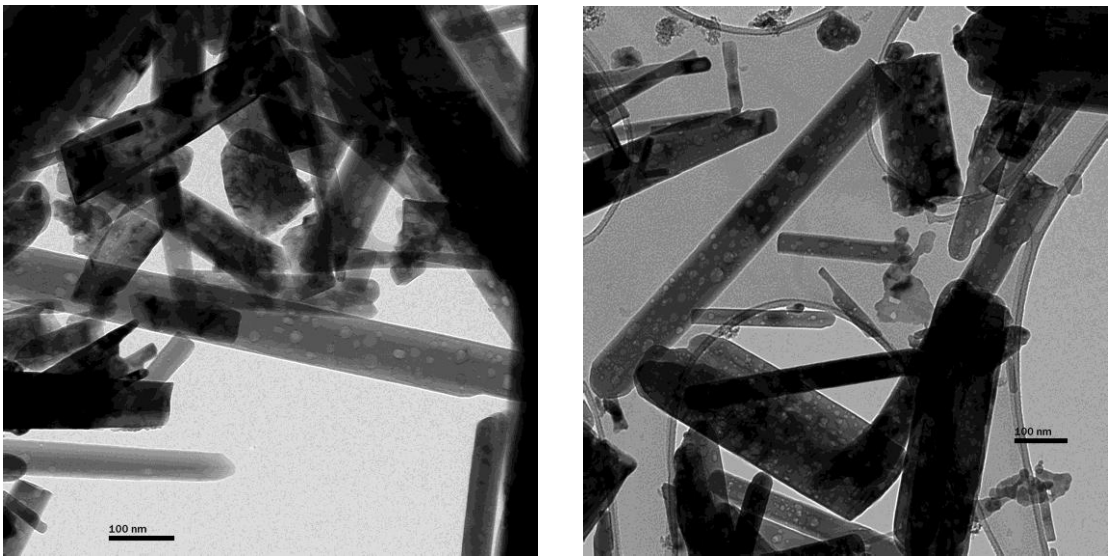


Figure 4.12 TEM results for the gold-based catalyst

4.3.2 Effect of temperature on product selectivity and CO conversion over Au/ZnO/γ-Al_2O_3

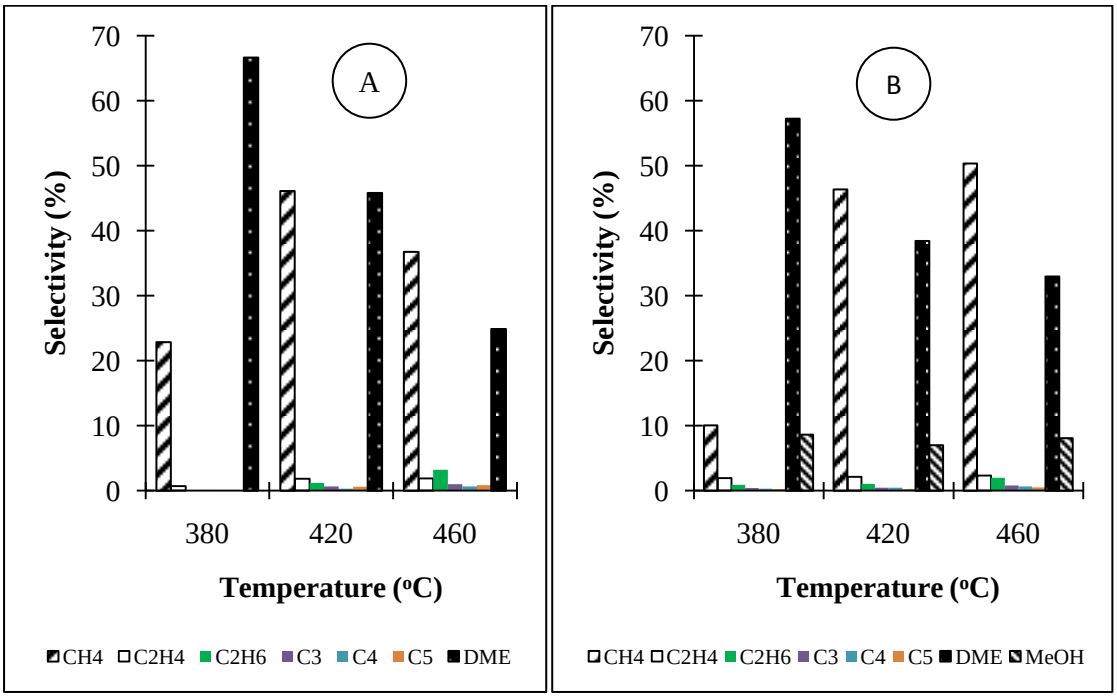


Figure 4.13 Selectivity of products as a function of temperature at a SV of 0.75 $dm^3.h^{-1}.g^{-1}$, and pressures of 20 bar (A) and 35 bar (B)

Figure 4.13A shows the selectivity of DME and hydrocarbons in the product (outlet) as a function of temperature at constant pressure and a SV of 20 bar and 0.75$dm^3.h^{-1}.g^{-1}$

respectively. The selectivity of DME declined with an increase in temperature, while the selectivity of CH_4 reached a maximum at 420^oC, and afterwards reduced at 460^oC. The selectivity to C_2 paraffin was higher than that to C_2 olefin. No MeOH production was noticed under these operating conditions at any of the chosen temperatures. The higher temperatures proved favourable for the formation of hydrocarbons (C_2–C_5).[70]

At 35 bar and 0.75 $dm^3.h^{-1}.g^{-1}$ (Figure 4.13B), DME selectivity dropped lower with an increase in temperature than under the previous set of conditions (20 bar). CH_4 selectivity was very low at 380^oC, but increased fourfold with the rise in temperature from 380 to 420^oC. However, when the temperature was raised once more, to 460^oC, only a 5% increase in CH_4 selectivity was noted. The selectivity of light hydrocarbons grew steadily. MeOH formation could be observed, and its selectivity was similar to that obtained at 380^oC. The drop in DME selectivity is probably due to unconverted MeOH, as some MeOH always undergoes conversion to light hydrocarbons. The actual product distribution seen was dependent on the reaction temperature. [15]

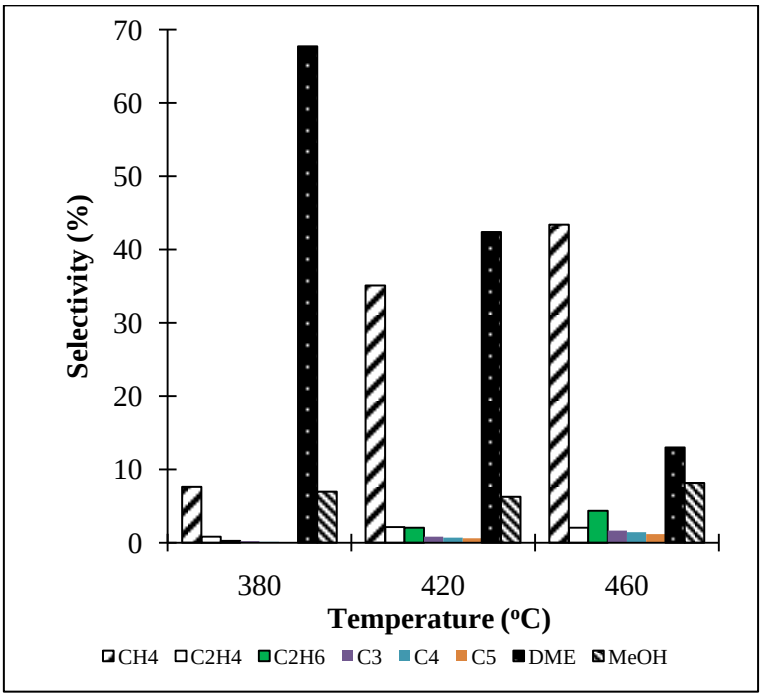


Figure 4.13C Selectivity of products as a function of temperature at a SV of 0.75 $dm^3.h^{-1}.g^{-1}$ and pressure of 50 bar

At 50 bar and 0.75 $dm^3.h^{-1}.g^{-1}$ (Figure 4.13C), high DME selectivity was achieved at a low temperature. Trends similar to those depicted in Figures 4.13A and 4.13B were observed, but the C_2 olefin-to-paraffin ratio decreased with the rise in temperature. Furthermore, the selectivity of C_2–C_5 hydrocarbons rose with the temperature to a greater degree than in the 20 bar operating conditions.

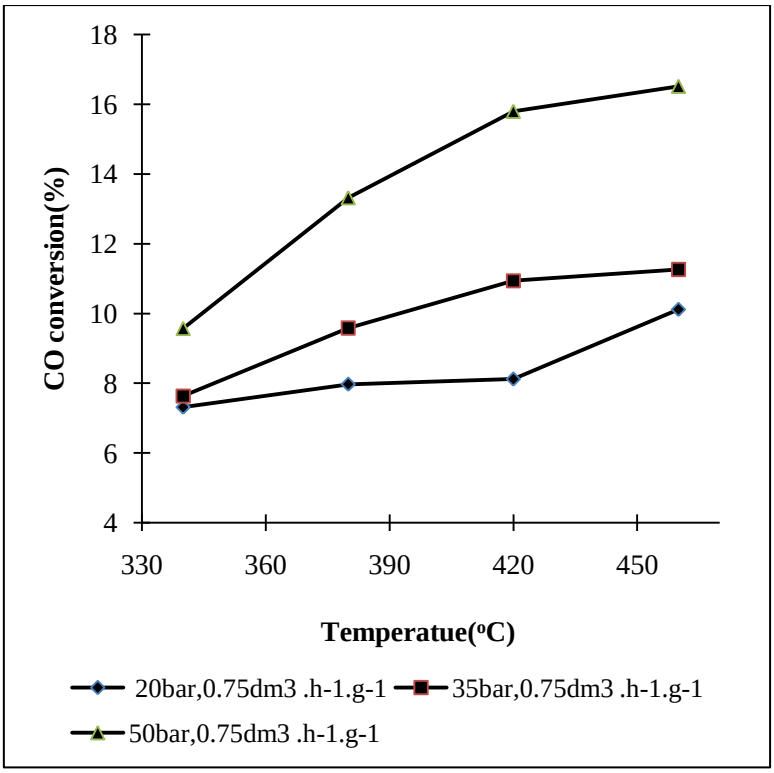


Figure 4.14 CO conversion as a function of temperature at a SV of 0.75 $dm^3.h^{-1}.g^{-1}$, and pressures of 20, 35 and 50 bar

Figure 4.14 shows that CO conversion increased with a rise in temperature at constant pressure and SV. This behaviour is different to that expected when the conversion is limited by thermodynamics, as the equilibrium conversion declines with an increment in temperature (see Figure 4.5). Thus we can conclude that the conversion is limited by kinetics rather than thermodynamics. The activity of the catalyst was favoured by the rise in temperature, but the catalyst was deactivated above 460°C. Water formation is also likely to reduce the acidity of the catalyst.[71]

4.3.3 Effect of pressure on product selectivity and CO conversion over Au/ZnO/γ-Al_2O_3

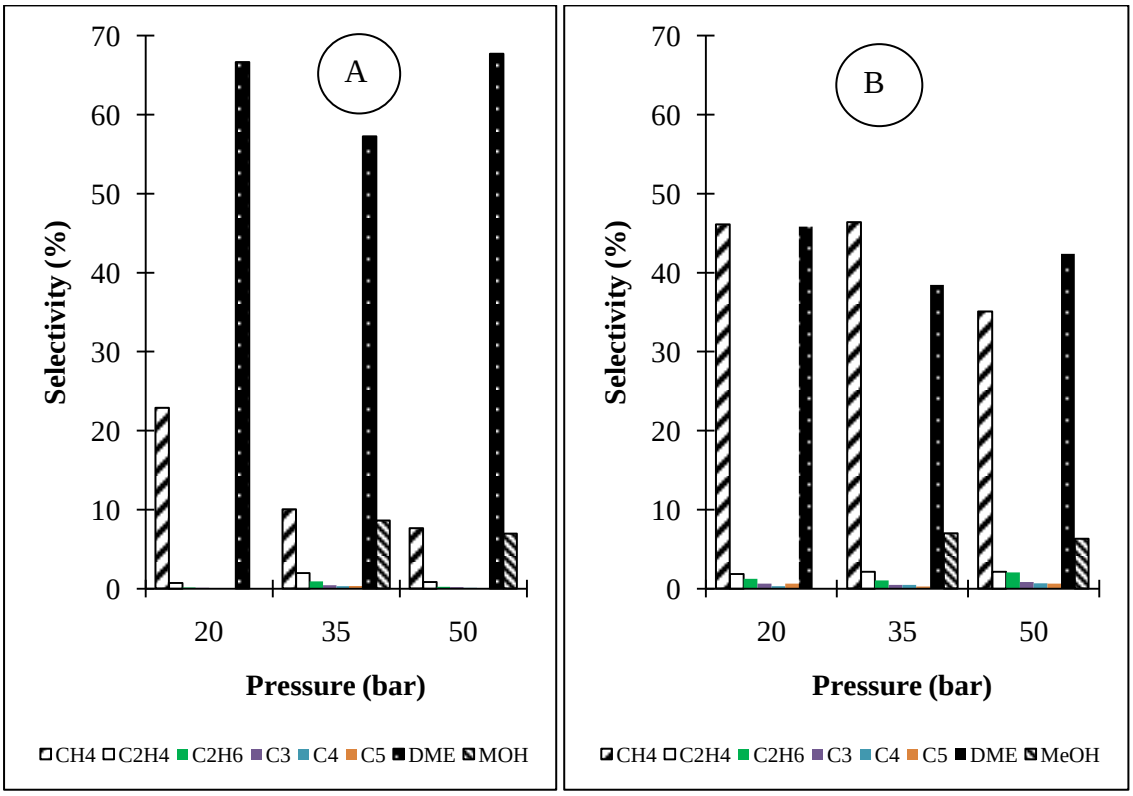


Figure 4.15 Selectivity of products as a function of pressure at a SV of 0.75 $dm^3.h^{-1}.g^{-1}$, and temperatures of 380°C (A) and 420°C (B)

Figures 4.15A-B reveal that the selectivity of methane reduced with an increase in pressure, while the selectivity of DME reached a minimum at 35 bar but remained dominant in the reaction products. No MeOH was present in the products at 20 bar. C_2 hydrocarbons were observed, and selectivity improved as both temperature and pressure rose. The ratio of C_2H_4 : C_2H_6 dropped with an increase in temperature and pressure. The formation of C_3–C_5 was observed at 420°C and 460°C. Selectivity to these products improved as the pressure increased.

Higher pressures favour the formation of MeOH, leading to improved DME selectivity, but the dehydration of MeOH to DME is not complete, because of secondary reactions of MeOH

to hydrocarbons, which are also present and competing under the operating conditions used.[72]

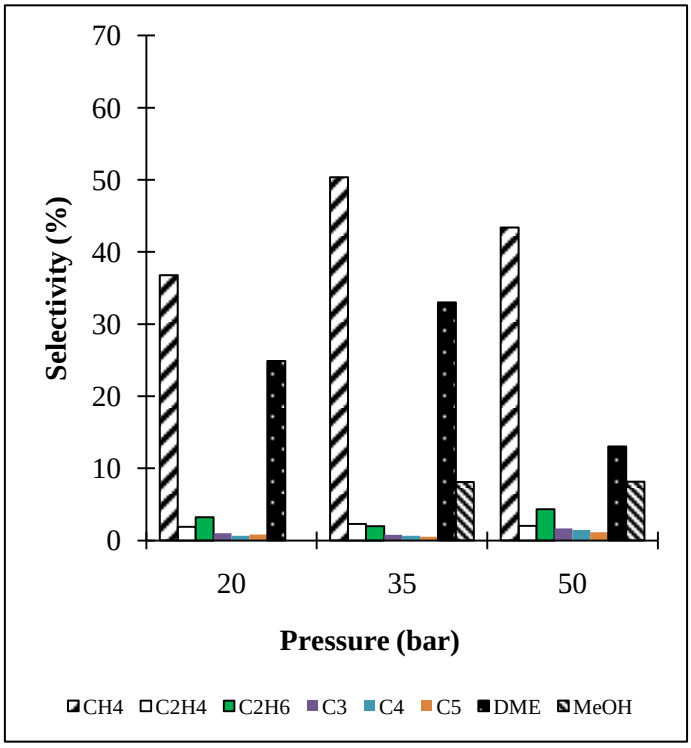


Figure 4.15C Selectivity of products as a function of pressure at a SV of 0.75 $dm^3.h^{-1}.g^{-1}$ and a temperature of 460^oC

In Figures 4.15C show also that the selectivity of DME reached a maximum at 35 bar, but then declined with a further rise in pressure. The ratio of selectivity CH_4 : DME improved with an increase in pressure, probably owing to kinetic limitations, because the MeOH dehydration reaction (as intermediate) is not favoured at higher temperatures, and the effect of temperature is greater than the effect of pressure.[55]

The CO conversion increased when the pressures were raised, as shown in Figure 4.14. The highest conversion was achieved when both the pressure and temperature were high (50 bar and 460^{o}C respectively).

4.3.4 Effect of space velocity on product selectivity and CO conversion Au/ZnO/γ-Al_2O_3

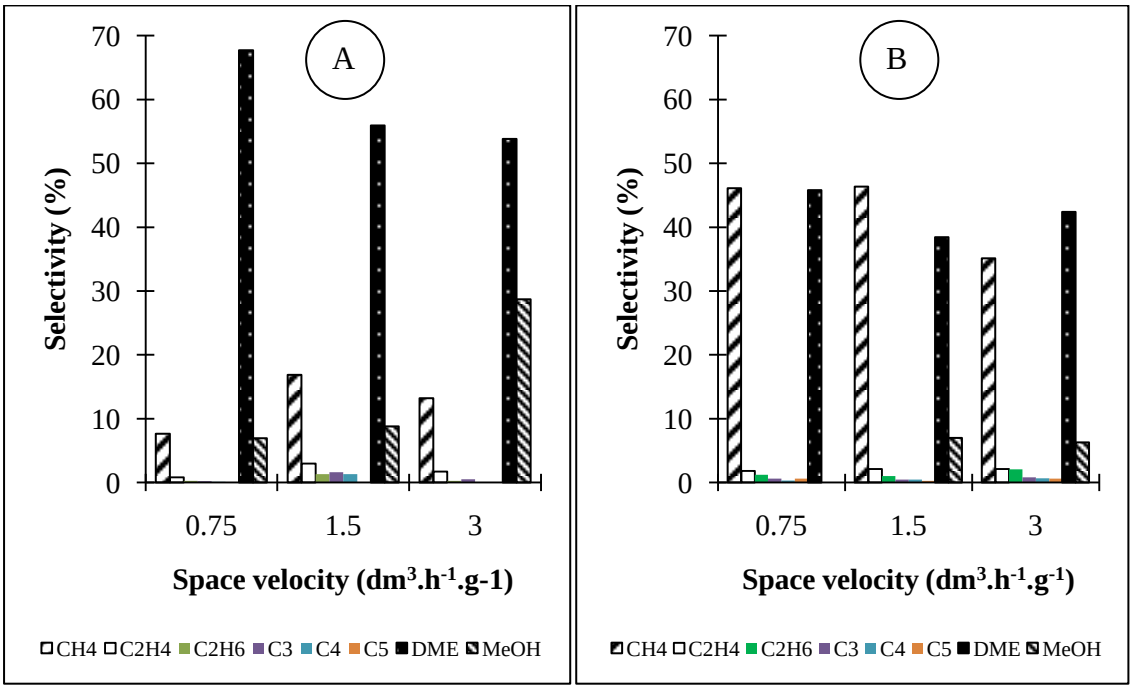


Figure 4.16 Selectivity of products as a function of SV at a constant pressure of 50 bar and temperatures of 380°C (A) and 420°C (B)

At constant pressure (50 bar), the highest DME and MeOH selectivities were observed at 380°C for a SV of 0.75 $dm^3.h^{-1}.g^{-1}$ and 3 $dm^3.h^{-1}.g^{-1}$ respectively, as shown in Figure 5.4. The highest CH_4 selectivity was found at 460°C and 3 $dm^3.h^{-1}.g^{-1}$ (see Figure 5.10 below). Figures 4.15 (A-B) and 5.10 show that the product distribution varied with the changes in SV and temperature. Moreover, the hydrocarbon selectivity was better at the high temperature 460°C and high SV of 3 $dm^3.h^{-1}.g^{-1}$, but the SV does not exert much influence on the MeOH selectivity (see Figure 4.16). This implies that MeOH decomposition occurs at a much higher rate than MeOH conversion to light hydrocarbons, since a longer residence time is realised at a lower SV.[73] Low space velocity promote the MeOH synthesis reaction, as the rate of MeOH dehydration is faster than that of methanol formation, much of MeOH produced is converted to DME.

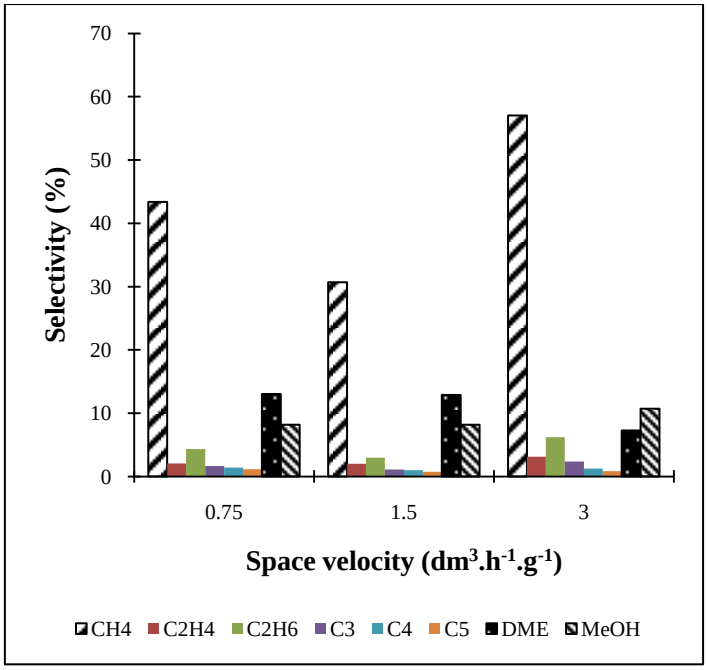


Figure 4.17 Selectivity of products as a function of SV at a constant pressure of 50 bar and temperature of 460°C

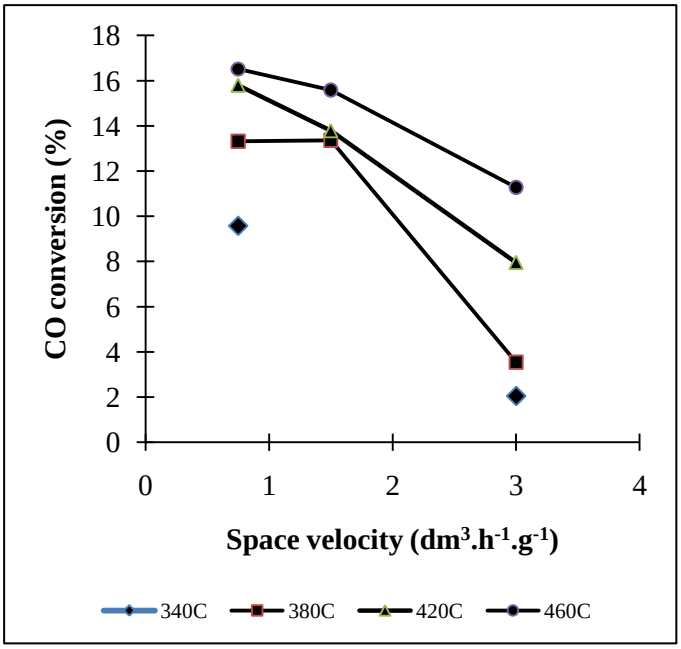


Figure 4.18 CO conversion as a function of SV at temperatures of 340, 380, 420 and 460°C

Figure 4.17 shows that the CO conversion declined with an increase in SV. CO conversion dropped more quickly for SVs higher than 1.5 $dm^3.h^{-1}.g^{-1}$ at all the temperatures examined. Increasing the SV leads to an increase in reactants velocity which improves the mass transfer

but reduces the contact time of the reactants. It is therefore very important to operate at low SV in order to achieve higher CO conversions.[57]

4.3.5 Catalyst stability

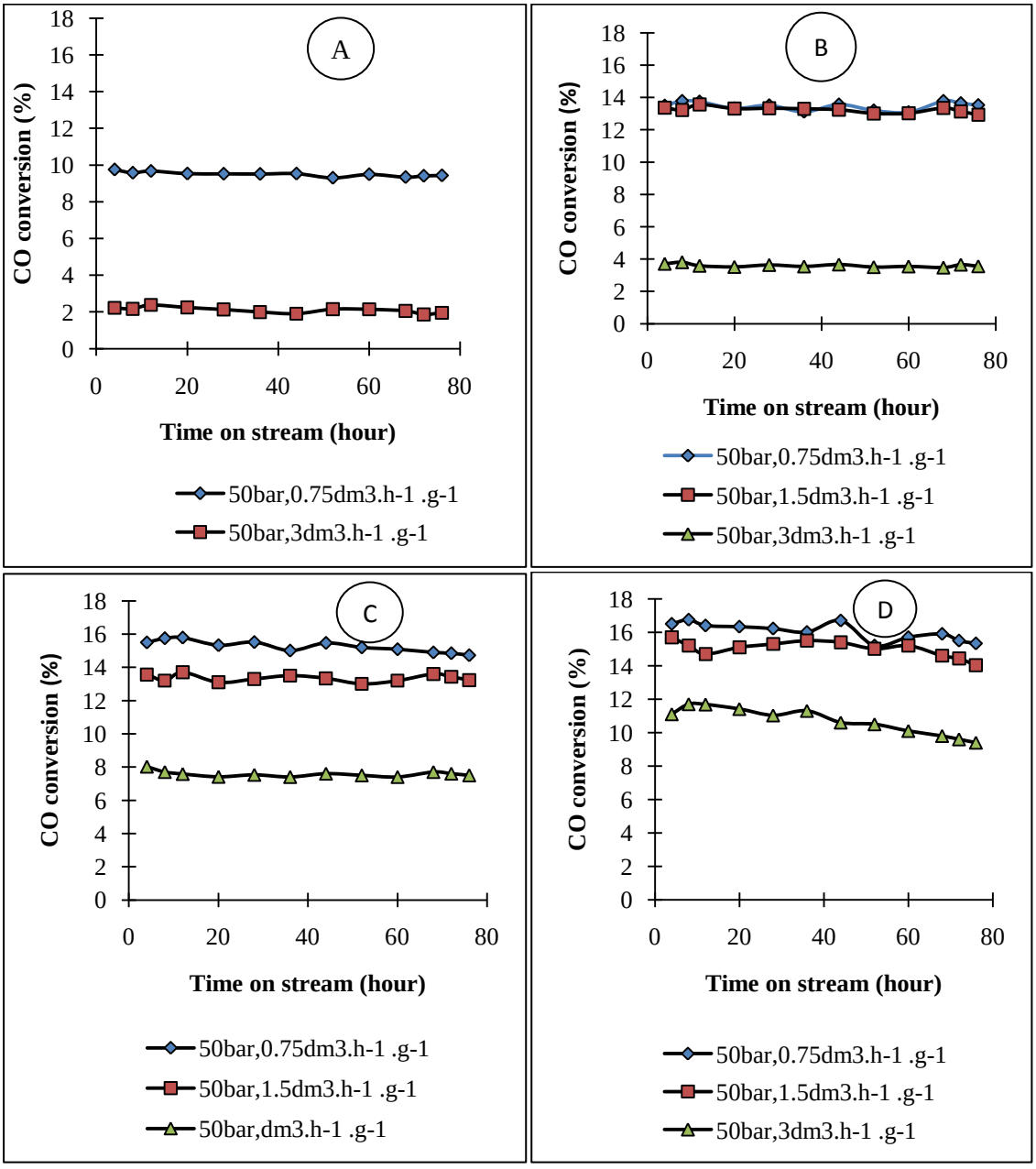


Figure 4.19 CO conversion as a function of time on stream at 340 (A), 380 (B), 420 (C) and 460°C (D) respectively

The stability of the Au/ZnO/γ-Al_2O_3 was studied for a period of 72 hours, as represented in Figure 5.18, A–D. The pressure was maintained at 50 bar while the temperatures and SVs

were varied. The catalyst was quite stable at 340^{o}C and 380^{o}C for the three different SVs. At 420^{o}C the CO conversion decreased slightly with further time on stream for all the chosen SVs.

The CO conversion dropped sharply at high temperature (460^{o}C) and high SV (3 $dm^3.h^{-1}.g^{-1}$) because under these conditions some of hydrocarbons tended to lead to carbon deposition on the surface of the catalyst. This resulted in blockage of the catalyst pores or active sites.[29]

4.3.6 Effect of the temperature on the equilibrium constant

In order to determine whether the reactions for MeOH formation (4.1), DME synthesis (4.2), WGS (4.3), and CH_4 production (4.4) are equilibrium-limited or far from equilibrium, we calculated the ratio of product to reactant compositions in the outlet of the reactor. These data were taken from each experimental run, and were compared with the theoretical equilibrium constants derived from the thermodynamic data appropriate for reactions 4.1–4.[67] The Gibbs free energies of formation $G_{f,T}$ and reaction $G_{rx,T}$ of the different products were determined using the equations 4.15 and 4.16.

$$Ln\left(K_p\right) = -\frac{\Delta G_{rx,T}}{RT} \qquad (4.29),$$

where T is the temperature in K; R is the molar gas constant; and the Gibbs free energy is expressed in $kJ.mol^{-1}$.

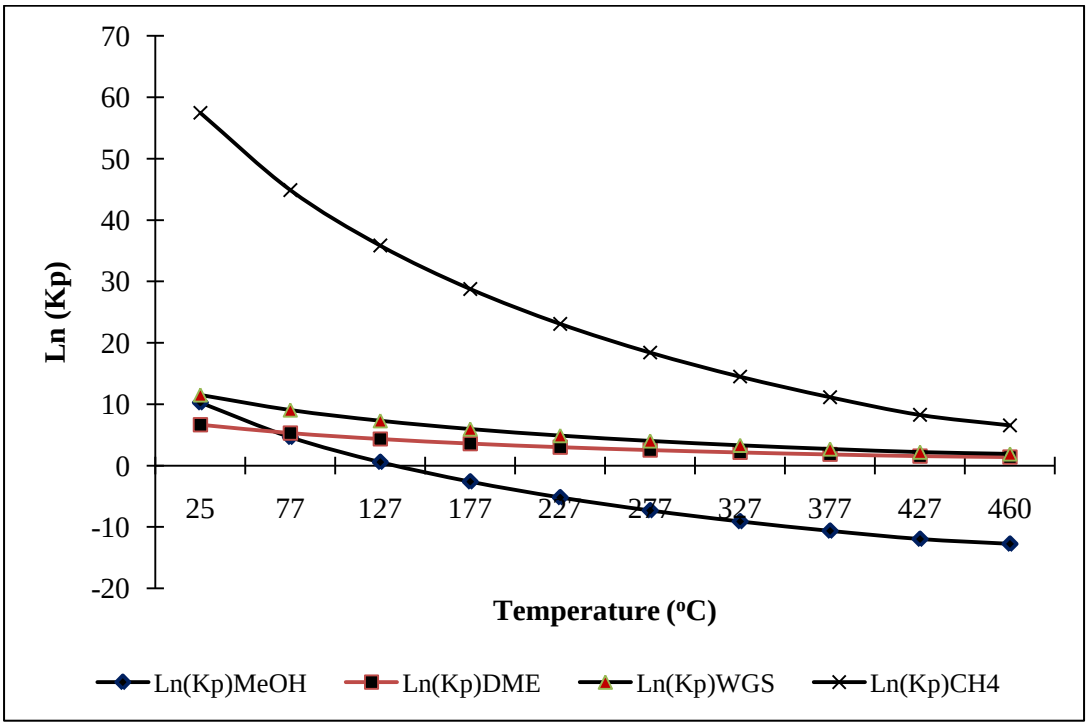


Figure 4.20 Theoretical Ln (Kp) function of temperature for the reactions 4.1 for MeOH; 4.2 for WGS; 4.3 for DME; and 4.4 for CH_4 formation

As can be seen in Figure 4.20, the formation of CH_4 is favoured above that of MeOH, WGS and DME in the 25–460^{o}C range. This indicates that the formation of CH_4 is kinetically limited over the tested catalyst. Furthermore, lower temperatures are best suited thermodynamically to MeOH formation. Below 25^{o}C, the equilibrium constant for 4.1 is higher than that of either the WGS or DME reactions.

The Ln (K_p) values (theoretical and experimental) are compared in Figure 4.20. These indicate that the WGS reaction (A) tends toward equilibrium with an increase in the temperature, while the opposite trend can be observed in the DME formation reaction (B), where the experimentally calculated ratio of products to reactant moves away from equilibrium constant derived from the thermodynamic data. Methane formation (C) is also far

from equilibrium at all the temperatures studied. Only the MeOH formation reaction (D) is a near-equilibrium situation found.

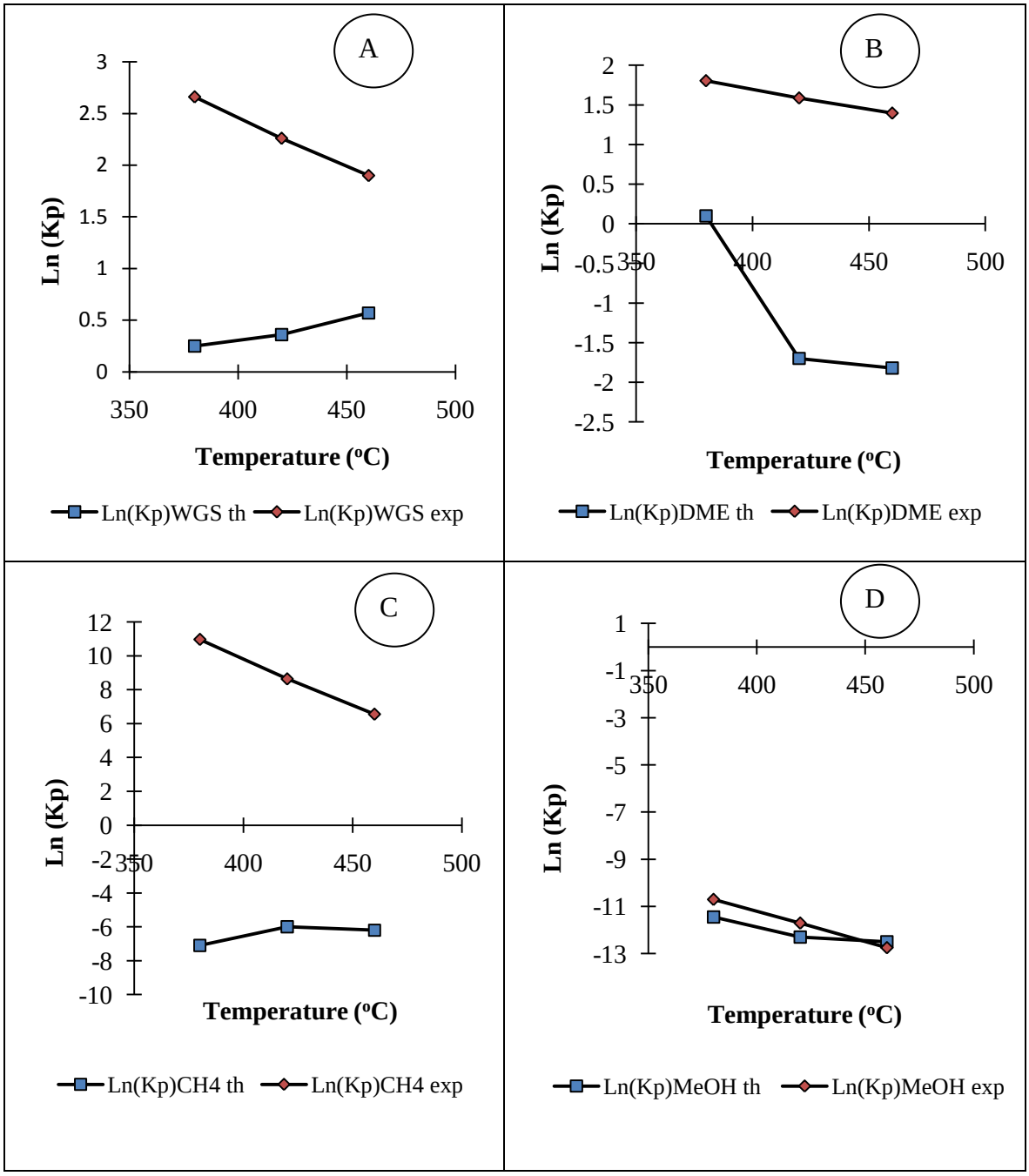


Figure 4.21 Calculated Ln (Kp) and experimental Ln (Kp) as a function of temperature at 35 bar and 0.75 $dm^3.h^{-1}.g^{-1}$, of the WGS reaction (A), DME formation (B), CH_4 formation (C) and MeOH synthesis (D)

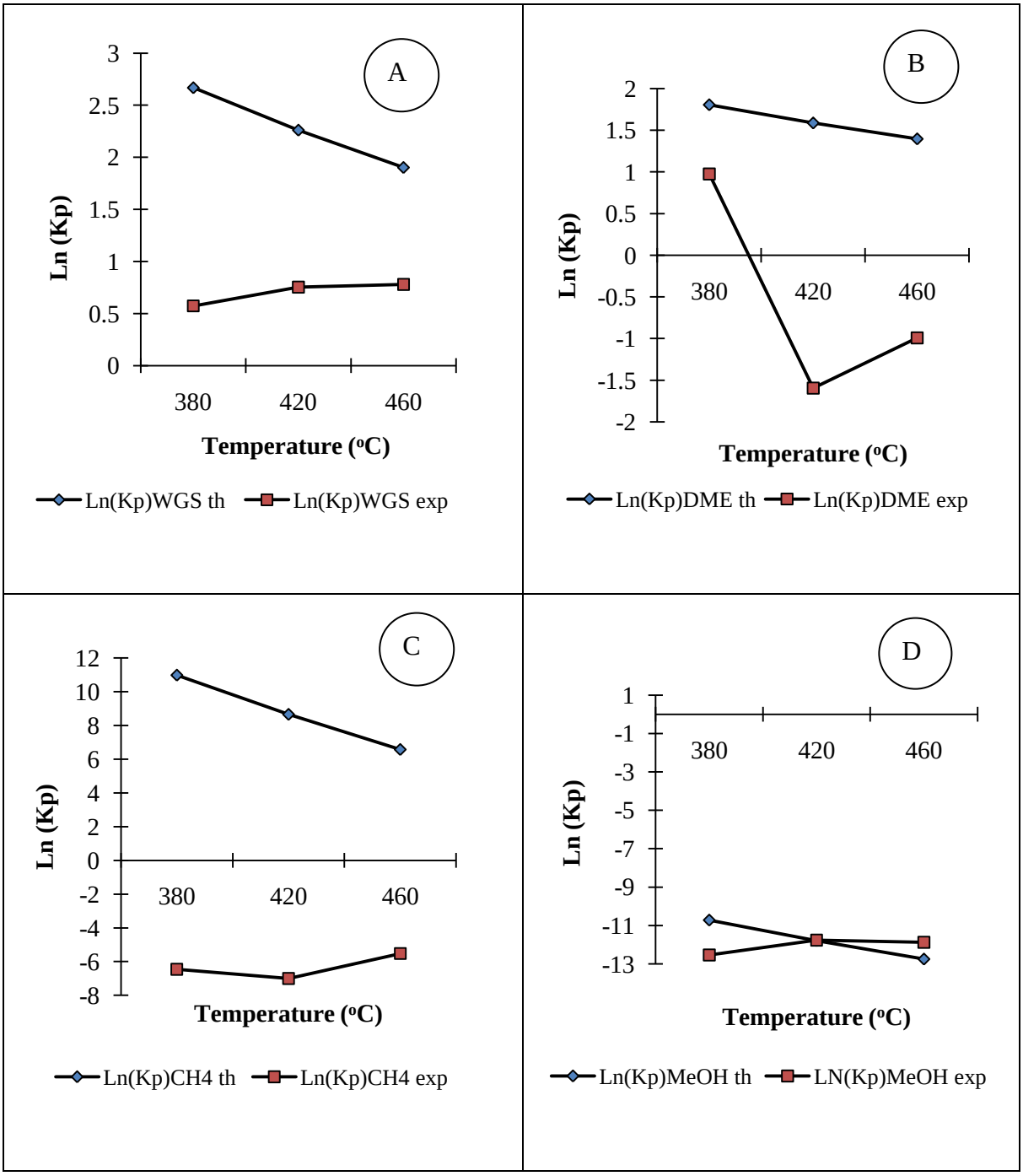


Figure 4.22 Calculated Ln (Kp) and experimental Ln (Kp) as a function of temperature at 50 bar and 0.75 $dm^3h^{-1}g^{-1}$ for WGS reaction (A), DME formation (B), CH_4 formation (C), and MeOH synthesis (D)

Figure 4.21 depicts a comparison of theoretical calculations of Ln (Kp) values and experimental Ln (Kp) values for WGS, DME, CH_4 and MeOH at 50 bar. We observed that the theoretical and experimental Ln (Kp) values differed substantially in all but, except in the case of the MeOH formation reaction, where there was close agreement at 420^{o}C and 460^{o}C. Equilibrium was more closely approached when the pressure was raised from 35 to 50 bar (compare Figures 4.20 and 4.21). This result is consistent with a model that postulates that the MeOH synthesis reaction is fairly rapid and reaches equilibrium, and that the conversion of methanol to DME and hydrocarbon synthesis is kinetically limited.

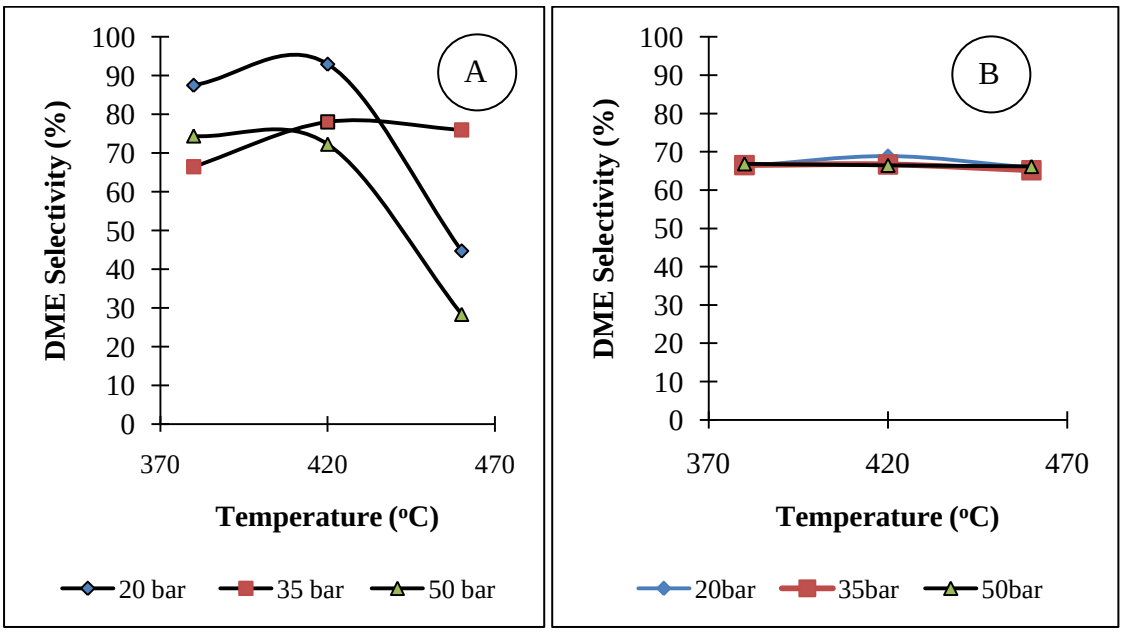


Figure 4.23 Experimental DME selectivity (A) and theoretical DME selectivity (B) for the DME–MeOH–WGS system at different temperatures and pressures

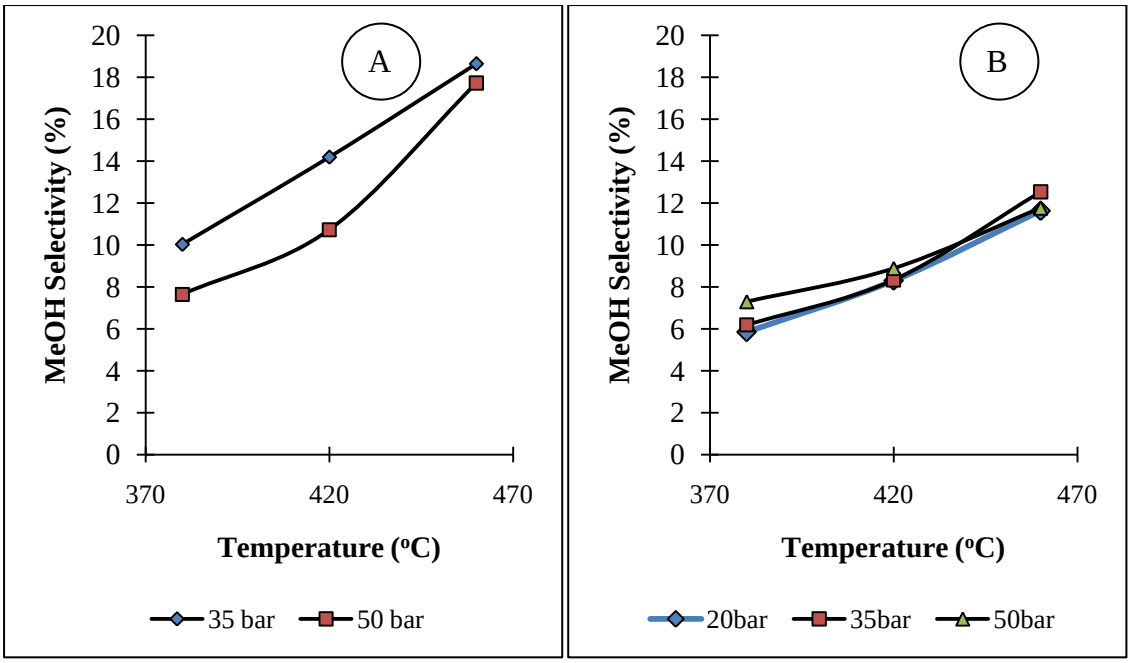


Figure 4.24 Experimental MeOH selectivity (A) and theoretical MeOH selectivity (B) for the DME–MeOH–WGS system at different temperatures and pressures

Methane production is obviously an important factor, in that at thermodynamic equilibrium, the dominant product would be methane (see Figure 4.11). However, we might ask whether the other products (DME, MeOH and, CO_2) achieve or approach equilibrium. The experimental selectivities were calculated based on the amount of oxygenates and carbon dioxide in the products of the reaction:

$$Selectivity\,component_i = \frac{molar\ \ flowrate\,of\ \ component\,i}{molar\ \ flowrate\,of\ \ CO_2 + 2\times DME + MeOH} \qquad (4.30),$$

where component *i* is either DME or MeOH. The theoretical selectivities were determined as in Figures 4.6 and 4.7. The experimentally observed selectivities of DME are pressure-dependent as predicted theoretically. The experimental selectivities increased with an increment in temperature from 380°C to 420°C, and then declined as the temperature rose further. Figure 4.22 shows that the theoretical and experimental DME selectivities were close

only at 35 bar. Our explanation is that the experimental DME selectivies dropped because of the increase in production of CO_2 at higher temperatures and a lower conversion of MeOH to DME. Experimental MeOH selectivities (Figure 4.23) are higher than the theoretically predicted MeOH selectivies, which implies that the conversion of MeOH to DME is kinetically limited.

4.4 Conclusion

When designing a process, one has to decide on a number of factors. The kinds of questions that need to be answered include:

- Which route will be most technically and economically profitable?
- What range of operating temperatures and pressures should be feasible?
- What are the maximum conversions that could be achieved?
- What range of selectivities could be expected?
- What is the effect of changes in temperature and pressure on conversion and selectivity?

The earlier these factors are determined, the more thoroughly one can screen the activities of the catalyst to be used in the process.

We have used thermodynamic tools to demonstrate that it is possible, by means of simple, rapid calculations, to combine the main reactions and to see how they affect the process under different operating conditions in the earliest stages of the design and catalyst development.

In this chapter we have shown that combining the MeOH and DME reactions makes an increase in the overall conversion of CO thermodynamically feasible. For example, at 500 K

and 40 bar the MeOH reaction would achieve an equilibrium conversion of 69.2%, while the combined MeOH–DME system would obtain 86.6%. This means that we can consider operating at lower pressures while continuing to achieve reasonable conversions. The selectivity is relatively pressure-insensitive, and low temperatures favour the production of DME, while higher temperatures increase the amount of MeOH produced rather than DME. Therefore if the aim is to produce DME, using low temperatures would favour that selectivity.

The WGS reaction increases the achievable CO conversion significantly in the MeOH–DME–WGS system. However, at high temperatures much of the improvement in CO conversion is attributable to the increase CO_2 production caused by the WGS reaction, which is not particularly useful in terms of CO_2 emission. Thus a balance between producing CO_2 and increasing the DME selectivity (by decreasing the temperature) has to be achieved. However, if the CO_2 that is produced in the process is recycled, this would inhibit CO_2 production in the reactor. It follows that the lower operating temperature would probably be the more important consideration, because it would increase the overall CO conversion and maximize DME selectivity.

Methane production from syngas is the most favour thermodynamically when it is in equilibrium in a system of reactions containing MeOH, DME, WGS, and CH_4, and it is the main product and theoretically no MeOH and/or DME are produced, therefore the choice of a better catalyst which is has higher selectivity toward DME and MeOH is crucial as they are the desirable product.

The gold hybrid catalyst was active in the range of temperatures 340–460^{o}C, which is higher than the traditional range of 280–300^{o}C employed when the commercial $ZnO/CuO/Al_2O_3 + \gamma$-

Al_2O_3 catalyst is used. Lower temperatures tended to result in poor catalytic activity, while higher temperatures led to the deactivation of the catalyst. The highest conversion in the synthesis gas to DME process was achieved at high pressure (50 bar), low SV (0.75 $dm^3.h^{-1}.g^{-1}$) and high temperature (460^oC). Lower temperatures and lower space velocities led to higher DME and low hydrocarbon selectivity. The catalyst was more stable between 340–420^oC.

CHAPTER 5

GENERAL CONCLUSIONS

The results from the study of synthesis gas conversion to DME and light hydrocarbons lead to the following conclusions.

The thermodynamic study of the process confirmed that the one-step synthesis gas to DME process is economically profitable because it achieves higher conversions and reduces separation costs. We also found that low temperatures are favourable for DME production, and that the maximum theoretical CO conversion is obtained at low temperatures and high pressures.

The formation of CH_4 over a $ZnO/CuO/Al_2O_3 + \gamma\text{-}Al_2O_3$ catalyst is kinetically limited, while that of MeOH is thermodynamically suited to lower temperatures.

A comparison of Ln (K_p) values (theoretical and experimental) showed that the MeOH synthesis reaction is in equilibrium compared with the other main reactions. Furthermore, the equilibrium is closely approached with an increase in pressure. High pressures and high temperatures favour the tendency to reach equilibrium.

The selectivities of DME obtained experimentally are pressure-dependent, as predicted theoretically. Experimental DME selectivities declined because of the increased production of CO_2 at higher temperatures and the lower conversion of MeOH to DME. Experimental MeOH selectivities are higher than those theoretically predicted. This means that the conversion of MeOH to DME is kinetically limited.

The gold-based catalyst $ZnO/CuO/Al_2O_3 + \gamma\text{-}Al_2O_3$ was proved to be stable between 340–420^{o}C, but catalyst deactivation occurs at 460^{o}C. DME selectivity is improved when the SV and temperature are low. These conditions limit the formation of hydrocarbons.

REFERENCES

[1] C.W. Corti, R.J. Holliday, Increasing gold demand: new industrial applications, *Applied Earth Science*, 114 (2005) 115-121.

[2] Recognizing the best in innovation: breakthrough catalyst. R&D Magazine, (September 2005) pp.20.

[3] J. Hagen, *Industrial Catalysis. A Practical Approach*, in: WILEY-VCH Verlag GmbH & Co. KGaA (Ed.), Weinheim, Germany, 2006, pp. 179-180,270-272.

[4] P. Stoltze, *Introduction to heterogeneous catalysis*, Department of Chemistry and Applied Engineering Science, Aalborg University, Denmark, (2000),pp 59-70
.
[5] J. Haber, J.H. Block, B. Delmon, Manual ofmethods and procedures for catalyst characterization (Technical Report), *Pure and Applied Chemistry*, 67 (1995) 1257-1306.

[6] M. Haruta, Catatysis of gold nanoparticles deposited on metal oxides, *Cattech*, 6 (2002) 102-115.

[7] S. Biella, G.L. Castiglioni, C. Fumagalli, L. Prati, M. Rossi, Application of gold catalysts to selective liquid phase oxidation, *Catalysis Today*, 72 (2002) 43-49.

[8] A. Ueda, M. Haruta, Nitric Oxide Reduction with Hydrogen, Carbon Monoxide, and Hydrocarbons over Gold Catalysts, *Gold Bulletin*, 32 (1999) 3-11.

[9] A.I. Kozlov, A.P. Kozlova, H. Lui, Y. Iwasawa, A new approach to active supported Au catalysts, *Applied Catalysis A: General*, 182 (1999) 9-28.

[10] G.J. Hutchings, Catalysis by gold, *Catalysis Today*, 100 (2005) 55-61.

[11] S. Schimpf, M. Lucas, C. Mohr, U. Rodemerck, A. Bruckner, J. Radnik, H. Hofmeister, P. Claus, Supported gold nanoparticles: in-depth catalyst characterization and application in hydrogenation and oxidation reactions, *Catalysis Today*, 72 (2002) 63-78.

[12] M. Haruta, Size and support dependency in the catalysis of gold, *Catalysis Today*, 36 (1997) 153-166.

[13] D. Cameron, R. Hollyday, D. Thompson, Gold's future role in fuel cell systems, *Journal of Power Sources*, 118 (2003) 298-303.

[14] H.B. Calvin, J.F. Robert, *Fundamentals of Industrial catalytic processes*, second ed., John Wiley & Sons, Inc, Hoboken, New Jersey, 2006.

[15] G. Olah, A. Goeppert, S.P.G. K., *Beyond Oil and Gas: The Methanol Economy*, Second ed., Federal Republic of Germany, 2009.

[16] M.V. Twigg, *Catalyst handbook*, Second ed., Wolfe Publishing Ltd, Frome, England, 1989.

[17] F. Yaripour, M. Mollavali, S.M. Jam, H. Atashi, Catalytic Dehydration of Methanol to Dimethyl Ether Catalyzed by Aluminum Phosphate Catalysts, *Energy & Fuels*, 23 (2009) 1896-1900.

[18] E.F. Sousa-Aguiar, L.G. Appel, C. Mota, Natural gas chemical transformations: The path to refining in future, *Catalysis Today*, 101 (2005) 3-7.

[19] T. Ogawa, N. Inoue, T. Shikada, Y. Ohno, Direct dimethyl ether synthesis, *Journal of Natural Gas Chemistry* 12 (2003) 219-227.

[20] D. Varisli, T. Dogu, Production of Clean Transportation Fuel Dimethylether by Dehydration of Methanol Over Nafion Catalyst, *G.U. Journal of Science*, 21 (2008) 37-41.

[21] Y. Adachi, M. Komoto, I. Watanabe, Y. Ohno, K. Fujimoto, Effective utilisation of remote coal through dimethyl ether synthesis, *Fuel* 79 (2000) 229-234.

[22] M. Yao, Z. Chen, Z. Zheng, B. Zhang, Y. Xing, Study on the controlling strategies of homogeneous charge compression ignition combustion with fuel of dimethyl ether and methanol, *Fuel*, 85 (2006) 2046-2056.

[23] Y. Seo, S.-H. Jo, H.-J. Ryu, C.-K. Yi, G.T. Jin, One-step DME Synthesis from Coal-Derived,CO-Rich Syngas in a Slurry Reactor, *Journal of Chemical Engineering of Japan*, 41 (7) (2008) 585-589.

[24] T.A. Semelesberger, R.L. Borup, H.L. Greene, Dimethyl ether (DME) as an alternative fuel, *Journal of Power Sources*, 156 (2006) 497-511.

[25] M. Marchionna, R. Patrini, D. Sanfilippo, G. Migliavacca, Fundamental investigations on di-methyl ether(DME) as LPG substitute or make-up for domestic uses, *Fuel Processing Technology*, 89 (2008) 1255-1261.

[26] T.A. Semelsberger, R.L. Borup, H.L. Greene, Dimethyl ether (DME) as an alternative fuel, *Journal of Power Sources*, 156 (2006) 497-511.

[27] Y. Tanaka, R. Kikuchi, T. Takeguchi, K. Eguchi, Steam reforming of dimethyl ether over composite catalysts of γ-Al2O3 and Cu-based spinel, *Applied Catalysis A: Environmental*, 57 (2005) 211-222.

[28] G.R. Moradi, S. Nosrati, F. Yaripour, Effect of the hybrid preparation method upon synthesis of dimethyl ether from synthesis gas, *Catalysis Communications*, 8 (2007) 598-606.

[29] A.T. Aguayo, J. Erena, I. Siera, M. Olazar, J. Bilbao, Deactivation and regenaration of hybrid catalysts in the single-step synthesis of dimethyl ether from syngas and CO_2, *Catalysis Today* 106 (2005) 265–270.

[30] J.-L. Li, X.-G. Zhang, T. Inui, Improvement in the catalyst activity for direct synthesis of dimethyl ether from synthesis gas through enhancing the dispersion of CuO/ZnO/γ-Al_2O_3, *Applied Catalysis A: General*, 147 (1996) 23-33.

[31] Y. Fu, T. Hong, J. Chen, A. Auroux, J. Shen, Surface acidity and the dehydration of methanol to dimethyl ether, *Termochimica Acta*, 434 (2005) 22-26.

[32] K. Sun, W. Lu, F. Qiu, S. Lui, X. Xu, Direct synthesis of DME over bifunctional catalyst: surface poperties and catalytic performance, *Applied Catalysis A: General*, 252 (2003) 243-249.

[33] X. An, Y.-Z. Zuo, Q. Zhang, D.-Z. Wang, J.-F. Wang, Dimethyl Ether Synthesis from CO_2 Hydrogenation on a CuO-ZnO-Al2O_3-ZrO_2/HZSM-5 Bifunctional, *Catalyst, Industrial Engineering Chemical Resouces*, 47 (2008) 6547-6554.

[34] G.R. Moradi, J. Ahmadpour, F. Yaripour, J. Wang, Equilibrium calculations for direct synthesis of dimethyl ether from syngas, *The Canadian Journal of Chemical Engineering*, 89 (2011) 108-115.

[35] V. Vishwanathan, K.-W. Jun, J.-W. Kim, H.-S. Roh, Vapour phase dehydration of crude methanol to dimethyl ether over Na-modified H-ZSM-5 catalysts, *Applied Catalysis A: General*, 276 (2004) 251-255.

[36] F. Hayer, H. Bakhtiary-Davijany, R. Myrstad, A. Holmen, P. Pfeifer, H.J. Venvik, Synthesis of dimethyl ether from syngas in a microchannel reactor-Simulation and experimental study, *Chemical Engineering Journal*, 167 (2010) 610-15.

[37] L. Wang, Y. Qi, Y. Wei, D. Fang, S. Meng, Z. Liu, Research on the double-function catalyst for DME synthesis from syngas, *Catalysis Letters*, 106 (2006) 61-66.

[38] D. Mao, W. Yang, J. Xia, B. Zhang, Q. Song, Q. Chen, Highly effective hybrid catalyst for the direct synthesis of dimethyl ether from syngas with magnesium oxide-modifed HZSM-5 as a dehydration component, *Journal of Catalysis*, 230 (2005) 140-149.

[39] L. Liu, W. Huang, Z. Gao, L. Yin, The Dehydration of Methanol to Dimethyl Ether over Novel Slurry Catalyst, Energy Sources, Part A: Recovery, *Utilization, and Environmental Effects*, 32 (2010) 1379-1387.

[40] F. Yaripour, M. Mollavali, S.M. Jam, H. Atashi, Catalytic dehydration of methanol to dimethyl ether catalyzed by aluminum phosphate catalysts, *Energy & Fuels*, 23 (2009) 1896-1900.

[41] Y. Zhao, A. Mpela, D.I. Enache, S.H. Taylor, D. Hilderbrandt, D. Glasser, G.J. Hutchings, M.P. Atkins, M.S. Scurrell, Study of carbon monoxide hydrogenation over supported Au catalyst, *Studies in surface Science and Catalysis*, 163 (2007) 141-151.

[42] A. Mpela, D. Hilderbrandt, D. Glasser, M.S. Scurrell, G.J. Hutchings, Low pressure methanol/dimethyl ether synthesis from syngas on gold-based catalyst, *Gold Bulletin*, 40 (3) (2007) 219-224.

[43] E.S. Yoon, C. Han, A Review of Sustainable Energy - Recent Development and Future Prospects of Dimethyl Ether (DME), in: C.A.O.d.N. Rita Maria de Brito Alves, Evaristo Chalbaud Biscaia, Jr. (Eds.) *Computer Aided Chemical Engineering, Elsevier*, 2009, pp. 169-175.

[44] C.-J. Lee, Y. Lim, H.S. Kim, C. Han, Optimal Gas-To-Liquid product Selection from Natural Gas under Uncertain Price Scenarios, *Industrial Engineering Chemical Resouces*, 48 (2009) 794-800.

[45] D.J. Wilhelm, D.R. Simbeck, A.D. Karp, R.L. Dickenson, Syngas production for gas-to-liquids applications: technologies,issues and outlook, *Fuel Processing Technology*, 71 (2001) 139-148.

[46] X.D. Peng, A.W. Wang, B.A. Toseland, P.J.A. Tijm, Single-Step Synthesis-to-Dimethyl Ether Process for Optimal Productivity,Minimal Emissions, and Natural Gas-Dirived Syngas, *Industrial Engineering Chemical Resouces*, 38 (1999) 4381-4388.

[47] D. Song, W. Cho, G. Lee, D.K. Park, E.S. Yoon, Numerical Analysis of a Pilot-Scale Fixed-Bed Reactor for Dimethyl Ether (DME) Synthesis, *Industrial Engineering Chemical Resouces*, 47 (2008) 4553-4559.

[48] T. Wang, J. Wang, Y. Jin, Slurry Reactors for Gas-to-Liquid Processes: A Review, *Industrial Engineering Chemical Resouces*, 46 (2007) 5824-5847.

[49] H. Hom-Larsen, Synthesis and New applications of DME-a review of alternative, in, Natal, 2007, pp. 1-23.

[50] M. Kumar, V.C. Srivastava, Simulation of a Fluidized-bed Reactor for Dimethyl Ether Synthesis, *Chemical Engineering Technology*, 33 (2010) 1967-1978.

[51] W.-Z. Lu, L.-H. Teng, W.-D. Xiao, Simulation and experimental study of dimethyl ether synthesis from syngas in a fluidized-bed reactor, *Chemical Engineering Science*, 59 (2004) 5455-5464.

[52] R. Vakili, E. Pourazadi, P. Setoodeh, R.M. Rahimpour, Dimethyl ether(DME) synthesis through a thermally coupled heat exchanger reactor, *Applied Energy*, 88 (2011) 1211-1223.

[53] Y.I. Pyatnitskii, P.E. Strizhak, N.K. Lunev, Kinetic Modeling for the conversion of synthesis gas to dimethyl ether on a mixed Cu-ZnO-Al2O3 catalyst with γ-Al2O3, *Theoretical and Experimental Chemistry*, 45 (5) (2009) 312-316.

[54] Y. Zhu, S. Wang, X. Ge, Q. Liu, Z. Luo, K. Cen, Experimental study of improved two step synthesis for DME production, *Fuel Processing Technology*, 91 (2010) 424-429.

[55] S.B. Lee, W. Cho, D.K. Park, E.S. Yoon, Simulation of fixed bed reactor for dimethyl ether synthesis, *Korean journal of Chemical Engineering*, 23 (4) (2006) 522-530.

[56] L. Wang, D. Fang, X. Huang, S. Zhang, Y. Qi, Z. Liu, Influence of Reaction Conditions on Methanol Synthesis and WGS Reaction in Syngas-to-DME Process, *Journal of Natural Gas Chemistry*, 15 (2006).

[57] G. Moradi, J. Ahmadpour, M. Nazari, F. Yaripour, Effects of Feed Composition and Space Velocity on Direct Synthesis of Dimethyl Ether from Syngas, *Industrial Engineering Chemical Resouces*, 47 (2008) 7672-7679.

[58] E.D. Larson, R. Tingjin, Synthetic fuel production by indirect coal liquefaction, *Energy for Sustainable Development*, 7 (2003) 79-102.

[59] E.S. Yoon, C. Han, A Review of Sustainable Energy - Recent Development and Future Prospects of Dimethyl Ether (DME), in: C.A.O.d.N. Rita Maria de Brito Alves, Evaristo Chalbaud Biscaia, Jr. (Eds.) *Computer Aided Chemical Engineering, Elsevier*, (2009), pp. 169-175.

[60] J. Ereña, R. Garoña, J.M. Arandes, A.T. Aguayo, J. Bilbao, Direct synthesis of dimethyl ether from (H_2+CO) and (H_2+CO_2) feeds. Effect of feed composition, *International Journal of Chemical reator Engineering*, 3 (2005) 1-15.

[61] G.R. Moradi, R. Ghanei, F. Yaripour, Determination of Optimum Operating Conditions for Direct Synthesis of Dimethyl Ether from Syngas, *International Journal of Chemical reator Engineering*, 5(A14) (2007).

[62] Z.L. Wang, *Characterization of Nanophase Materials*, First ed., Wiley-VCH Verlag GmbH, Weinheim Federal Republic of Germany (2000), pp. 37-78.

[63] I. Cherkendorff, J.W. Niemantsverdriet, *Concepts of Modern Catalysis and Kinetics*, Second ed., Wiley-VCH Verlag GmbH & Co. KGaA, (2007), pp. 143-146.

[64] J.W. Niemantsverdriet, Spectroscopy in Catalysis. *An Introduction and Kinetics*, Third ed., Wiley-VCH Verlag GmbH & Co. KGaA, (2007), pp. 182-184.

[65] P. Stoltze, *Introduction to heterogeneous catalysis*, Department of Chemistry and Applied Engineering Science, Aalborg University, Denmark, (2000), pp. 46-70

[66] A. Ebadi, J.S.S. Mohammadzadeh, A. Khudiev, What is the correct form of BET isotherm for modeling liquid phase adsorption?, *Adsorption*, 15 (2009) 65-73.

[67] R.C. Reid, J.M. Prausnitz, B.E. Poling, *The Properties of Gases and Liquids*, in, McGraw-Hill, New York 1987, pp. 656–732.

[68] G. Jia, Y. Tan, Y. Han, Synthesis of dimethyl ether from CO hydrogenation: a thermodynamic analysis of the influence of water gas-shift reaction, *Journal of Natural Gas Chemistry*, 14 (2005) 47-53.

[69] A.I. Kozlov, A.P. Kozlova, H. Liu, Y. Iwasawa, A new approach to active supported Au catalysts, *Applied Catalysis A: General*, 182 (1999) 9-28.

[70] S. Svelle, P.O. Ronning, U. Olsbye, S. Kolboe, Kinetic studies of zeolite-ctalyzed methylation reactions. Part 2. Co-raction of [^{12}C] propene or [^{12}C] n-butene and [^{13}C] methanol, *Journal of Catalysis*, 234 (2005) 385-400.

[71] P. Dutta, S.C. Roy, L.N. Nandi, P. Samuel, S.M. Pillai, B.D. Bhat, M. Ravindranathan, Synthesis of lower olefins from methanol and subsequent conversion of ethylene to higher olefins via oligomerisation, *Journal of Molecular Catalysis A: Chemical*, 223 (2004) 231-235.

[72] X. Wu, M.G. Abraha, R.G. Anthony, Methanol conversion on SAPO-34: reaction condition for fixed-bed reactor, *Applied Catalysis A: General*, 260 (2004) 63-69.

[73] Q. Zhang, X. Li, K. Asami, S. Asaoka, K. Fujimoto, Synthesis of LPG from synthesis gas, *Fuel Processing Technology*, 85 (2004) 1139-1150.

[74] T. Shikada, Y. Ohno, T. Ogawa, M. Ono, M. Mizuguchi, K. Tomura, K. Fujimoto Fujimoto, Synthesis of dimethyl ether from natural via synthesis gas, *Kinetics and Catalysis* (*Translation of Kinetika i Kataliz*), 40 (3) (1999) 395-400.